

Strong coupling constant and quark masses from lattice QCD

Javad Komijani^a, Peter Petreczky^{b,*}, Johannes Heinrich Weber^c

^a*Department of Physics, University of Tehran, Tehran 1439955961, Iran*

^b*Physics Department, Brookhaven National Laboratory, Upton, NY 11973, USA*

^c*Department of Computational Mathematics, Science and Engineering, and Department of Physics and Astronomy, Michigan State University, East Lansing, MI 48824, USA*

Abstract

We review lattice determinations of the charm and bottom quark masses and the strong coupling constant obtained by different methods. We explain how effective field theory approaches, such as Non-Relativistic QCD (NRQCD), potential Non-Relativistic QCD (pNRQCD), Heavy Quark Effective Theory (HQET) and Heavy Meson rooted All-Staggered Chiral Perturbation Theory (HMrAS χ PT) can help in these determinations. After critically reviewing different lattice results we determine lattice world averages for the strong coupling constant, $\alpha_s(M_Z, N_f=5) = 0.11803^{+0.00047}_{-0.00068}$, as well as for the charm quark mass, $m_c(m_c, N_f=4) = 1.2735(35)$ GeV, and the bottom quark mass, $m_b(m_b, N_f=5) = 4.188(10)$ GeV. The above determinations are more precise than the ones obtained by Particle Data Group (PDG).

Keywords: QCD, strong coupling constant, quark masses, lattice

Contents

1	Introduction	3
2	General remarks on lattice calculations and determinations of the light and strange quark masses	5
3	Static $q\bar{q}$ energy	7
3.1	Static energy in the weak-coupling approach	8
3.1.1	Static energy at N ³ LO	8
3.1.2	Resummation of the ultrasoft logarithms	10
3.1.3	Perturbative uncertainty	11
3.1.4	OPE calculation of the renormalon subtracted singlet potential	12
3.2	Static energy determination on the lattice	13

*Corresponding author

Email addresses: jkomijani@ut.ac.ir (Javad Komijani), petreczk@quark.phy.bnl.gov (Peter Petreczky), weberjo8@msu.edu (Johannes Heinrich Weber)

3.2.1	Interpolating operator dependence	13
3.2.2	Discretization artifacts at short distances	14
3.2.3	Sea quark effects in lattice simulations	17
3.3	α_s from the static energy	17
3.4	α_s from the singlet free energy	19
3.5	Summary and pre-averaging	22
4	Moments of quarkonium correlators	23
4.1	General definitions and properties	24
4.2	Lattice setup and continuum limit	27
5	Comparison of the reduced moments from various groups	29
6	Heavy quark masses and α_s from the moments	31
7	Heavy quark masses from a combined EFT and lattice QCD analysis	36
7.1	Relations between heavy-light meson and quark masses	38
7.1.1	Minimal-Renormalon-Subtracted mass	38
7.1.2	Simulation and renormalized masses	41
7.1.3	Heavy-light mesons in EFTs and construction of a fit function	41
7.2	Lattice setup and simulations parameters	43
7.3	Quark mass results from EFT fit to lattice data	44
8	Other determination of α_s	49
8.1	α_s determination from step scaling	50
8.2	α_s from small Wilson loops	51
8.3	The strong coupling constant from hadronic vacuum polarization	51
8.4	The strong coupling constant from QCD vertices	52
8.5	The strong coupling constant from eigenvalues of the Dirac operator	53
9	Other heavy quark mass determinations	53
9.1	Charm quark mass determination	54
9.2	Bottom quark mass determination	54
10	Executive summary of the strong coupling constant and heavy quark mass determinations	55
11	Conclusions	58

1. Introduction

The strong coupling constant and quark masses are important parameters of the Standard Model (SM) and thus their knowledge is required for its testing. Heavy quark masses are needed to test the Higgs mechanism of mass generation [1] and accurate determination of the SM parameters [2–4]. The accurate determination of the strong coupling constant is needed for predictions of the Higgs boson branching ratios [1, 5] and stability of the SM vacuum [6, 7].

Traditionally the quark masses and the strong coupling constant α_s have been obtained from a comparison of perturbative QCD calculations to the experimental data involving a hard scale. For example, α_s can be extracted from jets [8–12], e^+e^- annihilation [13–20], deep inelastic scattering [21–26], or τ -decay [27–30]. The charm and bottom quark masses can be extracted from the e^+e^- annihilation data above the open charm threshold [31, 32] or from deep inelastic scattering [33].

Lattice QCD calculations play an increasingly important role in the determination of the quark masses and α_s because of the increase in available computation resources and algorithmic improvements. The basis of lattice QCD is the formulation of the QCD path integral on a discretized Euclidean space-time lattice with lattice spacing a . This formulation allows for ultraviolet regularization of QCD at the level of the path integral and not only at the level of Feynman diagrams. The path integral can be calculated non-perturbatively using Monte-Carlo simulations. Finally, to recover the continuum physics, the limit $a \rightarrow 0$ should be taken. There are different ways to discretize the gauge and fermions fields on a lattice, i.e. different lattice QCD actions. For the gauge degrees of freedom one can use the standard Wilson plaquette action or the improved Lüscher-Weisz action. For quark fields different improved actions are used, such as the clover-improved Wilson quark action, AsqTad staggered quark action [34], Highly Improved Staggered Quark (HISQ) action [35], twisted mass quark action [36], or any domain wall fermion (DWF) action [37]. For a recent review on the basics and current status of lattice QCD we refer the reader to Ref. [38].

Phenomenological determinations of the strong coupling constant typically give α_s defined at large energy scales. The only low energy determination of α_s comes from the τ decay. For some applications it is important to know the running of the strong coupling constant at low energy scales. An example is the testing the applicability of the weak-coupling approach to QCD thermodynamics through comparison to lattice QCD results [39–45]. Here one needs α_s at relatively low scale $\mu \simeq \pi T$, with T being the temperature. As we will see, lattice QCD calculations are well suited to determine the running of α_s at low energy scales down to the charm quark mass.

In lattice QCD the quark masses are fixed by setting the masses of a set of hadrons composed of those quarks to their physical values. This procedure gives the so-called bare quark masses in a specific lattice scheme. To obtain the quark masses in the commonly used $\overline{\text{MS}}$ scheme one has to calculate the renormalization constant that converts the lattice scheme to the $\overline{\text{MS}}$ scheme. There are several methods to do this which will be discussed in this review.

The lattice determination of α_s is based on the idea that one calculates the quantity $O(\nu)$, that depends on some physical energy scale ν (not to be confused with the renormalization scale) non-perturbatively on a lattice. Then one compares the result with the perturbative calculation of $O(\nu)$ as an expansion in powers of $\alpha_s(\nu)$. From this one can obtain the value of $\alpha_s(\nu)$ provided that the truncated power series in $\alpha_s(\nu)$ yields a sufficiently accurate description of $O(\nu)$. One of the big challenges in the lattice determination of the quark masses and α_s is the so-called window problem. The scale ν has to be much smaller than the lattice cutoff (a^{-1}) to avoid large discretization effects (lattice artifacts), and at the same time sufficiently large to make the perturbative expansion accurate, i.e.

$$\Lambda_{QCD} \ll \nu \ll \frac{1}{a}. \quad (1)$$

This means one has to perform the calculations at small values of the lattice spacing, which is computationally very demanding and is limited by the critical slowing down of Monte-Carlo algorithms. Controlling discretization effects is the biggest challenge for an accurate determination of α_s and the quark masses. We will discuss this issue in detail for calculations of α_s from the energy of a static quark anti-quark ($q\bar{q}$) pair and the moments of quarkonium correlators as examples. As we will see, the interplay between lattice QCD calculations and effective field theory methods will play an important role in addressing this issue.

The rest of this review is organized as follows. In the next section we summarize some key aspects of lattice calculations including a discussion on determination of the light quark masses. In Sec. 3 we will discuss the determination of α_s from the energy of static $q\bar{q}$ states. In Sec. 4 we discuss the determination of α_s and heavy quark masses from the moments of quarkonium correlators. In Sec. 7 we present the determination of the quark masses using a combined effective field theory and lattice QCD calculations. The discussion of other lattice methods for the determination of α_s as well as the comparison of different results will be given in Sec. 8. Overview of different determinations of heavy quark masses will be given in Sec. 9. Readers not interested in technical details of the lattice calculations and perturbation theory can skip to Sec. 10 for the main results, where we present an executive summary of the present status. Finally, Sec. 11 contains our conclusions. The lattice determination of the strong coupling constant and the quark masses is also reviewed by the Flavor Lattice Averaging Group (FLAG) [46]. The FLAG findings will be incorporated into our discussions where appropriate.

2. General remarks on lattice calculations and determinations of the light and strange quark masses

Out of the six quarks present in the SM the up, down, and strange quarks have masses that are smaller or comparable to the nonperturbative QCD scale Λ_{QCD} . As a result, their effects cannot be taken into account by perturbation theory unlike the heavy quarks. Therefore, the effects of the u , d , and s quarks have to be included directly in any lattice QCD calculations. Since isospin symmetry is believed to be a good symmetry of QCD, most lattice calculations set $m_u = m_d$ and denote their masses by m_l . Therefore, lattice QCD calculations involving u , d , and s quarks are usually referred to as (2+1)-flavor or $N_f = 2 + 1$ calculations. The charm-quark mass is much larger than Λ_{QCD} , and therefore its effect can be reasonably well approximated by perturbation theory. This was also confirmed in a recent lattice study [47]. Nevertheless many lattice QCD calculations nowadays include the effect of dynamical charm quarks. These calculations are referred to as (2+1+1)-flavor or $N_f = 2 + 1 + 1$ calculations.

In order to perform the continuum ($a \rightarrow 0$) limit of a quantity of interest the lattice spacing has to be varied, which is performed by varying the bare gauge coupling g_0 in the lattice QCD action. It is customary to parametrize g_0 in terms of $\beta = 6/g_0^2$ or $\beta = 10/g_0^2$ if an improved gauge action is used, see e.g. Ref. [48]. To fix the lattice spacing we need to calculate a physical quantity, for example the pion decay constant f_π , in lattice units¹. Using the experimental value of the pion decay constant from the Particle Data Group [49] one can then determine the lattice spacing in physical units. It is also possible to determine the lattice spacing in terms of quantities that are not measured experimentally. Examples for such a quantity are the Sommer scale r_0 [50] and the r_1 [48] and r_2 [40] scales. These scales are defined in terms of the energy of a static quark-antiquark pair, $E(r)$, as

$$\left. \frac{r^2}{a^2} \frac{d[aE(r/a)]}{d[r/a]} \right|_{r=r_i} = r^2 \left. \frac{dE(r)}{dr} \right|_{r=r_i} = c_i, \quad \left\{ \begin{array}{llll} r_i & \rightarrow & r_0 & r_1 & r_2 \\ c_i & \rightarrow & 1.65 & 1.0 & 0.5 \end{array} \right. . \quad (2)$$

To use for example r_1 for scale setting one has to determine it in physical units. To do this one first calculates r_1/a and also $f_\pi a$ (or any other experimentally measured quantity) at several lattice spacings and performs the continuum extrapolation of the dimensionless quantity $r_1 f_\pi$. Using the known value of f_π one obtains r_1 in physical units. This value can be used to set the lattice spacing in a different lattice calculation. The same applies to the r_0 or the r_2 scales. Other similar quantities that can be used for scale setting are the gradient flow parameters t_0 [51] and w_0 [52]. The values of r_0 , r_1 , r_2 , w_0 and t_0 are now well established. In Secs. 3 and 4 we use the value $r_1 = 0.3106(8)(14)(4)$ fm [53] in the case of (2+1)-flavor QCD with HISQ action. The contributions to the uncertainty of r_1 are due to the continuum extrapolation, the chiral extrapolation, and

¹A quantity in lattice units refers to a dimensionless number obtained by multiplying the quantity by an appropriate power of the lattice spacing a . For instance, the pion decay constant f_π in lattice units is $a f_\pi$.

the experimental uncertainty of f_π . The calculations of the static energy using DWF formulation, discussed in Sec. 3 use $r_1 = 0.311(2)$ fm [54], which is based on the same lattice calculation of r_1 in terms of f_π .

As we vary the lattice spacing or equivalently β we also need to vary the quark masses such that the physical hadron masses remain constant in physical units. This procedure defines the line of constant physics $m_l = m_l(\beta)$, $m_s = m_s(\beta)$ and $m_c = m_c(\beta)$. The computational costs of lattice QCD calculations increase with decreasing quark masses and could be very large for physical values of m_l . For this reason many lattice QCD calculations fix the charm- and strange-quark masses to their physical values, while m_l is taken to be larger than the physical value. Performing calculations at several values of m_l that are larger than the physical one and performing chiral extrapolations the physical limit can be recovered. Currently many lattice calculations are performed directly at or very close to the physical value of m_l and no extrapolation is needed. Once the values of $m_l(\beta)$, $m_s(\beta)$ and $m_c(\beta)$ are determined in lattice calculations one has to calculate the renormalization factor that converts the quark masses in the lattice scheme to the $\overline{\text{MS}}$ scheme at a certain scale μ , which is conventionally set to 2 GeV. This can be done directly in perturbation theory on the lattice or indirectly by first converting the lattice quark masses to some intermediate scheme, like RI-MOM, and then matching the RI-MOM masses to the $\overline{\text{MS}}$ masses.

To determine the light quark masses in the isospin symmetric limit one has to consider the isospin symmetric hadron masses. Typically pseudoscalar meson masses are used to fix the quark masses and chiral perturbation theory is used to estimate the isospin symmetric masses. The status of the lattice determination of m_s and m_l is reviewed in detail by FLAG [46] and therefore we will only summarize their main findings here. The quark mass determinations in FLAG are grouped according to some quality criteria and only the lattice determinations that pass certain quality criteria are used to calculate the averaged values of the quark masses. The results from averaging $N_f = 2 + 1$ and $N_f = 2 + 1 + 1$ lattice calculations are reported separately. FLAG finds for the $\overline{\text{MS}}$ masses at $\mu = 2$ GeV [46]:

$$m_l = 3.364(41) \text{ MeV}, \quad m_s = 92.03(88) \text{ MeV}, \quad N_f = 2 + 1, \quad (3)$$

$$m_l = 3.410(43) \text{ MeV}, \quad m_s = 93.44(68) \text{ MeV}, \quad N_f = 2 + 1 + 1. \quad (4)$$

The quark mass ratios are scheme and scale independent, and thus can be evaluated directly from ratios of the bare masses. For the ratio m_s/m_l FLAG obtains [46]:

$$m_s/m_l = 27.42(12), \quad N_f = 2 + 1, \quad (5)$$

$$m_s/m_l = 27.23(10), \quad N_f = 2 + 1 + 1. \quad (6)$$

We see that the $N_f = 2 + 1$ and $N_f = 2 + 1 + 1$ determinations agree well with each other implying that the effects of dynamical charm quarks are small.

Calculating for instance charmonium ground state masses on a lattice one can obtain $m_c(\beta)$. Combining this with $m_s = m_s(\beta)$ and performing continuum extrapolation one obtains m_c/m_s ; see for example Ref.

[55] for $N_f = 2 + 1$, which finds

$$m_c/m_s = 11.877(91). \quad (7)$$

This agrees well with the FLAG average of $m_c/m_s = 11.82(16)$, $N_f = 2 + 1$, though it was excluded from the FLAG averaging procedure. For $N_f = 2 + 1 + 1$ FLAG finds: $m_c/m_s = 11.768(33)$.

To obtain m_u and m_d masses isospin breaking effects including QED effects have to be considered. The latter implies that one has to perform lattice calculations in QED + QCD. Many of the present day calculations consider QED effects only in the valence sector, i.e. use electro-quenched approximation. This approach has the advantage that no new lattice gauge configurations have to be generated. The lattice determination of m_u and m_d is also reviewed by FLAG in great detail and here we only give the summary of their findings:

$$m_u = 2.27(9) \text{ MeV}, \quad m_d = 4.67(9) \text{ MeV}, \quad m_u/m_d = 0.485(19), \quad N_f = 2 + 1, \quad (8)$$

$$m_u = 2.50(17) \text{ MeV}, \quad m_d = 4.88(20) \text{ MeV}, \quad m_u/m_d = 0.513(31), \quad N_f = 2 + 1 + 1. \quad (9)$$

The above lattice results for the up-, down-, and strange-quark masses are much more precise than the values quoted by PDG [49]. The determination of the charm and bottom quark mass may potentially suffer from large discretization effects and will be discussed separately in the following sections.

3. Static $q\bar{q}$ energy

The QCD static energy E of a quark-antiquark pair is an observable in QCD up to an additive constant. As an analog of positronium in QED, the QCD static energy is the most simple bound state problem of QCD. Due to the infinite mass of the static quark and antiquark the two color charges are strictly immobile, and their distance is a well-defined quantum number. The static energy $E(r)$ is defined in terms of the large time limit of the expectation value of the Wilson loop $W_S(r, t)$ as

$$E(r) = \lim_{t \rightarrow \infty} i \frac{1}{t} \langle \ln W_S(\mathbf{r}, t) \rangle = \lim_{t \rightarrow \infty} i \frac{\partial}{\partial t} \langle \ln W_S(\mathbf{r}, t) \rangle. \quad (10)$$

The Wilson loop is a smooth path-ordered contour in the continuum

$$W_S(\mathbf{r}, t) = e^{ig \oint_{\mathbf{r}, t} dz^\mu A_\mu}. \quad (11)$$

The Wilson loop has a self-energy divergence proportional to its circumference. The static energy cannot depend on the gauge fields at infinite time separation due to the cluster decomposition. Hence, the static energy may be defined as well by evaluating the correlation function of two temporal Wilson lines in a suitable gauge, e.g. Coulomb gauge,

$$C_S(\mathbf{r}, t) = e^{ig \int_0^t d\tilde{t} A_0(\mathbf{0}, \tilde{t})} e^{-ig \int_0^t d\tilde{t} A_0(\mathbf{r}, \tilde{t})}. \quad (12)$$

The definition in terms of the Wilson line correlation function avoids the self-energy divergence associated with the spatial distance between the two Wilson lines. The static energy E is a function of the fixed distance r between the static quark and antiquark, the QCD coupling $\alpha_s = g^2/4\pi$, and the masses of the N_f dynamical quarks in the sea. In particular, the static energy depends on α_s already at the tree-level, where it is up to a trivial color factor C_F and the different coupling constant formally the same as the QED Coulomb potential.

3.1. Static energy in the weak-coupling approach

The QCD static energy has been calculated in the weak-coupling approach since the earliest days of QCD [56–60] and is currently known at the next-to-next-to-next-to-leading log (N³LL) level [61–65]. At each loop order there is a one-to-one correspondence between the coupling α_s in the weak-coupling expression for the static energy and the QCD Lambda parameter. Since the masses of the up, down, and strange sea quarks are much smaller than the QCD Lambda parameter, their non-vanishing masses play only a negligible role for the running of the coupling at scales much higher than the Lambda parameter. For this reason, these sea quarks are generally taken to be in the massless limit in perturbation theory. Although there is an explicit dependence on the masses of the dynamical sea quark flavors as well, such contributions to the static energy are suppressed by positive powers of the distance between the quark and antiquark and of the coupling α_s itself [66]. These small contributions to the static energy can be neglected safely.

3.1.1. Static energy at N³LO

The QCD static energy E is a multi-scale problem, i.e. E depends on the scales $1/r$ and α_s/r , where r is the distance between the static quark and antiquark. It is a convention to call the former the soft scale, $\nu \sim 1/r$, and the latter the ultrasoft scale, $\mu_{\text{us}} \sim \alpha_s/r$. Such a multi-scale problem is ideally approached in an effective field theory approach, i.e. in potential nonrelativistic QCD (pNRQCD) [60, 67], which permits integrating out the higher scale, $1/r$, while solving the more simple problem at the lower scale, α_s/r . In pNRQCD the system is described in terms of the interactions among a heavy quark-antiquark pair at the relative distance r in the color-singlet or the color-octet configurations. These are the nonrelativistic degrees of freedom, whereas the light quarks and gluons, which are at the even lower scale Λ_{QCD} , are included in terms of nonperturbative matrix elements. The Wilson coefficients of pNRQCD have an explicit dependence on the distance r and represent various contributions to the quark-antiquark potential in QCD. The static energy has been calculated in the weak-coupling approach in the limit of N_f massless sea quarks. The static energy can be decomposed at the next-to-next-to-next-to-leading order into

$$E(r) = V_s(r, \mu_{\text{cut}}) + \Lambda_s + \delta E_{us}(r, \mu_{\text{cut}}). \quad (13)$$

Here, μ_{cut} is a cutoff scale between the soft and ultrasoft scales, $\nu \sim 1/r \gg \mu_{\text{cut}} \gtrsim \mu_{\text{us}} \sim \alpha_s/r$. The first term, V_s , is the color singlet potential of pNRQCD. Like its color octet counterpart V_o it is a Coulomb

potential up to the trivial color factors at the tree-level: $V_s^{\text{tree}}(r) = -C_F \frac{\alpha_s}{r}$, $V_o^{\text{tree}}(r) = +\frac{1}{2N_c} \frac{\alpha_s}{r}$. The singlet potential can be obtained through the Fourier transform

$$V_s(r, \mu_{\text{cut}}) = -4\pi C_F \int_{q^2 \geq \mu_{\text{us}}^2} \frac{d^3 q}{(2\pi)^3} e^{i\mathbf{q} \cdot \mathbf{r}} \frac{\alpha_V(q^2)}{q^2}, \quad (14)$$

where the coupling in the V scheme (also called the $q\bar{q}$ scheme) is given by

$$\alpha_V(q^2) = \alpha_s(\nu^2) \sum_{n=0}^L \{p_n[\ln(\nu^2/q^2)] + d_n[\ln(\nu^2/q^2)]\} \left(\frac{\alpha_s(\nu^2)}{4\pi} \right)^n. \quad (15)$$

The n -th order polynomials p_n and d_n are known at the next-to-next-to-next-to-leading order [57–60, 62–65]. In particular, $p_n[0] = a_n$, where the constants a_n are reproduced to this order in Appendix A. The latter (d_n) contain the IR divergent contributions that are regularized by the cutoff at or above the ultrasoft scale $\mu_{\text{cut}} \gtrsim \mu_{\text{us}} \sim \alpha_s/r$. The first nontrivial contribution d_n occurs for $n = 3$, i.e. it contributes at the next-to-next-to-next-to-leading order. The singlet potential $V_s(r, \mu_{\text{cut}})$ is affected by an r -independent renormalon². The second term Λ_s in Eq. (13) is the residual mass, which is also affected by a renormalon; see Ref. [56]. This renormalon exactly cancels the constant renormalon of the singlet potential [69]. The last term $\delta E_{\text{us}}(r, \mu_{\text{cut}})$ in Eq. (13) is called the ultrasoft contribution. It is the time integral of the chromoelectric correlation function regularized at the ultrasoft scale μ_{cut} ,

$$\delta E_{\text{us}}(r, \mu_{\text{cut}}) = -i \frac{g^2}{N_c} V_A^2 \int_0^\infty dt e^{-it[V_o - V_s](r)} \langle \text{tr } \mathbf{r} \cdot \mathbf{E}(t) \mathbf{r} \cdot \mathbf{E}(0) \rangle. \quad (16)$$

$\delta E_{\text{us}}(r, \mu_{\text{cut}})$ can be understood in pNRQCD as being due to the intermediate fluctuation of the static quark and antiquark into the color-octet configurations. The chromoelectric fields can be separated as the sum of the perturbative contribution $\mathbf{E}_{\text{us}}(t)$ at the ultrasoft scale, $\mu_{\text{us}} \sim \alpha_s/r$, and the nonperturbative contribution $\mathbf{E}_{\text{np}}(t)$ at the scale $\Lambda_{\text{QCD}} \ll \mu_{\text{us}}$, where the latter undergoes a very slow variation with time. Hence, the integral splits into two contributions³, where

$$-i \frac{g^2}{N_c} V_A^2 \int_0^\infty dt e^{-it[V_o - V_s](r)} \langle \text{tr } \mathbf{r} \cdot \mathbf{E}_{\text{np}}(0) \mathbf{r} \cdot \mathbf{E}_{\text{np}}(0) \rangle \sim -\frac{\frac{g^2}{N_c}}{\frac{N_c \alpha_s}{2r}} V_A^2 r^2 \langle \text{tr } \mathbf{E}_{\text{np}}^2(0) \rangle \sim -\frac{\pi}{N_c} r^3 \langle G^2 \rangle \quad (17)$$

is the nonperturbative contribution from the dimension four gluon condensate with r^3 power-law form, while

$$-i \frac{g^2}{N_c} V_A^2 \int_0^\infty dt e^{-it[V_o - V_s](r)} \langle \text{tr } \mathbf{r} \cdot \mathbf{E}_{\text{us}}(t) \mathbf{r} \cdot \mathbf{E}_{\text{us}}(0) \rangle \quad (18)$$

can be evaluated in perturbation theory with the UV cutoff μ_{cut} . Here, $\mu_{\text{us}} \sim \alpha_s/r \sim (V_o - V_s) \sim 1/t$ acts as an IR cutoff, namely, contributions from larger times $t \gg 1/\mu_{\text{us}}$ are suppressed due to the rapid oscillations.

²For a discussion on renormalons see Ref. [68]. For a brief discussion in the context of the pole mass see Sec. 7.1.1.

³ A mixed term is forbidden due to the rotational invariance of the problem.

At the level of the leading logarithms, the UV divergent contributions from this part of $\delta E_{\text{us}}(r, \mu_{\text{cut}})$ at the UV cutoff μ_{cut} cancel against the IR divergent contributions to $V_s(r, \mu_{\text{cut}})$ at the same IR cutoff μ_{cut} .

The renormalon of Λ_s may be evaded by instead considering the force $F = dE/dr$ [70], which is given at the next-to-next-to-next-to-leading order (N³LO) as

$$F(r, \nu) = \frac{C_F}{r^2} \alpha_s(\nu) \left[1 + \frac{\alpha_s(\nu)}{4\pi} (\tilde{a}_1 - 2\beta_0) + \frac{\alpha_s^2(\nu)}{(4\pi)^2} (\tilde{a}_2 - 4\tilde{a}_1\beta_0 - 2\beta_1) + \frac{\alpha_s^3(\nu)}{(4\pi)^3} (\tilde{a}_3 - 6\tilde{a}_2\beta_0 - 4\tilde{a}_1\beta_1 - 2\beta_2 + a_3^L \ln \frac{C_A \alpha_s(\nu)}{2}) + \mathcal{O}(\alpha_s^4, \alpha_s^4 \ln^2 \alpha_s) \right]. \quad (19)$$

The first three terms correspond to the tree-level, the one-loop, and the two-loop order, respectively. Both parts of the fourth term correspond to the three-loop order. Here and in the following, the coupling $\alpha_s(\nu)$ is understood as renormalized in the $\overline{\text{MS}}$ scheme at the soft scale ν , and can be traded for the corresponding QCD Lambda parameter, i.e. at three flavors in the $\overline{\text{MS}}$ scheme $\Lambda_{\overline{\text{MS}}}^{N_f=3}$. Large logarithms $\ln(r\nu)$ and their cancellations between different terms can be avoided, if the soft scale ν is chosen proportional to the inverse distance, e.g. a standard choice is $\nu = 1/r$, which we use hereafter. Integrating Eq. (19) one obtains a renormalon-free expression for the static energy up to an arbitrary but finite integration constant. The coefficients in Eq. (19) are defined in [71] and reproduced in Appendix A. At the three-loop order there is a contribution proportional to $\ln \alpha_s(1/r)$ as well as a non-logarithmic term. The origin of the former can be understood in pNRQCD [60] as the interplay between the singlet potential V_s and the last term in Eq. (13). The intermediate scale $\mu_{\text{us}} = C_A \alpha_s(1/r)/(2r) = V_o - V_s$ is the physical IR cutoff for the contribution from the singlet potential, V_s , and the UV cutoff for the ultrasoft contribution. For this reason, and to distinguish it from the soft scale ν , μ_{us} is called the ultrasoft scale. Note that there are alternative conventions to use an r -independent value for the ultrasoft scale, e.g. 0.8 GeV [72, 73], or $3 \Lambda_{\overline{\text{MS}}}^{N_f=3}$ or $4 \Lambda_{\overline{\text{MS}}}^{N_f=3}$ [74, 75] (using the PDG value of $\Lambda_{\overline{\text{MS}}}^{N_f=3}$).

3.1.2. Resummation of the ultrasoft logarithms

Eventually, for sufficiently small values of the coupling $\alpha_s(1/r)$, i.e. for short enough distances r , the ultrasoft logarithm $\ln \alpha_s(1/r)$ becomes very large. Hence, one could resum the terms $\alpha_s^{3+n} \ln^n(\alpha_s)$ or $\alpha_s^{4+n} \ln^n(\alpha_s)$ that contribute to the force. This resummation is accomplished using the renormalization group equations in pNRQCD [61, 76, 77]. In this case, it is not immediately clear, whether the naive power counting $\ln \alpha_s \sim \mathcal{O}(\alpha_s^0)$ could be appropriate. One may attempt a resummation of these contributions by treating the logarithm as $\ln \alpha_s \sim \mathcal{O}(\alpha_s^{-n})$, where $n = 0, 1, 2, \dots$. We show the different terms at the two- and three-loop orders of Eq. (19) in Fig. 1 for distances that are accessible in state-of-the-art lattice simulations. Inspecting the magnitude of the terms, i.e. first noting that the two-loop term is systematically larger than each three-loop term as demanded by the naive power counting, and second noting that all three-loop terms are of a similar magnitude, it is evident that the counting of the ultrasoft logarithms as of a lower

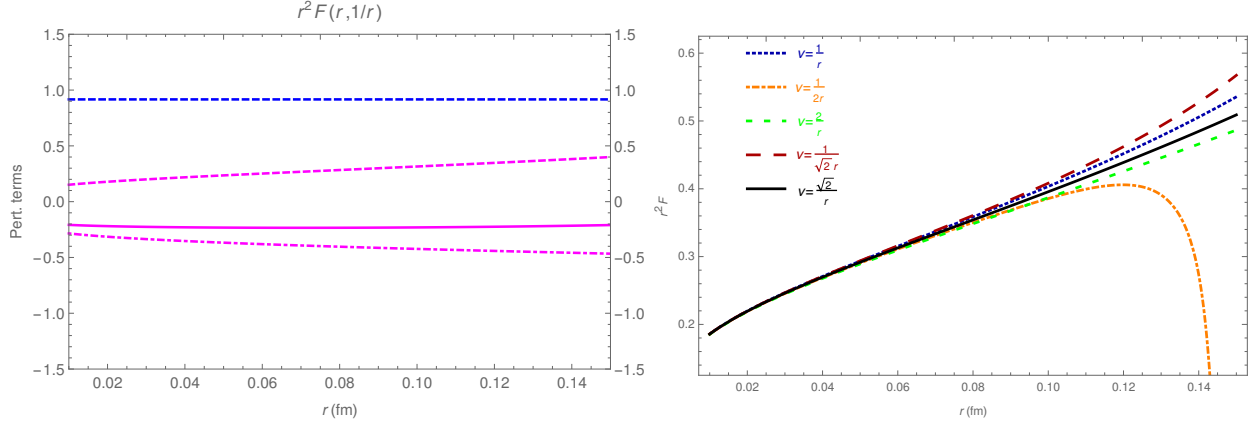


Figure 1: (left) The magenta lines represent three-loop contributions: dashed (soft term, the first term in the last line of Eq. (19)), solid (ultrasoft term, the second term in the last line of Eq. (19)), and dot-dashed (resummed ultrasoft term, the terms in the second line of Eq. (20)). The blue dashed line represents the two-loop contribution (last term in the first line of Eq. (19)). A factor $\alpha_s^3(1/r)$ has been dropped from all terms. (right) The three-loop force with resummed leading ultrasoft logarithms according to Eq. (20) at different values of the soft scale ν . The dependence on the soft scale is non-monotonic and has a minimum for $\nu \approx 1/(\sqrt{2}r)$. (both) The plots use $\Lambda_{\overline{\text{MS}}}^{N_f=3} = 315 \text{ MeV}$ and the standard value $\mu_{us} = C_A \alpha_s(1/r)/(2r)$ for the ultrasoft scale.

order, is not justified in this distance range. Nevertheless, using the naive power counting $\ln \alpha_s \sim \mathcal{O}(\alpha_s^0)$ one may still resum the leading ultrasoft logarithms as [73]

$$\begin{aligned}
 F(r, \nu) = \frac{C_F}{r^2} \alpha_s(\nu) & \left[1 + \frac{\alpha_s(\nu)}{4\pi} (\tilde{a}_1 - 2\beta_0) + \frac{\alpha_s^2(\nu)}{(4\pi)^2} (\tilde{a}_2 - 4\tilde{a}_1\beta_0 - 2\beta_1) \right. \\
 & - \frac{\alpha_s^2(\nu)}{(4\pi)^2} \frac{a_3^L}{2\beta_0} \ln \frac{\alpha_s(\mu_{us})}{\alpha_s(\nu)} + \frac{\alpha_s^2(\nu)\alpha_s(\mu_{us})}{(4\pi)^3} a_3^L \ln \frac{C_A \alpha_s(\nu)}{2\mu_{us}/\nu} \\
 & \left. + \frac{\alpha_s^3(\nu)}{(4\pi)^3} (\tilde{a}_3 - 6\tilde{a}_2\beta_0 - 4\tilde{a}_1\beta_1 - 2\beta_2) + \mathcal{O}(\alpha_s^4) \right]. \quad (20)
 \end{aligned}$$

The second term of the last line of Eq. (19) is recovered from the second line of Eq. (20) in the limit $\mu_{us} \rightarrow \nu$. Figure 1 shows that the resummed ultrasoft term partially cancels the r dependence of the soft term at three loops, which may be accidental, i.e. this may fail to happen at higher loop orders. For this reason, it is conservative to consider the perturbative uncertainties due to the soft or ultrasoft terms as independent uncertainties. In the following we refer to the static energy $E(r)$ obtained from integrating $F(r, 1/r)$ in Eq. (20) as the three-loop result with resummed leading ultrasoft logarithms.

3.1.3. Perturbative uncertainty

The perturbative uncertainty can be estimated by varying the details of the perturbative calculation. On the one hand, one may estimate the influence of unknown higher order terms by multiplying the soft

term at the highest known order (N³LO) by $\pm\alpha_s(\nu)$, and include this in the weak-coupling result. On the other hand, one may estimate the influence of unknown higher order terms by varying the soft scale ν in the calculation. It is customary to vary the soft scale by factor two, i.e. between $\nu = 1/(2r)$ and $\nu = 2/r$ for the standard choice of $\nu = 1/r$. Figure 1 shows that the soft scale dependence is non-monotonic and becomes rather large for the variation by a factor of two, if distances larger than $r \gtrsim 0.1$ fm are considered. The perturbative uncertainty due to the soft term is then given by the larger of these two estimates, where the upper error is always found to be determined in terms of the scale variation. Adopting this approach an asymmetric uncertainty due to the soft term could be obtained [78]. Moreover, the uncertainty originating in the ultrasoft contribution could be estimated similarly (by varying the ultrasoft scale). Alternatively, one could vary the resummation scheme for the ultrasoft term to estimate the related uncertainty, i.e. consider the difference between the N³LO result using Eq. (19) or the three-loop result with resummed leading ultrasoft logarithms using Eq. (20). This approach has been adopted to obtain a symmetric uncertainty due to the ultrasoft term [78].

3.1.4. OPE calculation of the renormalon subtracted singlet potential

An alternative procedure to addressing the renormalon of the singlet potential V_s in the weak-coupling approach relies on a very particular version of an operator product expansion (OPE) [79, 80]. For small distances r the exponential e^{iqr} in Eq. (14) can be multipole expanded into real and imaginary terms, and the momentum integral can be evaluated with the lower momentum cutoff $\nu_f \ll \sqrt{q^2}$. Using a deformed contour integration the singlet potential V_s can be separated into a renormalon-free singlet potential $V_s^{\text{RF}}(r)$ and a renormalon contribution $R(r, \nu_f)$ as

$$V_s(r, \nu_f) = V_s^{\text{RF}}(r) + R(r, \nu_f), \quad V_s^{\text{RF}}(r) = V_C(r) + \mathcal{C}_1 r, \quad R(r, \nu_f) = \mathcal{C}_0(\nu_f) + \mathcal{C}_2(\nu_f) r^2 \quad (21)$$

up to higher orders in the multipole expansion. It is not immediately clear, how the coefficients \mathcal{C}_1 or \mathcal{C}_2 , which would represent condensates of mass dimension two or three, respectively, could be related to the usual QCD condensates of at least mass dimension four. Here, the renormalon-free terms are independent of the momentum cutoff, i.e.

$$\mathcal{C}_{-1} = \frac{2C_F}{2\pi i} \int_{C_{\Lambda_{\text{QCD}}}} \frac{dq}{q} \alpha_V(q^2), \quad \mathcal{C}_1 = -\frac{C_F}{2\pi i} \int_{C_{\Lambda_{\text{QCD}}}} \frac{dq}{q} q^2 \alpha_V(q^2), \quad (22)$$

$$V_C(r) = -\frac{1}{r} \left\{ \frac{2C_F}{\pi} \int_0^\infty \frac{dq}{q} e^{-qr} \text{Im } \alpha_V(q^2 + i0) - \mathcal{C}_{-1} \right\}, \quad (23)$$

where $C_{\Lambda_{\text{QCD}}}$ is a closed contour around the singularity of the coupling $\alpha_V(q^2)$. $V_C(r)$ is defined via an integral whose contour has been rotated to the line iq with a real positive q . Explicit dependence on the momentum cutoff ν_f appears only through the imaginary terms in the multipole expansion,

$$\frac{2C_F}{\pi r} \text{Im} \int_{C_{\text{upper}}(\nu_f)} \frac{dq}{q} \left\{ iqr - \frac{i(qr)^3}{3!} \right\} \alpha_V(q^2) = \mathcal{C}_0(\nu_f) + \mathcal{C}_2(\nu_f) r^2, \quad (24)$$

where $C_{\text{upper}}(\nu_f)$ is a contour from 0 to ν_f in the upper half-plane above the singularity of the coupling $\alpha_V(q^2)$. The coefficients $\mathcal{C}_0(\nu_f)$ and $\mathcal{C}_2(\nu_f)$ have to be determined nonperturbatively. The second order renormalon proportional to r^2 can only be resolved at sufficiently large distances.

3.2. Static energy determination on the lattice

The static energy is also amenable to lattice-QCD calculations. For nonperturbative lattice calculations one is forced to use the imaginary-time formalism. After the Wick rotation $t \rightarrow -i\tau$ the static energy can be obtained as

$$aE\left(\frac{r}{a}\right) = \lim_{\tau \rightarrow \infty} -\frac{a}{\tau} \left\langle \ln W\left(\frac{\mathbf{r}}{a}, \frac{\tau}{a}\right) \right\rangle = \lim_{t \rightarrow \infty} -\frac{\partial}{\partial(\tau/a)} \left\langle \ln W\left(\frac{\mathbf{r}}{a}, \frac{\tau}{a}\right) \right\rangle. \quad (25)$$

W can be any lattice correlation function suitable for discretizing the Wilson loop W_S . The correlation function in the lattice approach is constructed as a product of gauge link variables (elementary parallel transporters by a single lattice step). Each of the gauge links has the same self-energy divergence, which is related to the charge renormalization factor, and results in an additive constant contribution to the QCD static energy in the lattice approach that diverges in the continuum limit. Since the lattice has a reduced symmetry in terms of the cubic group W_3 instead of the full rotation symmetry group $O(3)$, there is only a finite set of displacements between the static quark and antiquark that are geometrically equivalent. The static energy is accessible in the lattice approach at distances $r = \sqrt{n_x^2 + n_y^2 + n_z^2}a$, where $n_x, n_y, n_z \in [0, 1, 2, \dots]$. In order to resolve very small distances r , simulations with very fine lattice spacings are required. Moreover, for distances of the order of the lattice spacing, $r \sim a$, lattice calculations are affected by severe discretization artifacts. The origin of these discretization artifacts is apparent from the fact that the paths connecting the static quark and antiquark belong to different representations of the symmetry group. On the other hand, at distances larger than $r/a \sim 5$ the discretization artifacts of the QCD static energy are usually of a similar size as the statistical errors, and thus cannot be resolved clearly.

3.2.1. Interpolating operator dependence

A lattice regularized Wilson loop cannot be realized as a smooth contour, but has to be implemented as a rectangular Wilson loop. This rectangular Wilson loop introduces an additional problem of receiving large contributions from cusp divergences due to its four corners, whose precise cancellation requires very high statistical accuracy. Due to the UV noise associated with the cusp divergences the statistical error of the rectangular Wilson loops tends to be too large for obtaining a useful signal without any smoothing of the links. Typical link smoothing algorithms are the APE smearing [81], the HYP (hypercubic) smearing [82],

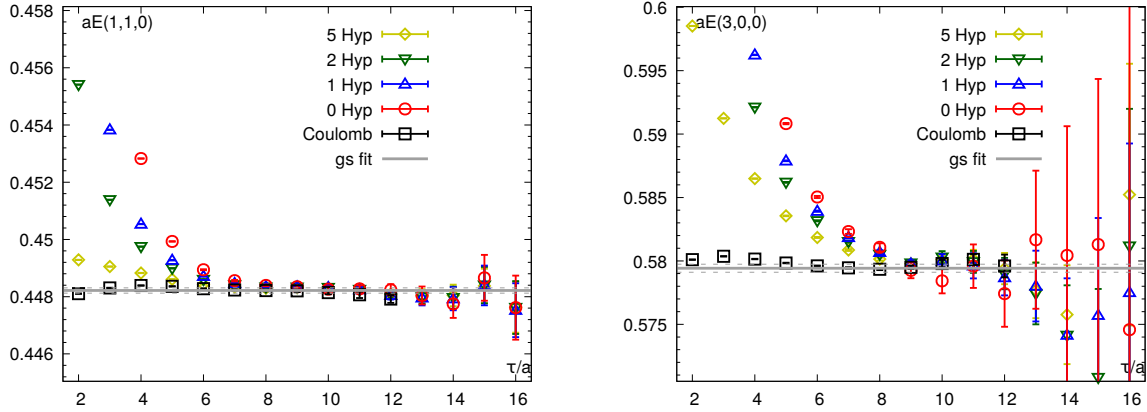


Figure 2: The effective masses $aE(\mathbf{r}) = -\ln(W(\mathbf{r}, \tau)/W(\mathbf{r}, \tau + a))$ of the Wilson line correlator in Coulomb gauge (black) and the Wilson loop with spatially (only cubic HYP) smeared spatial Wilson lines reach the same plateau value at large times. At larger distances larger amounts of smearing are required for the same extent of excited state suppression. The data are obtained in (2+1)-flavor QCD at $\beta = 7.825$ with the HISQ action.

stout smearing [83] or the Wilson flow [51, 84]. The spatial Wilson lines of the rectangular Wilson loop are path dependent, and bring about the linear self-energy divergences, which are suppressed by applying smoothing techniques for the gauge fields along the paths. Moreover, for the rectangular Wilson loops there are different levels of cusp divergences associated with non-straight paths. Nevertheless, as more and more smoothing is applied to the spatial links the signal-to-noise ratio of the Wilson loops steadily improves and the cusp divergences can be suppressed until they become numerically irrelevant. Alternatively, due to the cluster decomposition, the static energy may be defined in a suitably fixed gauge by evaluating Eq. (12), which evades all difficulties associated with the spatial paths. Whereas the two definitions have different levels of excited state contaminations, both correlators yield the same large-time behavior, and become independent of the details of the smearing, i.e. both reach the same ground state, which is the static energy in units of the lattice spacing, aE ; see Fig. 2.

3.2.2. Discretization artifacts at short distances

At very short distances that are most relevant to the comparison of the static energy calculated on a lattice and in the weak-coupling expansion, the static quark-antiquark correlators are beset by severe discretization artifacts. These discretization artifacts can be understood to a large extent in terms of the tree-level calculation,

$$E^{\text{lat, tree}}(\mathbf{r}) = -C_F g^2 \int \frac{d^3 k}{(2\pi)^3} D_{00}(\mathbf{k}, k_0 = 0) e^{i\mathbf{k} \cdot \mathbf{r}}, \quad (26)$$

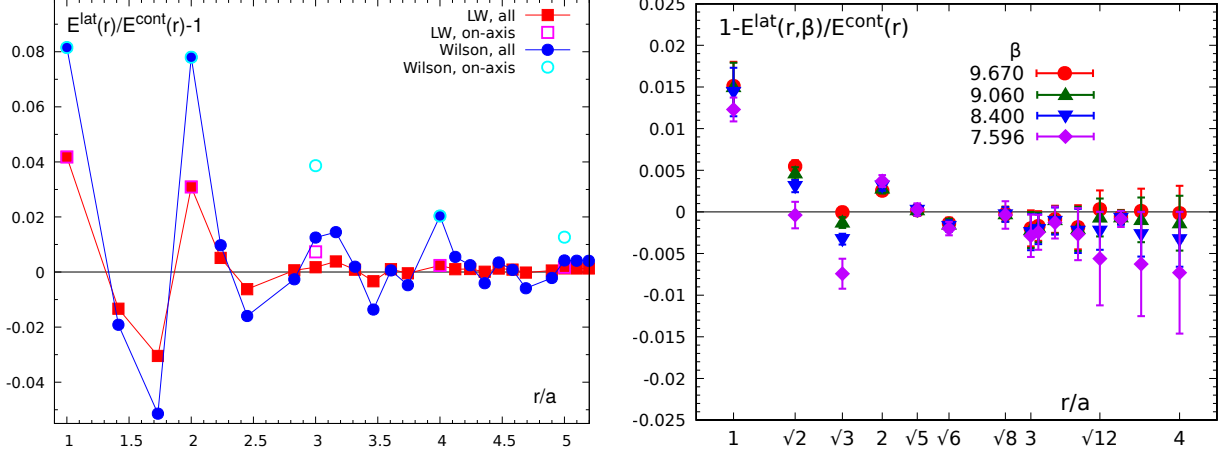


Figure 3: The ratio between the static energy on the lattice and in the continuum, $E^{\text{lat}}/E^{\text{cont}}$, shows a distinctive, non-smooth pattern of r/a -dependent discretization artifacts. (left) The discretization artifacts of the static energy in the lattice approach at the tree-level have a distinct pattern at the percent level as a function of r/a . Use of an improved gauge action reduces these discretization artifacts significantly, such that they become almost negligible (permille level) for $r/a > \sqrt{6}$. (right) The discretization artifacts of the QCD static energy in the lattice approach after the tree-level correction show a similar pattern with a reduced size and opposite sign.

i.e. one-gluon exchange between a static quark-antiquark pair without a running coupling. The discretization artifacts are due the lattice gluon propagator

$$D_{00}(\mathbf{k}, k_0 = 0) = \left(\sum_{j=1}^3 \sin^2 \left(\frac{ak_j}{2} \right) + c_w \sin^4 \left(\frac{ak_j}{2} \right) \right)^{-1}, \quad (27)$$

where $c_w = 0$ for the (unimproved) Wilson gauge action and $c_w = 1/3$ for the (improved) Lüscher-Weisz action [85]. In the continuum this calculation yields $E^{\text{cont,tree}}(r) = V_s^{\text{tree}}(r) = -C_F \alpha_s / r$. A tree-level improved distance r_I is defined by equating

$$E^{\text{lat,tree}}(\mathbf{r}) \equiv -C_F \alpha_s / r_I = E^{\text{cont,tree}}(r_I), \quad (28)$$

where r_I depends on the details of the path geometry, i.e. paths with the same length but geometries that belong to different representations of the cubic group W_3 correspond to different tree-level improved distances r_I . The assignment of the lattice data to the tree-level improved distances is called the tree-level correction. These improved distances r_I differ from the naive (bare) distances by up to 8% for the unimproved gauge action and by up to 4% for the improved gauge action (at $r/a = 1$), see Fig. 3 (left). On the one hand, the tree-level correction reduces the size of the residual discretization artifacts of the QCD static energy $E^{\text{lat}}(\mathbf{r})$ to the level of the typical statistical errors in QCD lattice simulations at distances $r/a \gtrsim 3$. On

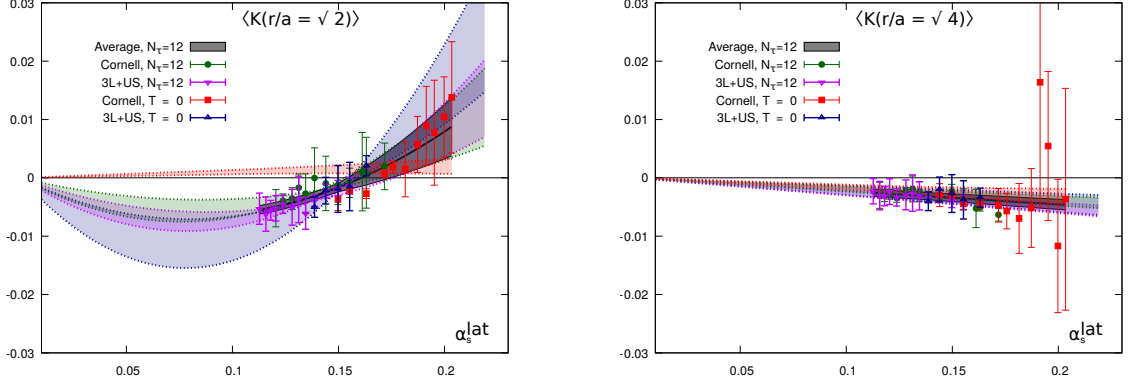


Figure 4: Nonperturbative correction of the tree-level corrected static energy in (2+1)-flavor QCD with improved gauge action and HISQ action. Results obtained using a Cornell Ansatz for interpolating the data on fine lattices, or using the integral of the three-loop force with resummed leading ultrasoft logarithms are numerically consistent. Substituting the QCD static energy (at $T = 0$) by the QCD singlet free energy at $T > 0$, and restricted to short enough distances, a similar result can be obtained at much smaller values of the gauge coupling.

the other hand, the tree-level correction accounts for the largest part of the discretization artifacts of the QCD static energy $E^{\text{lat}}(\mathbf{r})$ even at distances $r/a \lesssim 3$, since the QCD gauge coupling is small at such short distances. Nevertheless, a similar pattern of discretization artifacts remains even after applying the tree-level correction, see Fig. 3 (right). There are two possible approaches to account for these residual discretization artifacts. One may either calculate the corrections order by order in g^2 using the lattice perturbation theory, or one may use a continuum estimate for the QCD static energy, and calculate the necessary nonperturbative correction beyond the tree-level correction. This has been achieved in two schemes that ultimately yield quantitatively consistent answers.

First, the same distance r corresponds to different r/a on fine or coarse lattices. Thus, the static energy result on fine lattices (with the improved gauge action and after the tree-level correction) at distances where the discretization artifacts are statistically irrelevant may serve as a continuum estimate for determining the discretization artifacts in the static energy on coarser lattices. This approach introduces a systematic uncertainty, because this requires interpolating the data on the fine lattices to the distances where data are available on the coarse lattices. The other drawback of this correction scheme is that it does not provide accurate information on the nonperturbative correction for small r/a on fine lattices, which are most important for comparing to the weak-coupling result. Second, one may compare to the weak-coupling calculation directly to estimate the nonperturbative correction. In this scheme there are a few important ingredients. One has to ensure that the weights of the data where corrections are needed are small enough that these do not dominate the weighted residues in the comparison. Moreover, one has to marginalize over the details of

the weak-coupling result used in the comparison in order to not introduce a bias towards a specific value of the QCD Lambda parameter. Lastly, the comparison has to be restricted to the distance range where the weak-coupling result and the lattice data are expected to agree in the continuum limit, i.e. following [73] for $r \lesssim 0.5 r_1$ (or $r \lesssim 0.15$ fm). Due to the $\mathcal{O}(a^2)$ or $\mathcal{O}(\alpha_s a^2, a^4)$ forms of the dominant discretization errors of the Wilson or Lüscher-Weisz actions, the discretization artifacts of the tree-level corrected QCD static energy have to be of the form $\alpha_s^n a^2/r^2$, where $n \geq 1$. Namely, the discretization artifacts for the fixed r/a are polynomials in the bare gauge coupling α_s^{bare} . The nonperturbative corrections from either of these estimates may be extrapolated in the (tadpole-improved⁴) gauge coupling $\alpha_s^{\text{lat}} = \alpha_s^{\text{bare}}/u_0^4$ towards the continuum limit. This extrapolation indicates that corrections of the order $(\alpha_s^{\text{lat}})^2$ are required for $r/a < 2$, while the order α_s^{lat} is sufficient for $2 \leq r/a < \sqrt{8}$ at the present numerical accuracy, see Fig. 4 for two typical cases. After the nonperturbative correction lattice results for the static energy at different lattice spacings are statistically consistent with each other up to the divergent, additive constant.

3.2.3. Sea quark effects in lattice simulations

The nonperturbative lattice calculation of the static energy has a mild dependence on the sea quark masses or on the sea quark discretization. The former may be visualized most clearly in terms of a ratio of the static energy calculated with different sea quark masses and the same bare gauge coupling [40, 87], see Fig. 5 (left). Such a direct comparison shows that the sea quark mass dependence is not unambiguously resolved for $r \lesssim 0.55 r_1$ (or $r \lesssim 0.17$ fm). The latter may be observed at larger distances even by direct comparison of such results in the continuum limit or with sufficiently small lattice spacing, see Fig. 5 (right). The QCD static energy with the HISQ action or the DWF action and a similar pion mass are consistent at distances $r \gtrsim 0.4 r_1$ (or $r \gtrsim 0.13$ fm).

3.3. α_s from the static energy

The calculation of α_s from the QCD static energy is straightforward. The QCD static energy in any two regularizations differs by an additive constant, in which the zeroth order renormalon may be absorbed if necessary. In particular, this constant is different for each lattice spacing and has to be determined through a fit. First, one has to ensure that the lattice data of the QCD static energy are at sufficiently small distances that the perturbative expansion shows apparent convergence, i.e. that the residues per degree of freedom in a fit of the lattice data with the weak-coupling result (and with the necessary additive constants) become smaller as the perturbative order is increased. It has been demonstrated that this condition is satisfied for $r \lesssim 0.5 r_1$ [73]. Restriction to such distances automatically implies that the sea quark mass

⁴Here, the “average” link variable u_0 in the tadpole improvement is defined using the expectation value of the plaquette. An alternative approach would be to directly measure it in a smooth gaugelike Landau gauge. The tadpole improvement is used to enhance the convergent of the perturbative expansion of the discretized theory. See Ref. [86] for details.

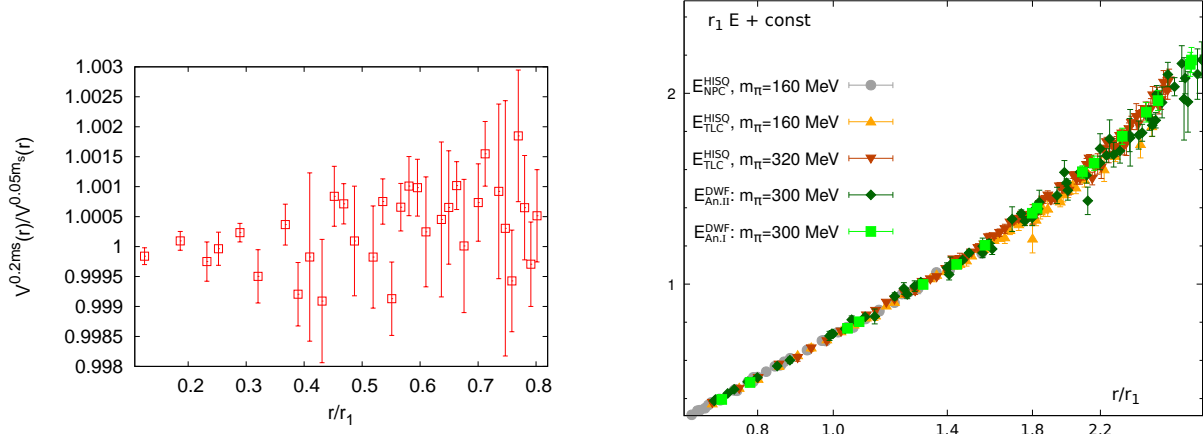


Figure 5: The sea quark mass dependence of the QCD static energy is negligible at short distances, $r \ll r_1$, but becomes numerically significant at larger distances. (left) The ratio of the QCD static energy for different sea quark masses corresponding to a pion mass of 160 MeV or 320 MeV in the continuum limit. The data are obtained in (2+1)-flavor QCD at $\beta = 7.825$ with the HISQ action [40, 87]. (right) The QCD static energy shows the clearly visible sea quark mass dependence at larger distances $r \gtrsim r_1$, which is quite independent of the discretization used for the sea quarks. The DWF data, which were obtained using spatially smeared Wilson loops in (2+1)-flavor QCD with a pion mass of 300 MeV were extrapolated to the continuum limit with two different analyses, i.e. in a two-step analysis I or in a one-step analysis II [74, 75], but are within errors consistent with the HISQ data at $\beta = 7.825$ at the similar pion mass at these rather large distances.

effects can be neglected. Second, one has to ensure that the lattice data are on sufficiently fine lattices that the discretization artifacts can be neglected (i.e. after the tree-level correction or after the nonperturbative correction). After meeting these two conditions, one may simply compare the lattice data with N_f sea quark flavors to the weak-coupling results with N_f massless quark flavors with a fit of $1 + N_{\text{lat}}$ parameters, where N_{lat} is the number of lattice spacings used as the data set in the fit. The result of this comparison does not show a strong dependence on the distance window used in the fit while $r \lesssim 0.45 r_1$ (or $r \lesssim 0.13$ fm). The analysis of the static energy in the (2+1)-flavor QCD lattice simulations with the HISQ action and up to six lattice spacings $0.08 r_1 \leq a \leq 0.20 r_1$ (or $0.025 \text{ fm} \leq a \leq 0.06 \text{ fm}$) [78] yields for $0.076 r_1 \leq r \leq 0.24 r_1$ (or $0.0237 \text{ fm} \leq r \leq 0.0734 \text{ fm}$)

$$\alpha_s(M_Z) = 0.11660^{+0.00110}_{-0.00056}, \quad \delta\alpha_s(M_Z) = (41)^{\text{stat}}(21)^{\text{lat}}(10)_{r_1}({}_{-13}^{+95})^{\text{soft}}(28)^{\text{us}}. \quad (29)$$

The uncertainty due to the residual lattice spacing dependence has been estimated from two analyses using the tree-level corrected or the nonperturbatively corrected lattice data with the HISQ action and a fit range delimited at small distances by $r/a \geq \sqrt{8}$. The uncertainty due to the lattice scale dependence has been included at the end, as it is largely independent of the lattice spacing. The scale uncertainty includes the uncertainty of the experimental input, f_π , which contributes to the uncertainty of the lattice

scale r_1 . Lastly, the perturbative uncertainty has been determined as described in Sec. 3.1.3. Soft scale variation by the factor 2 requires a stronger restriction than the apparent convergence of the perturbative expansion, namely, $r \lesssim (1/3)r_1$ (or $r \lesssim 0.1$ fm). The uncertainty estimate due to the soft scale variation is highly asymmetric due to the significant variation of the QCD coupling at such low-energy scales, and is the dominant uncertainty in the calculation. In order to estimate the influence of the ultrasoft term the difference between the results obtained via Eqs. (19) or (20) has been considered as a symmetric error. In fact all of the individual estimates of the perturbative uncertainty are substantially reduced when the comparison is restricted to a smaller maximal distance r as naively expected.

Two different analyses of the static energy in the (2+1)-flavor QCD lattice simulations with the DWF action and the three lattice spacings $0.14 r_1 \leq a \leq 0.26$ fm (or 0.044 fm $\leq a \leq 0.080$ fm) have been performed [74, 75]. In the two-step analysis I, the continuum limit is obtained by first interpolating the data on the two finer lattices to the distances, where the data on the coarsest lattice are available. Second, the (mock) data are extrapolated to the continuum limit at each distance r/a on the coarse lattice separately. Finally, this continuum limit is compared to the continuum OPE in the distance window $0.8 r_1 \leq r \leq 1.9 r_1$ (or 0.24 fm $\leq r \leq 0.6$ fm), which yields

$$\alpha_s(M_Z) = 0.1166^{+0.0021}_{-0.0020}, \quad \delta\alpha_s(M_Z) = (+0.0010)^{\text{stat}}(-0.0011)^{\text{syst}}. \quad (30)$$

In the one-step analysis II, the continuum limit is obtained by simultaneously fitting the data on all three lattices with the continuum OPE result and a parametrization of the discretization artifacts. This analysis is performed in the distance window $0.14 r_1 \leq r \leq 1.15 r_1$ (or 0.044 fm $\leq r \leq 0.36$ fm), which yields

$$\alpha_s(M_Z) = 0.1179^{+0.0015}_{-0.0014}, \quad \delta\alpha_s(M_Z) = (0.0007)^{\text{stat}}(+0.0014)^{\text{syst}}. \quad (31)$$

For further details of these systematic error budgets in both analyses see [74, 75]. The estimate of the contribution from the scale uncertainty, and hence from the experimental input, f_π , is the same as for the HISQ calculation. Note that the authors consider the one-step analysis II as superior to the two-step analysis I due to the smaller uncertainties and quote Eq. (31) as their final result [74, 75].

We show the comparison between the lattice and weak-coupling results in Fig. 6. At small distances the continuum results obtained in the one-step analysis II of the spatially smeared Wilson loops with the DWF action are systematically below the data from the Wilson line correlation function in Coulomb gauge with the HISQ action (nonperturbatively corrected at very small distances $r/a < \sqrt{8}$ or only tree-level corrected at larger distances $r/a \geq \sqrt{8}$).

3.4. α_s from the singlet free energy

The QCD singlet free energy is a thermal observable with many properties similar to those of the QCD static energy at zero temperature. It is defined in terms of the thermal expectation value of the Wilson line

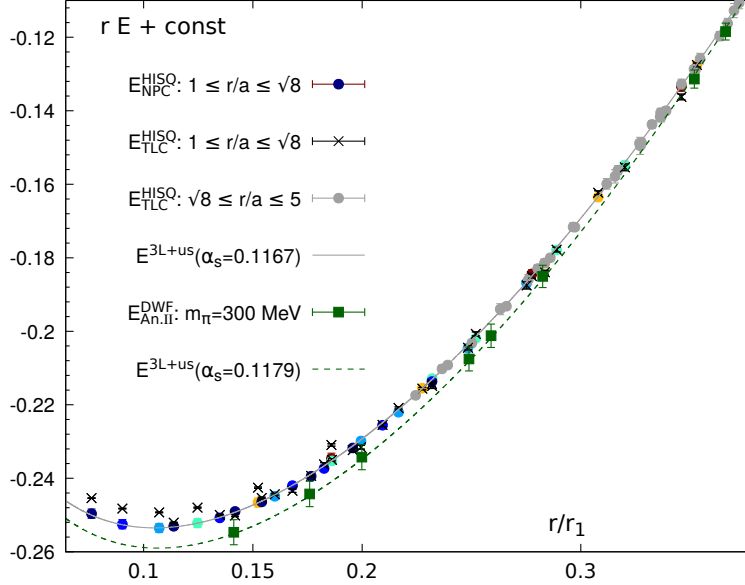


Figure 6: The nonperturbative lattice and the perturbative continuum results for the static energy multiplied by the distance, $rE(r)$. The HISQ data [78] are nonperturbatively corrected (NPC, colored bullets) or tree-level corrected (TLC, black crosses and gray bullets). The color indicates the lattice spacing in units of the r_1 scale, a/r_1 . The DWF data [74, 75] are from a one-step analysis II that mixes the continuum extrapolation with the fit to the OPE result at N³LO, Eq. (21), using a parametrization of discretization artifacts (green squares). The lines represent the three-loop result with resummed leading ultrasoft logarithms, Eq. (20), corresponding to $\alpha_s(M_Z, N_f = 5) = 0.1167$ (gray, solid) or $\alpha_s(M_Z, N_f = 5) = 0.1179$ (green, dashed). The former uses the central value $\alpha_s(M_Z, N_f = 5) = 0.1167$ of the analysis of the (TLC or NPC) HISQ data with $r/a \geq \sqrt{8}$ (gray bullets), the latter uses the central value $\alpha_s(M_Z, N_f = 5) = 0.1179$ of the OPE-based one-step analysis II of the DWF data [74, 75]. The NPC HISQ data with $r/a < \sqrt{8}$ are well-aligned with the fit excluding these data, while the TLC HISQ data with $r/a < \sqrt{8}$ cannot be consistently described by a continuum result for any value of $\alpha_s(M_Z, N_f = 5)$.

correlation function at $\tau = 1/T$ in a suitable gauge, i.e. in the Coulomb gauge, or in terms of the thermal expectation value of the cyclic Wilson loop with spatially smeared spatial Wilson lines,

$$F_S(r, T) = -T \left\langle \ln e^{ig \int_0^{1/T} d\tau A_0(\mathbf{0}, \tau)} e^{-ig \int_0^{1/T} d\tau A_0(\mathbf{r}, \tau)} \right\rangle_T, \quad (32)$$

$$F_W(r, T) = -T \ln \left\langle e^{ig \oint_{\mathbf{r}, 1/T} dz^\mu A_\mu} \right\rangle_T. \quad (33)$$

However, in contrast to the case of the QCD static energy at zero temperature these two quantities F_S and F_W are distinguished by their distinct and temperature-dependent UV structures. A particular advantage of the QCD lattice calculation at finite temperature is that it resolves the IR problem of QCD at zero temperature in an elegant way. Namely, at high temperatures $T \gtrsim T_c$ the chiral symmetry is not spontaneously broken, and there are no associated pseudo-Goldstone bosons at the pion scale. Those would cause severe finite volume effects in zero temperature lattice simulations by propagating across the periodic lattice

boundaries. At finite temperature, however, the smallest scale is the screening mass in the scalar channel, which scales as the temperature times the gauge coupling. Thus, a volume that is constant in units of the temperature as $TV^{1/3} \gtrsim 4$ is generally sufficient for avoiding the large finite volume effects.

In particular, $F_S(r, T)$ coincides up to the corrections at the order g^4 with the zero temperature singlet potential $V_s(r, \mu_{us})$,

$$F_S(r, T) = V_s(r, \mu_{us}) + \delta F_S(r, T, \mu_{us}), \quad (34)$$

and has the same constant renormalon contribution. Moreover, $F_S(r, T)$ and $E(r)$ share the same discretization artifacts at the tree-level. Hence, the renormalon-free difference $E(r) - F_S(r, T)$ is particularly convenient for comparing the weak-coupling result and the nonperturbative lattice calculation. The details of the finite temperature effects $\delta F_S(r, T, \mu_{us})$, however, depend on the hierarchy between the zero temperature and thermal scales. One might consider the cases $1/r \gg \alpha_s/r \gg T \gg m_D \sim gT$ or $1/r \gg T \gg m_D \sim gT \gg \alpha_s/r$. In the former hierarchy, which applies to small distances, the ultrasoft scale is the same as in the vacuum $\mu_{us} = (N_c \alpha_s (1/r))/(2r)$, and

$$\delta F_S(r, T, \mu_{us}) = \delta E_{us}(r, \mu_{us}) + \Delta F_S(r, T). \quad (35)$$

Thus, the thermal effects are expected to be suppressed since $T \ll \mu_{us}$. In the latter hierarchy, which applies to somewhat larger distances, F_S has been calculated up to the order $g^5(T)$ in the multipole expansion [88]. In this hierarchy $\delta F_S(r, T, \mu_{us})/T$ is a dimensionless polynomial in rT that receives the contributions at order $g^4(T)$ from the nonstatic Matsubara modes of the gluons and from the quarks, and at order $g^5(T)$ from the static Matsubara modes of the gluons. In particular, these contributions to $\delta F_S(r, T, \mu_{us})$ become smaller for smaller distances at both orders $g^4(T)$ or $g^5(T)$. However, the order g^6 contribution to $\delta F_S(r, T, \mu_{us})$ is not known for this hierarchy. For this reason one cannot be certain that the cancellation of the ultrasoft scale between $\delta F_S(r, T, \mu_{us})$ and $V_s(r, \mu_{us})$ takes place as in the zero temperature case. In particular, one has to expect that there is a temperature-dependent contribution $E(r) - F_S(r, T) \sim \alpha_s^3(T) \ln(rT)/r$. Moreover, there is an r -independent contribution at the order g^6 that can be understood as the matching coefficient between the NRQCD and the pNRQCD [88].

In the second hierarchy $1/r \gg T \gg m_D \sim gT \gg \alpha_s/r$ the two known contributions at the different orders $g^4(T)$ and $g^5(T)$ have opposite signs and – in the case of the phenomenologically interesting temperatures $300 \text{ MeV} \lesssim T \lesssim 10 \text{ GeV}$ that are accessible in the state of the art (2+1)-flavor QCD lattice simulations [39] – a similar magnitude and a similar r dependence. As a consequence, the absolute size of $\delta F_S(r, T, \mu_{us})$ is very small due to this approximate cancellation. Whereas the QCD lattice simulations do not exhibit a temperature dependence that is quite consistent⁵ with this expression at any fixed lattice scale, the

⁵ This may be caused by the strong discretization effects in this difference that become visible only after the dominant

general features are quite similar for distances up to $r \lesssim 0.3/T$. In particular, the approximate cancellation between the contributions from the nonstatic and from the static Matsubara modes appears to be realized nonperturbatively. At even shorter distances $r/a \lesssim \sqrt{6}$ the finite temperature effects are not even resolved at the level of the statistical errors. Hence, after restriction to such small distances a direct comparison to the zero temperature result for the static energy is feasible and appropriate.

After meeting the same two conditions as at zero temperature, and restricting to small $r \ll 0.3/T$, one may simply compare the finite temperature lattice data with N_f sea quark flavors to the weak-coupling results at zero temperature with N_f massless quark flavors in a fit of $1 + N_{\text{lat}}$ parameters, where N_{lat} is the number of lattice spacings used as the data set in the fit. The result of this comparison does not show a strong dependence on the distance window used in the fit while $r \lesssim 0.45 r_1$ (or $r \lesssim 0.13 \text{ fm}$), and is always perfectly consistent with the zero temperature calculation. The analysis of the singlet free energy in the (2+1)-flavor QCD lattice simulations with the HISQ action and up to fifteen lattice spacings $0.027 r_1 \leq a \leq 0.20 r_1$ (or $0.0085 \text{ fm} \leq a \leq 0.06 \text{ fm}$) [78] yields for $0.026 r_1 \leq r \leq 0.1 r_1$ (or $0.0081 \text{ fm} \leq r \leq 0.030 \text{ fm}$)

$$\alpha_s(M_Z) = 0.11638^{+0.00095}_{-0.00087}, \quad \delta\alpha_s(M_Z) = (80)^{\text{stat}}(21)^{\text{lat}}(17)^{T>0}(10)^{r_1}(+40)^{\text{soft}}_{-06}(15)^{\text{us}}. \quad (36)$$

In order to escape a possible contamination by finite temperature effects the analysis has been performed with $r/a \leq 2$.⁶ The uncertainty due to the finite temperature calculation has been estimated by comparing the results obtained with $N_\tau = 12$, or $N_\tau = 16$ with each other, or with the zero temperature calculation for the same upper limit of the distance window both in terms of r/a and r/r_1 . The scale uncertainty includes the uncertainty of the experimental input, f_π , which contributes to the uncertainty of the lattice scale r_1 . All of the individual estimates of the perturbative uncertainty are dramatically reduced when the comparison is restricted to the smallest maximal distance r , cf. Eq. (29).

3.5. Summary and pre-averaging

At this point we proceed to the summary and pre-averaging the present status of the determination of the strong coupling constant obtained from the QCD static energy in (2+1)-flavor QCD lattice simulations. The older calculations [72, 73] with the HISQ action have been superseded by the most recent calculation [78] that is reproduced in Eq. (29). The comparison with the QCD singlet free energy [78] is a statistically and systematically independent result that is reproduced in Eq. (36). Finally, the calculations [74, 75] with the DWF action are not independent. Hence, we calculate the averages for $\Lambda_{\overline{\text{MS}}}^{N_f=3}$ and $\alpha_s(M_Z, N_f = 5)$ using either the DWF result from the one-step analysis II, Eq. (31), or from the two-step analysis I, Eq. (30).

contributions have canceled between $E(r)$ and $F_S(r, T)$, see [39] for a detailed discussion of the discretization effects.

⁶A similar analysis with $r/a \leq 3$ or $r/a \leq \sqrt{12}$ produces a consistent result with smaller statistical uncertainties.

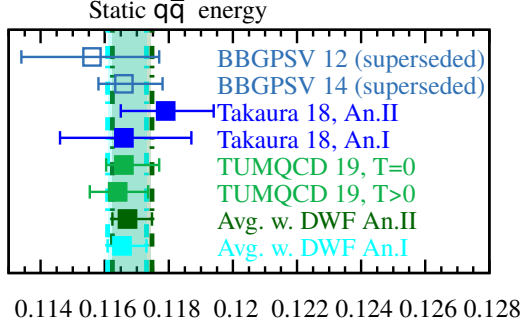


Figure 7: The results for $\alpha_s(M_Z, N_f = 5)$ obtained from the static $q\bar{q}$ energy in (2+1)-flavor QCD, i.e. the DWF result with a two-step analysis I and a one-step analysis II, Takaura 18 [74, 75], and the HISQ result using $T = 0$ and $T > 0$ ensembles, TUMQCD 19 [78]. The superseded results BBGPSV 12 [72] and BBGPSV 14 [73] (both are superseded by TUMQCD 19 [78]) are shown, too.

The lattice averages are obtained by propagating the asymmetric errors of the individual results with the bootstrap method, and then calculating the central values and the asymmetric errors from the cumulative distribution function. The average of the strong coupling constant at the Z pole reads

$$\alpha_s^{\text{stat}}(M_Z) = 0.11671^{+0.00076}_{-0.00047}, \quad \chi^2/\text{d.o.f.} = 0.914/2, \quad \text{with DWF An. II, Eq. (31),} \quad (37)$$

$$\alpha_s^{\text{stat}}(M_Z) = 0.11654^{+0.00076}_{-0.00045}, \quad \chi^2/\text{d.o.f.} = 0.040/2, \quad \text{with DWF An. I, Eq. (30).} \quad (38)$$

Treating the uncertainties instead as symmetric (the average of the upper or lower error) one would obtain $\alpha_s(M_Z, N_f = 5) = 0.11696(75)$ at $\chi^2/\text{d.o.f.} = 0.580/2$, or $\alpha_s(M_Z, N_f = 5) = 0.11653(78)$ at $\chi^2/\text{d.o.f.} = 0.016/2$ for the two averages, respectively. The variation between the different possible averages and individual results is covered in all cases by the uncertainties. However, the central value of the DWF result from the one-step analysis II [74, 75] is not fully covered by the propagated uncertainty in either way of taking the average, see Fig. 7.

4. Moments of quarkonium correlators

Quarkonium correlation functions or the corresponding quarkonium spectral functions are observables that are amenable to direct experimental studies or to calculation in QCD with perturbative or nonperturbative methods. On the one hand, the vector channel is the most favorable for the experimental study, since it is known to the best accuracy from the R -ratio $R = \frac{\sigma^{(0)}[e^+e^- \rightarrow \text{hadrons}]}{\sigma^{(0)}[e^+e^- \rightarrow \mu^+\mu^-]}$. On the other hand, the pseudoscalar channel is the most favorable for a lattice study, since it offers the best signal-to-noise ratio among the lattice observables, and has the least contamination by the discretization artifacts. In the following we focus exclusively on the pseudoscalar channel.

4.1. General definitions and properties

The renormalization group invariant quarkonium correlation function in the pseudoscalar channel is defined using the lattice discretization as

$$G(t, a, V, m_h) = \frac{a^3}{V} \sum_{\mathbf{n} \in \frac{V}{a^3}} (am_{h0})^2 \langle j_5(\mathbf{n}, t) j_5(\mathbf{0}, 0) \rangle, \quad j_5(\mathbf{n}, t) = \bar{\psi}(\mathbf{n}, t) \gamma_5 \psi(\mathbf{n}, t). \quad (39)$$

Here, $t = \tau/a$ is the Euclidean time in lattice units, m_h is the mass of the heavy quark, and am_{h0} is its bare mass in lattice units. Then the n th time moment of this quarkonium correlation function is defined for the infinite time direction as

$$G_n(a, V, m_h) = \sum_{t=0}^{\infty} t^n G(t, a, V, m_h). \quad (40)$$

Due to the periodic boundary condition in the time direction that is used in most QCD lattice calculations, which implies a backward propagating contribution, this time moment has to be generalized in the lattice approach as

$$G_n(a, V, m_h) = \sum_{t=0}^{N_\tau/2} t^n \{G(t, a, V, m_h) + G(N_\tau - t, a, V, m_h)\}. \quad (41)$$

Due to the symmetry of the correlation function, odd moments vanish exactly. The time moments $G_n(a, V, m_h)$ are finite for $n \geq 4$, since the correlation function defined in Eq. (39) diverges at small t only as t^{-4} . Obviously the larger values of the heavy quark mass m_h result in larger discretization artifacts $(am_h)^n$ for the time moments $G_n(a, V, m_h)$ with the same lattice spacing. Moreover, it is clear from Eq. (41) that, on the one hand, the lower time moments have a stronger sensitivity to the discretization artifacts caused by the larger influence of the lattice correlation function at small times $\tau \sim a$, whereas, on the other hand, the higher time moments have a stronger sensitivity to the finite time direction (as the missing contribution with $t > N_\tau/2$ would be given a larger weight).

The time moments of the quarkonium correlation function can be calculated in the weak-coupling approach using the $\overline{\text{MS}}$ scheme,

$$G_n(a, V, m_h)|_{\nu, \nu_m} = \frac{g_n \left[a, V; \alpha_s(\nu), \frac{\nu}{m_h(\nu_m)} \right]}{[am_h(\nu_m)]^{n-4}}, \quad (42)$$

where $m_h(\nu_m)$ is the $\overline{\text{MS}}$ heavy quark mass at the scale ν_m , and $\alpha_s(\nu)$ is the $\overline{\text{MS}}$ strong coupling constant at the scale ν . In principle the renormalization scale ν of the strong coupling constant could differ [32] from the renormalization scale ν_m of the heavy quark mass, although most studies assume $\nu = \nu_m$. The coefficients $g_n \left[a, V; \alpha_s(\nu), \frac{\nu}{m_h(\nu_m)} \right]$ are known for the continuous space-time $a \rightarrow 0$ and in the infinite volume limit $V \rightarrow \infty$ at the four-loop order, i.e. to the order α_s^3 [89–91].

It has been pointed out [92] that it is favorable to consider the reduced moments R_n for the calculation in the lattice approach. The reduced moments R_n are ratios of the moments in QCD and in the free field theory,

$$R_n(a, V, m_h) = \begin{cases} \left(\frac{G_4^{\text{QCD}}(a, V, m_h)}{G_4^{(0)}(a, V, m_h)} \right) & (n = 4) \\ \left(\frac{G_n^{\text{QCD}}(a, V, m_h)}{G_n^{(0)}(a, V, m_h)} \right)^{\frac{1}{n-4}} & (n > 4) \end{cases}. \quad (43)$$

There are various cancellations between the systematic effects in these ratios of the lattice moments. These cancellations are particularly relevant with regard to the effects of the finite lattice spacing a , of the heavy quark mass m_h , and of the periodic time direction, aN_τ , and to some extent, with regard to the finite volume V , too. In particular, the tree-level contribution to the discretization artifacts, $\alpha_s^0 a^n$, cancels exactly in the reduced moments to all orders n . Moreover, the uncertainties of the lattice time moments in QCD and in the free field theory due to the error of the numerical tuning of the heavy quark mass are subject to a strong compensation in the reduced moments R_n .

Furthermore, the contribution for $t > N_\tau/2$ is missing both in the numerator and in the denominator. It is possible to account for this systematic effect in the moments by replacing the correlator for t by $\cosh[am_0(t - N_\tau/2)]$ with m_0 being the ground state quarkonium mass. Then one can consider large enough N_τ such that the systematic effects are negligibly small. In the free theory calculations it is easy to do calculations at large enough N_τ , where the effects of finite temporal extent can be neglected.

Finally, the finite volume effects may also be subject to a partial compensation. However, this last effect is expected to be less pronounced than any of the other compensations. A general parametrization of the finite volume error is

$$\frac{R_n(a, \infty, m_h) - R_n(a, V, m_h)}{R_n(a, V, m_h)} = \left[\left(\frac{\delta_V G_n^{\text{QCD}}(a, V, m_h)}{G_n^{\text{QCD}}(a, V, m_h)} \right) - \left(\frac{\delta_V G_n^{(0)}(a, V, m_h)}{G_n^{(0)}(a, V, m_h)} \right) \right] \times \begin{cases} 1 & (n = 4) \\ \frac{1}{n-4} & (n > 4) \end{cases}, \quad (44)$$

but simplifies considerably under the reasonable assumption that the free field theory result is much more sensitive to the finite volume effects, i.e. that the first term in square brackets can be neglected. This assumption can be justified from the fact that, on the one hand, the QCD result is dominated by the rather volume insensitive bound state contributions below the open heavy flavor threshold. On the other hand, the free field theory result is dominated by the volume sensitive scattering states of a pair of fictitious heavy fermions in a finite box. With a free field theory calculation using multiple sizes of the box it is straightforward to estimate $\delta_V G_4^{(0)}(a, V, m_h)$.

In the weak-coupling approach, the reduced moments in the continuum at infinite volume are given as

Table 1: The constant coefficients r_{nj} of the perturbative expansion of the reduced moments R_n for the continuous space-time and in the infinite volume limit with the scales $\nu = \nu_m = m_h$.

n	r_{n1}	r_{n2}	r_{n3}
4	2.3333	-0.5690	1.8325
6	1.9352	4.7048	-1.6350
8	0.9940	3.4012	1.9655
10	0.5847	2.6607	3.8387

$$R_n(0, \infty, m_h)|_{\nu, \nu_m} \equiv r_n \left[\frac{\nu}{m_h(\nu_m)}, \alpha_s(\nu) \right] \left\{ \begin{array}{ll} 1 & (n=4) \\ \left(\frac{m_{h0}}{m_h(\nu_m)} \right) & (n>4) \end{array} \right. + \text{nonperturbative}, \quad (45)$$

$$r_n \left[\frac{\nu}{m_h(\nu_m)}, \alpha_s(\nu) \right] = 1 + \sum_{j=1}^3 r_{nj} \left(\frac{\nu}{m_h(\nu_m)} \right) \left(\frac{\alpha_s(\nu)}{\pi} \right)^j. \quad (46)$$

For the choice of scales $\nu = \nu_m = m_h$ the coefficients $r_{nj} \left(\frac{\nu}{m_h(\nu_m)} \right)$ simplify to the mass-independent constants r_{nj} that are reproduced in Tab. 1. These constants are of order one without any evident pattern. The quarkonium correlation functions also receive nonperturbative contributions through the coupling between the scalar density and the QCD condensates. The leading contribution among these is due to the gluon condensate [93], namely, and the reduced moments can be written as

$$R_n(0, \infty, m_h)|_{\nu, \nu_m} = \left(1 + \sum_{j=1}^3 r_{nj} \left(\frac{\nu}{m_h(\nu_m)} \right) \left(\frac{\alpha_s(\nu)}{\pi} \right)^j + \frac{1}{m_h^4(\nu_m)} \frac{11}{4} \left\langle \frac{\alpha_s}{\pi} G^2 \right\rangle \right) \times \left\{ \begin{array}{ll} 1 & (n=4) \\ \left(\frac{m_{h0}}{m_h(\nu_m)} \right) & (n>4) \end{array} \right., \quad (47)$$

where the value of the gluon condensate is known from the τ decays [94],

$$\left\langle \frac{\alpha_s}{\pi} G^2 \right\rangle = -0.006(12) \text{ GeV}^4. \quad (48)$$

Lastly, from the perspective of the use of data from the lattice calculation or from the experimental observation, it is particularly attractive to consider the ratios of the reduced moments,

$$R_{m,n}(a, V, m_h) = \frac{R_m(a, V, m_h)}{R_n(a, V, m_h)} \quad \text{and} \quad r_{m,n} \left[\frac{\nu}{m_h(\nu_m)}, \alpha_s(\nu) \right] = \frac{r_m \left[\frac{\nu}{m_h(\nu_m)}, \alpha_s(\nu) \right]}{r_n \left[\frac{\nu}{m_h(\nu_m)}, \alpha_s(\nu) \right]}, \quad (49)$$

where the nonperturbative contributions have been omitted. The obvious reason is that the fluctuations of the gauge ensembles that estimate the QCD path integral modify the underlying quarkonium correlation

function, and thus also the moments. In the ratio of two (reduced) moments of one and the same correlation function, the cancellation of some of the statistical fluctuations is natural. Moreover, one also expects a partial cancellation of the uncertainties of the reduced lattice moments due to the error of the numerical tuning of the heavy quark mass in these ratios. Lastly, the similar compensation may happen as well for the discretization artifacts, for the effects of the periodic time direction, and for the finite volume effects, although these compensations can be effective only to a lesser extent. In the weak-coupling calculation one might consider expanding the numerator and the denominator separately in powers of the strong coupling constant $\alpha_s(\nu)$, or expanding the full ratio of the reduced moments as a total. For a fit the difference between both approaches is numerically irrelevant in practice.

4.2. Lattice setup and continuum limit

The time moments of the heavy quarkonium correlation functions in Eq. (41) have been calculated using the lattice approach in the (2+1)-flavor QCD with the HISQ action [35] for the valence quarks by the HPQCD collaboration, HPQCD 08 [92], or HPQCD 10 [95], in a partially quenched setting on the MILC gauge ensembles [38, 48] with the asqtad action [34]. The time moments have also been calculated on a much wider range of gauge ensembles generated for the calculation of the (2+1)-flavor QCD equation of state [40, 96] with the HISQ action, in particular, using unprecedentedly fine lattice spacings, Maezawa and Petreczky (MP 16) [55], or Petreczky and Weber (PW 19) [97]. Moreover, the time moments have also been calculated by the JLQCD collaboration, JLQCD 16 [98], in the (2+1)-flavor QCD with the domain-wall fermion (DWF) action [37] for the valence quarks on DWF gauge ensembles with three steps of stout smearing [83]. Lastly, the time moments have also been calculated in the (2+1+1)-flavor QCD by the HPQCD collaboration, HPQCD 14 [99], using the HISQ action for the valence quarks on the MILC gauge ensembles [100] with the HISQ action, but no continuum extrapolated results have been given in terms of the moments.

In the following we focus on the most recent calculation in the (2+1)-flavor QCD lattice simulations with the HISQ action. Since the underlying gauge ensembles have been generated for the study of the (2+1)-flavor QCD equation of state [40, 96], they suffer from the rather small spatial volumes and rather short Euclidean time directions. These two restrictions are partly responsible for the fact that the finite size effects tend to be the dominant systematic uncertainties for the finer lattices, whereas the mis-tuning of the valence heavy quark masses tends to be the dominant systematic uncertainty for the coarser lattices. The experimental errors of the pseudoscalar or spin-averaged meson masses are statistically insignificant in this calculation. Moreover, since the bulk properties in the QCD thermodynamics have only a relatively mild dependence on the sea quark masses, the light sea quark masses are not fixed at the physical point, but at $m_l = m_s/20$ or $m_l = m_s/5$. The strange-quark mass has been tuned using the fictitious $\eta_{s\bar{s}}$ meson. These choices of the parameters (m_l/m_s) correspond to a pion mass of 160 MeV or 320 MeV in the continuum limit, respectively.

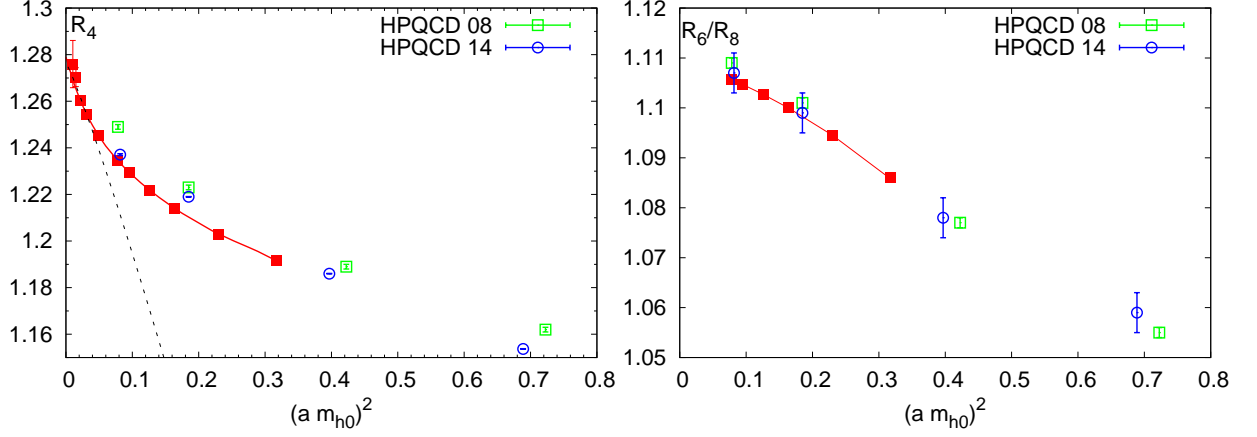


Figure 8: The lattice spacing dependence of the reduced moment R_4 , or of the ratio $R_{6,8}$ with the HISQ action at the valence charm quark mass. The red filled squares correspond to the most recent valence HISQ result on the (2+1)-flavor HISQ ensembles, PW19 [97], and clearly resolve the logarithmic lattice spacing dependence. The green open squares correspond to the first valence HISQ result on the (2+1)-flavor asqtad ensembles, HPQCD08 [92], while the blue open circles correspond to the most recent valence HISQ result on the (2+1+1)-flavor HISQ ensembles, HPQCD14 [99]. The most simple fit of R_4 using only $\alpha_s^{\text{lat}} (am_h)^2$ (black dashed line) is only feasible upon restricting the coarsest lattice spacing to $a \lesssim 0.04$ fm.

The kaon mass of the former corresponds to 504 MeV in the continuum. The valence heavy quark masses were tuned with the spin-average of the pseudoscalar and vector channels for the $m_l = m_s/20$ ensembles, and with just the pseudoscalar mass for the very fine $m_l = m_s/5$ ensembles. In the HISQ calculations with the exception of [55] the random color wall sources have been utilized, i.e. gaussian $Z(2)$ noise distributed over an entire time slice. The expectation values from the random color wall sources reproduce the expectation values from the more simple point sources, but achieve a reduction of the statistical errors by more than one order of magnitude. The quarkonium correlation functions have been calculated on ensembles with multiple light sea quark masses and/or multiple strange sea quark masses. Effects due to the different sea quark masses are generally at the same level as the statistical or systematic errors (due to finite volume or mis-tuning of the valence quark mass), i.e. they do not cause a statistically significant trend, and thus can be neglected.

In all of these calculations, the tree-level or the one-loop improved Symanzik gauge action has been used. Improved lattice fermions (asqtad, HISQ, or DWF) guarantee that there are no odd powers of the lattice spacing a permitted for the discretization artifacts. Moreover, with the exception of the contributions from the condensates, which are from the scale Λ_{QCD} , or from the even lower and less important scales of the sea quark masses, the relevant scale in the problem is given by the (bare) heavy valence quark mass m_{h0} . As the contribution from the condensates has 200% uncertainty in the continuum limit, cf. Eq. (48), and is

suppressed by four powers of the heavy valence quark mass, $1/m_h^4$, cf. Eq. (47), the associated discretization errors are completely negligible and cannot be resolved in the analysis. Hence, in the infinite volume limit the most general fit form for the discretization artifacts is given by

$$R_n(a, \infty, m_h) - R_n(0, \infty, m_h) = \sum_{n=1}^N \sum_{j=1}^J c_{nj} [\ln(am_{h0})] (\alpha_s^{\text{lat}})^j (am_{h0})^{2n}, \quad (50)$$

where the coefficients c_{nj} could depend logarithmically on the heavy valence quark mass am_{h0} . Here, the tadpole-improved gauge coupling $\alpha_s^{\text{lat}} = \alpha_s^{\text{bare}}/u_0^4$ is a function of the bare lattice gauge coupling and of the “average” link variable u_0 ⁷. The tadpole-improved gauge coupling α_s^{lat} parametrizes the logarithmic dependence on the lattice spacing; see Fig. 8. For lattice spacings coarser than $a \lesssim 0.04 \text{ fm}$ some higher order terms in $(\alpha_s^{\text{lat}})^j$ or $(am_{h0})^{2n}$ have to be included in a fit, i.e. see [97] for a systematic discussion of the continuum extrapolation with up to eleven different lattice spacings in the range $0.025 \text{ fm} \lesssim a \lesssim 0.109 \text{ fm}$. If not enough data at fine enough lattice spacings or at different lattice spacings are available for such a fit, Bayesian techniques have to be employed to include additional constrained fit parameters, i.e. see [92, 95, 99], where only four lattice spacings in the range $0.059 \text{ fm} \lesssim a \lesssim 0.154 \text{ fm}$ were available and high powers $(am_{h0})^{2n}$ of the heavy valence quark mass were used. These more sophisticated analyses indicate the upward curvature for R_4 , and the downward curvature for the ratios R_6/R_8 , or R_8/R_{10} in the approach to the continuum limit for all heavy valence quark masses; see Fig. 8. However, with the larger statistical uncertainties due to the use of point sources such subtle effects could not be resolved in some of the presented analyses [55, 98], which used the simplest linear fits without even the factor $(\alpha_s^{\text{lat}})^1$. For these reasons, these analyses failed to identify the logarithmic lattice spacing dependence. In particular, in the JLQCD analysis three lattice spacings $a = 0.080, 0.055$ and 0.044 fm were used and simple $(am_{h0})^2$ extrapolations were performed. The $\chi^2/\text{d.o.f.}$ of such extrapolations turned out to be large. For example $\chi^2/\text{d.o.f.} = 2.1, 4.1$ and 5.1 for R_6/m_{h0} , R_8/m_{h0} and R_{10}/m_{h0} , respectively. On the other hand, for the higher moments the overall uncertainty is dominated by the error of the lattice scale. For this reason, the most simple fit form $\alpha_s^{\text{lat}}(am_{h0})^2$ is often sufficient, i.e. including any higher order terms does not have a statistically significant impact on the continuum limit.

The continuum extrapolated results of the most recent valence HISQ results [97] on the (2+1)-flavor HISQ ensembles are reproduced in Tab. 2. Given that no statistically significant sea quark effects are observed, these results can be considered to correspond to physical quark masses.

5. Comparison of the reduced moments from various groups

In the previous section we discussed the calculations of the moments of quarkonium correlators and demonstrated the main features of such calculations using the HISQ action with $N_f = 2 + 1$. We showed

⁷ Here, u_0 in the tadpole improvement is defined using the expectation value of the plaquette.

Table 2: The continuum results for R_4 , R_6/R_8 , or R_8/R_{10} , or R_n/m_{h0} , $n \geq 6$ at the different valence heavy quark masses, m_h , in (2+1)-flavor QCD with the HISQ action, PW19 [97]. The continuum extrapolation for $m_h = 4m_c$ or $m_h = m_b$ was not possible due the lack of a sufficiently large number of fine lattice spacings. Note that the error of the R_n/m_{h0} is dominated by the error of lattice scale in units of the lattice spacing, r_1/a , which includes the error of the experimental input, f_π , that was used for setting the lattice scale.

m_h	R_4	R_6/R_8	R_8/R_{10}	R_6/m_{h0}	R_8/m_{h0}	R_{10}/m_{h0}
$1.0m_c$	1.279(4)	1.1092(6)	1.0485(8)	1.0195(20)	0.9174(20)	0.8787(50)
$1.5m_c$	1.228(2)	1.0895(11)	1.0403(10)	0.7203(35)	0.6586(16)	0.6324(13)
$2.0m_c$	1.194(2)	1.0791(7)	1.0353(5)	0.5584(35)	0.5156(17)	0.4972(17)
$3.0m_c$	1.158(6)	1.0693(10)	1.0302(5)	0.3916(23)	0.3647(19)	0.3527(20)
$4.0m_c$				0.3055(23)	0.2859(12)	0.2771(23)
m_b				0.2733(17)	0.2567(17)	0.2499(16)

that the continuum extrapolation of the lowest moment or the ratio of the moments is quite challenging. Since the reliable continuum results for the moments are pre-requisite for an accurate determination of heavy quark masses and the strong coupling constant, it is important to compare different lattice calculations at the level of the continuum results for the moments. Comparison with perturbation theory and estimates of the corresponding systematic errors introduces another level of complications.

In Fig. 9 we show the continuum extrapolated results for R_4 , R_6/R_8 and R_8/R_{10} from different groups. We calculated the weighted average of different lattice results excluding MP 16 [55], since it was superseded by PW 19 [97]. The averaging procedure gives $\chi^2/\text{d.o.f.} = 1.24$ (R_4), 2.26 (R_6/R_8) and 0.79 (R_8/R_{10}). There is some scattering in the data, which together with large $\chi^2/\text{d.o.f.}$ may indicate that some errors are underestimated. In Fig. 10 we show a comparison of different lattice results for R_6/m_{h0} , R_8/m_{h0} , and R_{10}/m_{h0} . We also performed averaging of the different lattice results, which resulted in $\chi^2/\text{d.o.f.} = 2.61$, 2.93 and 2.73 for R_6 , R_8 and R_{10} , respectively. The JLQCD 16 value is lower than the average in all cases. This may indicate that there is a problem with the continuum extrapolation in the JLQCD 16 analysis, which would not be too surprising, since the a^2 extrapolation did not work well. If we omit the JLQCD 16 results from the average we obtain $\chi^2/\text{d.o.f.} = 0.81$ (R_6), 0.52 (R_8) and 0.53 (R_{10}), which appears to be much more reasonable. Therefore, we will quote the averages for R_6/m_{h0} , R_8/m_{h0} , and R_{10}/m_{h0} excluding the JLQCD 16 result. The average continuum values for the moments and their ratios are summarized in Tab. 3. These can be used to extract the strong coupling constant and heavy quark masses in an independent way by other groups.

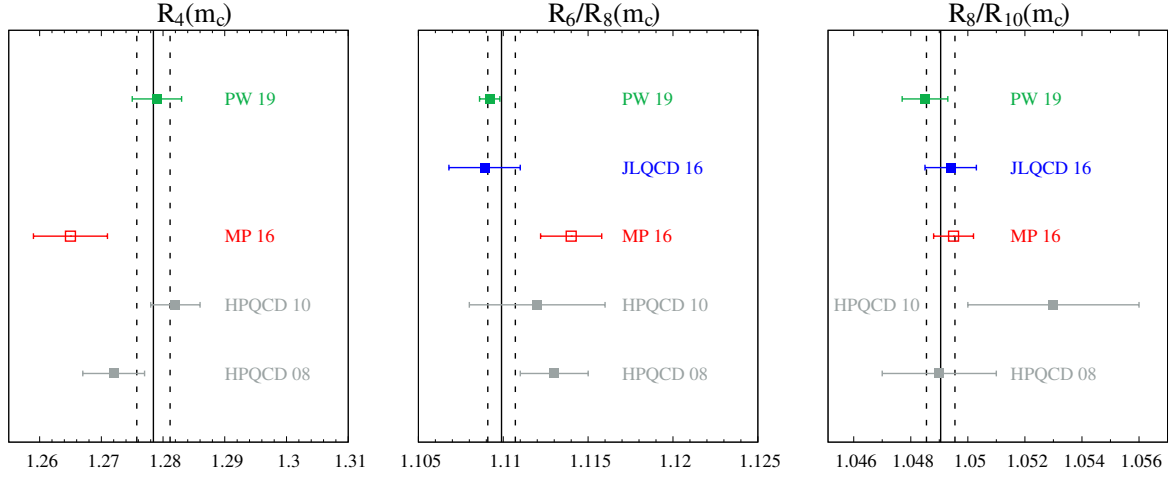


Figure 9: Comparison of different lattice results for R_4 (left), R_6/R_8 (middle), and R_8/R_{10} (right). Shown are the lattice results from HPQCD 08 [92], HPQCD 10 [95], JLQCD 16 [98], Maezawa and Petreczky (MP 16) [55], Petreczky and Weber (PW 19) [97]. The vertical solid and dashed lines show the weighted average and the corresponding uncertainty. The data corresponding to the open symbols do not enter the averages since they are superseded by PW 19.

Table 3: Lattice averages for R_4 , R_6/R_8 , or R_8/R_{10} , or R_n/m_{h0} , $n \geq 6$ at the charm quark mass. The errors of the experimental inputs, i.e. the scale setting error originating in the different experimental scales (here: f_π or m_Ω), and the mass min-tuning error originating the experimental meson masses, are sub-leading among the error sources of the averages.

R_4	R_6/R_8	R_8/R_{10}	R_6/m_{h0}	R_8/m_{h0}	R_{10}/m_{h0}
1.2784(27)	1.10990(81)	1.04905(50)	1.0211(16)	0.9188(14)	0.8744(13)

6. Heavy quark masses and α_s from the moments

Given the time moments of the quarkonium correlation function and their ratios in the continuum limit, one may proceed with the extraction of the heavy quark masses and the strong coupling constant in the $\overline{\text{MS}}$ scheme at the next-to-next-to-next-to-leading order.

First of all, one may choose the common renormalization scale $\nu = \nu_m = m_h$ for the strong coupling and the quark masses in Eq. (47), leading to the simplification $r_n[\nu/m_h(\nu_m), \alpha_s(nu)] \rightarrow r_n[\alpha_s(m_h)]$ as in PW 19 [97]. Then, using the continuum extrapolated HISQ results for R_4 , R_6/R_8 , or R_8/R_{10} that are given in Tab. 2 in a first step, one may solve for the strong coupling constant $\alpha_s(m_h, N_f = 3)$ in $N_f = 3$ QCD. In a second step, one may use this $\alpha_s(m_h, N_f = 3)$ and fit the higher moments R_n/m_{h0} for $n > 4$, which are given in Tab. 2, too. These higher moments satisfy the scheme independent relation $m_h^{(a)}/m_h^{(b)} = R_n^{(a)}/R_n^{(b)}$ for any schemes a and b , and thus

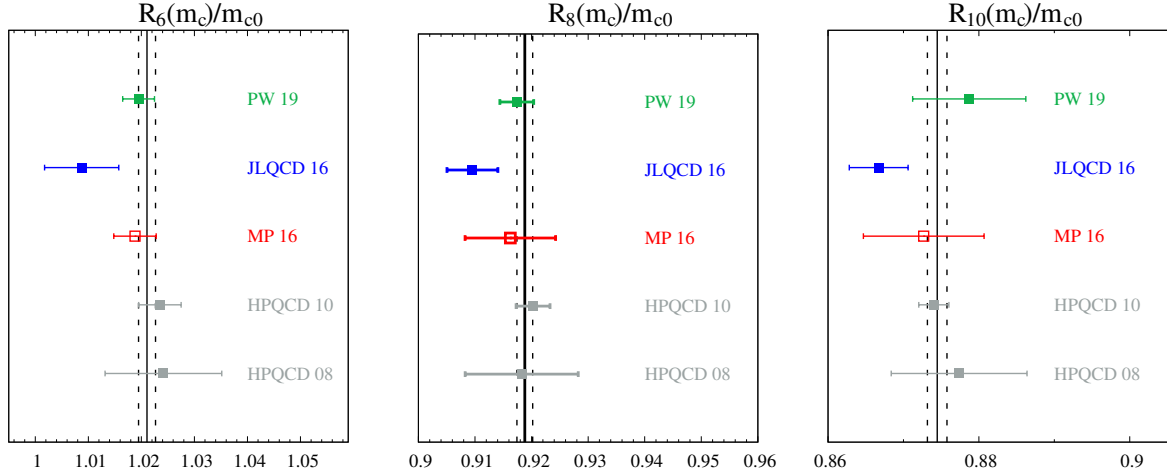


Figure 10: Comparison of different lattice results for R_6/m_{h0} (left), R_8/m_{h0} (middle), and R_{10}/m_{h0} (right). Shown are the lattice results from HPQCD 08 [92], HPQCD 10 [95], JLQCD 16 [98], Maezawa and Petreczky (MP 16) [55], Petreczky and Weber (PW 19) [97]. The vertical solid and dashed lines show the weighted average and the corresponding uncertainty. The data corresponding to the open symbols do not enter the averages since they are superseded by PW 19.

$$m_h(m_h) = \frac{r_n[\alpha_s(m_h)]}{R_n} m_{h0}. \quad (51)$$

Hence, one can directly calculate the heavy quark mass $m_h(m_h)$ in the $\overline{\text{MS}}$ scheme.

For the first step one could proceed with multiple levels of combined or separate fits. On the one hand, one might fit either multiple results among the R_4 , R_6/R_8 , and R_8/R_{10} at multiple valence heavy quark masses in a simultaneous fit, which, however has to include (reasonable) assumptions about the running of the strong coupling. On the other hand, one might use a combined fit of R_4 , R_6/R_8 , and R_8/R_{10} at each heavy quark mass, or one could even consider these results in separate fits. The latter provides the advantage of a consistency check of the three individual continuum extrapolations, which is the approach used in PW 19 [97]. In order to estimate the perturbative truncation error, one may consider including a generic higher order term $r_{n4}(\alpha_s(m_h)/\pi)^4$ in the analysis. In order to be conservative its coefficient has been varied between $-5r_{n3} \leq r_{n4} \leq +5r_{n3}$ in PW 19 [97]. The r_{nj} can be considered as independent for R_4 , R_6/R_8 , or R_8/R_{10} . Since the strong coupling constant $\alpha_s(m_h)$ becomes much smaller for the higher scales, appropriate for higher masses, the perturbative error is systematically reduced for the larger heavy quark masses. The nonperturbative contribution from the gluon condensate is just added as a constant shift, and varied within its error. Since it is weighted with the fourth power of the inverse heavy quark mass, this uncertainty quickly becomes numerically insignificant for the larger heavy quark masses. We

Table 4: The values of $\alpha_s(m_h, N_f = 3)$ for different heavy quark masses, m_h , extracted from R_4 , R_6/R_8 , and R_8/R_{10} . The first, second, and third errors correspond to the lattice error, the perturbative truncation error, and the error due to the gluon condensate. The error of the experimental inputs, i.e. the scale setting error originating in the experimental error of f_π , and the mass min-tuning error originating the experimental meson masses are subleading contributions to the lattice error. In the fifth column the averaged value of $\alpha_s(m_h, N_f = 3)$ is shown (see text). The last column gives the value of $\Lambda_{\overline{MS}}^{N_f=3}$ in MeV.

$\frac{m_h}{m_c}$	R_4	R_6/R_8	R_8/R_{10}	av.	$\Lambda_{\overline{MS}}^{n_f=3}$ MeV
1.0	0.3815(55)(30)(22)	0.3837(25)(180)(40)	0.3550(63)(140)(88)	0.3782(65)	314(10)
1.5	0.3119(28)(4)(4)	0.3073(42)(63)(7)	0.2954(75)(60)(17)	0.3099(48)	310(10)
2.0	0.2651(28)(7)(1)	0.2689(26)(35)(2)	0.2587(37)(34)(6)	0.2648(29)	284(8)
3.0	0.2155(83)(3)(1)	0.2338(35)(19)(1)	0.2215(367)(17)(1)	0.2303(150)	284(48)

reproduce the results for $\alpha_s(m_h, N_f = 3)$ in the \overline{MS} scheme from the different possible fits in Tab. 4. On the one hand, the $\alpha_s(m_h, N_f = 3)$ value for $m_h = m_c$ or $m_h = 1.5 m_c$ from the (2+1)-flavor HISQ result for R_8/R_{10} is slightly lower than the corresponding values from R_4 or R_6/R_8 . A possible reason might be that the (2+1)-flavor HISQ result for R_{10} is slightly higher, than the associated (2+1)-flavor world average, whereas the (2+1)-flavor HISQ results for R_6/R_8 , R_6/m_{h0} , and R_8/m_{h0} are much closer to their respective averages; see Fig. 10. On the other hand, for $m_h = 2 m_c$ the agreement between the three values from R_4 , R_6/R_8 , or R_8/R_{10} is better. Lastly, the $m_h = 3 m_c$ result has quite a large lattice error, which appears to be slightly lower $\alpha_s(m_h, N_f = 3)$ value from R_4 . The averages in Tab. 4 can be obtained as weighted averages, since the dominant uncertainties, i.e. the perturbative truncation errors, can be considered as sufficiently independent for the different quantities.

In the second step, one may use the thus obtained $\alpha_s(m_h, N_f = 3)$ to calculate values of $m_h(m_h)$ for $m_h \leq 3 m_c$ from the different reduced moments R_6/m_{h0} , R_8/m_{h0} , or R_{10}/m_{h0} , which are generally in very good agreement. This is not surprising, since their approach to the continuum limit is quite simple. We reproduce the results for $m_h(m_h)$ in the \overline{MS} scheme from the different possible fits in Tab. 5. The averages in Tab. 5 can be obtained straightforwardly, since the agreement is generally better than the errors would suggest.

Combining the results for $\alpha_s(m_h)$ and $m_h(m_h)$ at each heavy quark mass, one may use the perturbative running to obtain the values of the QCD Lambda parameter $\Lambda_{\overline{MS}}^{N_f=3}$. A small systematic error estimate due the difference between the implicit or explicit schemes⁸ has been included. Together with the errors of the numerical results for $\alpha_s(m_h, N_f = 3)$ and $m_h(m_h)$ all errors are added in quadrature to determine the uncertainty of $\Lambda_{\overline{MS}}^{N_f=3}$. The central values and errors are reported in the last column of Tab. 4.

⁸The implicit/explicit schemes are defined in terms of Eqs. (5) or (4) in [101].

Table 5: The heavy quark masses $m_h(m_h)$ in the $\overline{\text{MS}}$ scheme in units of GeV for the different values of m_h . The first, second, third, and fourth errors correspond to the errors of the lattice result, the perturbative truncation error, the error due to the gluon condensate, and the error from $\alpha_s(m_h, N_f = 3)$, respectively. The last column shows the average of the masses determined from R_6/m_{h0} , R_8/m_{h0} , and R_{10}/m_{h0} . This error budget does not include the overall error of the lattice scale, r_1 .

$\frac{m_h}{m_c}$	m_h from R_6/m_{h0} [GeV]	m_h from R_8/m_{h0} [GeV]	m_h from R_{10}/m_{h0} [GeV]	average m_h [GeV]
1.0	1.2740(25)(17)(11)(61)	1.2783(28)(23)(00)(43)	1.2700(72)(46)(13)(33)	1.2741(42)(29)(8)(46)
1.5	1.7147(83)(11)(03)(60)	1.7204(42)(14)(00)(40)	1.7192(35)(29)(04)(30)	1.7181(53)(18)(2)(43)
2.0	2.1412(134)(07)(01)(44)	2.1512(71)(10)(00)(29)	2.1531(74)(19)(02)(21)	2.1481(93)(12)(1)(31)
3.0	2.9788(175)(06)(00)(319)	2.9940(156)(08)(00)(201)	3.0016(170)(16)(00)(143)	2.9915(167)(10)(0)(220)
4.0	3.7770(284)(06)(00)(109)	3.7934(159)(08)(00)(68)	3.8025(152)(15)(00)(47)	3.7910(198)(10)(0)(75)
$\frac{m_b}{m_c}$	4.1888(260)(05)(00)(111)	4.2045(280)(07)(00)(69)	4.2023(270)(14)(00)(47)	4.1985(270)(9)(0)(76)

There is some concern that the central value of $\Lambda_{\overline{\text{MS}}}^{N_f=3}$ obtained from the data at $m_h = 2m_c$ is 2.5σ lower than the central values obtained from the lattice data at the smaller heavy quark masses, $m_h = m_c$ or $m_h = 1.5m_c$. This could imply that some continuum extrapolations at $m_h = 2m_c$ might suffer from underestimated systematic uncertainties. However, given the good consistency between the corresponding results in Tab. 4, it appears unlikely that multiple among the separate continuum extrapolations are flawed in order to produce such a result. Moreover, even eliminating the lowest or the lower two results of $\alpha_s(2m_c, N_f = 3)$ does not change the outcome of the analysis in a statistically significant manner. For these reasons, the spread between the different results has to be taken as a more conservative estimate for the error than the smaller result from the direct error propagation. Hence, the (unweighted) average of the results is

$$\Lambda_{\overline{\text{MS}}}^{N_f=3} = 298(16) \text{ MeV}. \quad (52)$$

This result has been used to determine the strong coupling $\alpha_s(m_h, N_f = 3)$ and the heavy quark masses $m_h(m_h)$ at the higher scales $m_h = 4m_c$ or $m_h = m_b$; see Tab. 5.

The determination of the strong coupling constant from the moments is strongly affected by the uncertainties in the continuum extrapolation of the moments. Using the perturbative decoupling of the charm quark at 1.5 GeV and of the bottom quark at 4.7 GeV this average result for $\Lambda_{\overline{\text{MS}}}^{N_f=3}$ can be converted to the strong coupling constant at the Z pole, $\nu = M_Z$,

$$\alpha_s(M_Z, N_f = 5) = 0.1159(12). \quad (53)$$

In particular, we show the four separate results of PW 19 [97] due to the four values of the QCD Lambda parameter obtained with the four different valence heavy quark masses, cf. Tab. 4, as separate symbols and

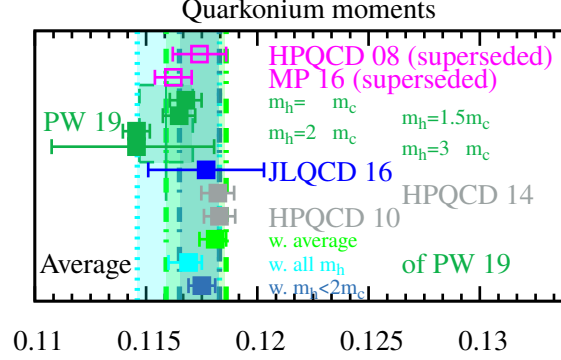


Figure 11: The results for $\alpha_s(M_Z)$ obtained from the time moments of quarkonium correlation functions in (2+1)-flavor QCD, i.e. HPQCD 10 [95], JLQCD 16 [98], Petreczky and Weber (PW 19) [97], or in (2+1+1)-flavor QCD from HPQCD 14 [99]. The superseded results HPQCD 08 [92] (superseded by HPQCD 10 [95]), and Maezawa and Petreczky (MP 16) [55] (superseded by PW 19 [97]) are shown, too.

the average in Eq. (53) as a shaded region. One might calculate a lattice average using either this average, or the individual results obtained with all four different valence heavy quark masses, or the results obtained by restricting to the smaller valence heavy quark masses $m_h < 2m_c$ (the largest valence heavy quark mass $m_h = 3m_c$ has practically no impact on the average). For these three averages one obtains

$$\alpha_s(M_Z) = 0.1180^{+0.0006}_{-0.0006}, \quad \chi^2/\text{d.o.f.} = \frac{3.35}{3}, \quad \text{with PW 19 average, Eq. (53),} \quad (54)$$

$$\alpha_s(M_Z) = 0.1169^{+0.0006}_{-0.0009}, \quad \chi^2/\text{d.o.f.} = \frac{22.7}{7}, \quad \text{with PW 19 all } m_h, \quad (55)$$

$$\alpha_s(M_Z) = 0.1175^{+0.0006}_{-0.0006}, \quad \chi^2/\text{d.o.f.} = \frac{5.24}{4}, \quad \text{with PW 19 } m_h < 2m_c, \quad (56)$$

respectively. The $\chi^2/\text{d.o.f.}$ is never below 1, which suggests that the errors in at least some of the averaged results are indeed underestimated as mentioned earlier on the level of the continuum extrapolated moments. The last average in Eq. (56) excluding the two larger valence heavy quark masses of PW 19 [97] appears to be the most consistent with the individual lattice results, and covers the central values of the other averages, too. We assign the spread between all individual results that enter this average as the estimate of the uncertainty and show this as a colored band in Fig. 11, namely,

$$\alpha_s^{\text{mom}}(M_Z) = 0.1175^{+0.0008}_{-0.0010} \quad \text{pre-average from the moments.} \quad (57)$$

On the contrary, the quark masses are in much better agreement between the different lattice calculations. Here, we reproduce the most recent (2+1)-flavor QCD results with the HISQ action, PW 19 [97]. After combining the uncertainty of the lattice scale r_1 with the result in Tab. 5, we obtain the $\overline{\text{MS}}$ charm quark mass in the three and four flavor theories,

$$m_c(\nu_m = m_c, N_f = 3) = 1.2741(101) \text{ GeV}, \quad (58)$$

$$m_c(\nu_m = m_c, N_f = 4) = 1.265(10) \text{ GeV}, \quad (59)$$

$$m_c(\nu_m = 3 \text{ GeV}, N_f = 4) = 1.001(16) \text{ GeV}. \quad (60)$$

Finally, we obtain the $\overline{\text{MS}}$ bottom quark mass in the three and five flavor theories,

$$m_b(\nu_m = m_b, N_f = 3) = 4.1985(371) \text{ GeV}, \quad (61)$$

$$m_b(\nu_m = m_b, N_f = 5) = 4.188(37) \text{ GeV}. \quad (62)$$

As previously, the matchings to the four or five flavor theories has been performed at 1.5 GeV or 4.7 GeV, respectively.

So far we discussed the determination of α_s using reduced moments by different lattice groups. Very recently the continuum extrapolated lattice results on the reduced moments of pseudoscalar correlators have been combined with the reduced moments of vector correlation function extracted from the experimental results on e^+e^- collisions to obtain α_s [102] (see also Ref. [103] for a related extraction). This study used a different methodology to extract the strong coupling constant and its uncertainty. The perturbative error has been estimated by varying the scale ν in $\alpha_s(\nu)$ as well as the scale ν_m at which the heavy quark mass $m_h(\nu_m)$ is defined contrary to the analysis by the lattice groups. This resulted in a perturbative error which is significantly larger. Since the renormalization scale dependence of the heavy quark masses is known to high order it is not clear if one should count the scale dependence of the quark masses at fixed order as part of the perturbative error. In any case these issues need further studies.

7. Heavy quark masses from a combined EFT and lattice QCD analysis

Because of confinement, one cannot determine quark masses by isolating them from the rest of the world and measuring their rest masses. For a heavy quark, however, there are physical states, such as a heavy-light meson composed of the heavy quark and a light antiquark, with this property that the bulk of the meson mass comes from the mass of the heavy quark; thus, the mass of the heavy quark can be identified at leading order with the masses of these physical states. Investigating the dependence of the mass of such a system on the mass of the heavy quark, one can in principle extract the heavy quark mass. We now discuss how a combination of effective field theories and lattice QCD can be used to quantify this dependence and in turn determine the charm- and bottom-quark masses.

Heavy quark effective theory (HQET) formula for the mass of a heavy-light pseudoscalar meson is [104]

$$M_H = m_h + \bar{\Lambda} + \frac{\mu_\pi^2}{2m_h} - \frac{\mu_G^2(m_h)}{2m_h} + \mathcal{O}(m_h^{-2}), \quad (63)$$

where m_h is the heavy-quark mass and \bar{A} , μ_π^2 , and $\mu_G^2(m_h)$ are matrix elements of HQET operators with dimension 4 and 5. These matrix elements have simple physical meanings. They correspond, respectively, to the energy of the light quarks and gluons, the heavy quark's kinetic energy, and the chromomagnetic energy, which has an anomalous dimension and, therefore, has a logarithmic dependence on the mass m_h .

A precise determination of the HQET matrix elements is necessary for precise determination of a heavy quark mass from Eq. (63). Lattice QCD makes it possible to compute many quantities including these matrix elements. One approach is to exploit the very Eq. (63): use lattice QCD to compute M_H as a function of m_h (for many fictitious values of the heavy quark mass) and fit Eq. (63) to compute the HQET matrix elements on the right-hand side including higher orders in $1/m_h$ [105]. When the HQET matrix elements are determined, one can plug them into Eq. (63) along with the physical masses of the D and B systems, and extract the masses of the charm and bottom quarks, respectively.

There are several challenges that should be addressed in order to implement the above program. First, as we discuss below, one should give a precise definition for the HQET matrix elements; this is tied to a precise definition for m_h in Eq. (63). Second, the simulation masses of quarks on a lattice must be renormalized in order to be used in expressions such as Eq. (63). The renormalization can be performed using lattice perturbation theory, which is in practice very limited and consequently restricts the accuracy, or using nonperturbative approaches such as the one we explain below, which is designed to improve the accuracy. Third, one should include the effects of light quark masses in Eq. (63). These effects can be incorporated into the analysis using heavy-meson chiral perturbation theory (HM χ PT) [106–108], which is a merger of HQET and χ PT. Fourth, because the data calculated by lattice simulations suffer from lattice artifacts that depend on the employed lattice action and are present at any nonzero lattice spacing, one cannot simply rely on HQET and χ PT to describe how the computed mass of a heavy-light meson on a lattice depends on the masses of its heavy and light quarks.⁹ In many cases the lattice artifacts can be modeled by simple analytic expansions in powers of the lattice spacing. This might not be a useful practice when light quarks are involved. In this case, to take the lattice artifacts into account, one can modify HM χ PT within the framework of another EFT: the Symanzik effective theory [109].

When all these challenges are addressed one obtains an effective formula to describe the mass of a heavy-light meson in terms of its quark masses as well as the lattice artifacts related to the employed lattice-QCD action. The free (mass-independent) parameters of such a formula would consist of several HQET matrix elements, such as those introduced in Eq. (63), several low energy constants in χ PT, as well as many parameters that describe the dependence on the lattice spacing a , which disappear at the continuum limit where $a = 0$. Fitting such a formula to lattice-QCD data, one can extract the free parameters of the function. Then by setting $a = 0$, one passes to the continuum, where the masses of the charm and bottom quarks can

⁹Except for electromagnetic effects, we use the term “quark” to refer to both components of a heavy-light meson.

be obtained at points where, for example, the D_s - and B_s -meson masses take their physical values.

In a series of papers [105, 110–114] by members of the Fermilab lattice, MILC, and TUMQCD collaborations, different aspects of the above program have been discussed and implemented leading to a precise determination of the charm- and bottom-quark masses. Combining the analysis with a separate determination of ratios of light-quark masses, they present one of the most precise determinations of the up-, down-, strange-, charm-, and bottom-quark masses [113]. In this section we highlight the main features of this program, and present the results for the quark masses. For details one should consult with Ref. [113].

This section is organized as follows. In Sec. 7.1, we address the mentioned challenges and present our formula for describing heavy-light meson masses. Then, in Sec. 7.2, we briefly describe the lattice data used in this analysis, including a discussion on tuning quark masses and dealing with unequilibrated topological charge. Finally, in Sec. 7.3, we summarize the analysis and present the quark masses.

7.1. Relations between heavy-light meson and quark masses

In this part, we discuss different aspects of relating heavy-light meson masses to quark masses. We start with a definition of a quark mass in the continuum that is useful in our analysis. We then discuss how such a mass can be calculated from the simulation mass of a quark on a lattice. Equipped with this definition of mass for a heavy quark, we present the EFT description of the mass of a heavy-light meson simulated on a lattice with staggered quarks.

7.1.1. Minimal-Renormalon-Subtracted mass

In HQET in general and in Eq. (63) in particular, the meaning of the matrix elements such as $\bar{\Lambda}$ is tied to the definition of the heavy-quark mass m_h used in the expansion. The natural definition, which was initially assumed when HQET was introduced, is the pole mass of the heavy quark. The pole mass is infrared finite [115] and gauge independent [115, 116] at every order in perturbation theory, but it is not well-defined when all orders are considered because at large orders the coefficients grow factorially rendering a divergent series [117, 118]. This particular pattern of divergence in the pole mass is referred to as a renormalon divergence. An interpretation of the divergent series is possible via Borel summation up to ambiguities caused by a series of (renormalon) singularities. In particular, the leading renormalon introduces an intrinsic ambiguity of order of QCD Lambda in the Borel sum of the pole mass. From Eq. (63), one can see that because the meson mass is unambiguous, this ambiguity must be canceled by another quantity of similar order: $\bar{\Lambda}$. Similar ambiguities from subleading infrared renormalons must be canceled by higher-dimension matrix elements such as μ_π^2 .

Several so-called threshold masses, such as the kinetic mass [119, 120], the renormalon-subtracted (RS) mass [121], the MSR mass [122], the 1S mass [123], and the potential-subtracted mass [124], have been introduced to handle the renormalon divergence in the pole mass. These threshold masses are defined

by introducing an arbitrary factorization scale as an infrared cutoff to remove the renormalon from the pole mass. Instead of the above threshold masses, here we briefly describe a recently introduced mass, the minimal renormalon-subtracted (MRS) mass [112], which is used by the Fermilab lattice, MILC, and TUMQCD collaborations in their analysis. It is a gauge- and scale-independent mass with an asymptotic expansion identical to the perturbative pole mass. Because of the last feature, one can use the MRS mass of a heavy quark for the HQET expansion. The main advantage of using the MRS mass is that it handles the renormalons without introducing any factorization scale unlike the other threshold masses listed above. This simplifies the analysis (with one less scale) and improves the precision of the analysis.

The MRS mass is defined based on an investigation of the large-order behavior of the pole mass in perturbation theory in Ref. [111]. Using r_n to denote the coefficients relating the $\overline{\text{MS}}$ mass to the pole mass and R_n to denote their asymptotic behavior, the idea behind the MRS mass is to interpret the pure asymptotic part, i.e. $\sum R_n \alpha_s^{n+1}$, via Borel summation, split the resulting integral into an unambiguous piece and an ambiguous one, and finally discard the ambiguous piece. The last step has an interesting meaning in the context of HQET. As discussed below, it means to sweep the ambiguous piece into a specific quantity related to the concept of residual mass in HQET [125]. The MRS mass defined in Eq. (2.24) of Ref. [112] is

$$m_{\text{MRS}} = \bar{m} \left(1 + \sum_{n=0}^{\infty} [r_n - R_n] \alpha_s^{n+1}(\bar{m}) + J_{\text{MRS}}(\bar{m}) \right), \quad (64)$$

where $\bar{m} = m_{\overline{\text{MS}}}(m_{\overline{\text{MS}}})$, and $J_{\text{MRS}}(\bar{m})$, defined in Eqs. (2.25) and (2.26) of Ref. [112], is the unambiguous part of the Borel sum of $\sum R_n \alpha_s^{n+1}$. Note that the R_n depend only on the coefficients of the beta function up to an overall normalization [111, 126].

Although the MRS mass is introduced such that one can in principle handle the effects of all renormalons, in practice (with four-loop calculations) one needs only to take care of the leading renormalon. To see that m_{MRS} admits a well-behaved perturbative expansion in α_s , even when the possible subleading renormalons are overlooked, let us briefly discuss the relation between the MRS and $\overline{\text{MS}}$ masses in a theory with three massless quarks in the sea ($n_l = 3$). Exploiting four-loop calculations in Ref. [127], and setting the overall normalization of the leading renormalon to $R_0^{(n_l=3)} = 0.535$ [111], one obtains [112]

$$r_n^{(n_l=3)} = (0.4244, 1.0351, 3.6932, 17.4358, \dots), \quad (65)$$

$$R_n^{(n_l=3)} = (0.5350, 1.0691, 3.5966, 17.4195, \dots), \quad (66)$$

for $n = 0, 1, 2, 3, \dots$. The differences

$$r_n^{(n_l=3)} - R_n^{(n_l=3)} = (-0.1106, -0.0340, 0.0966, 0.0162, \dots) \quad (67)$$

are much smaller than the r_n ; consequently, the series in powers of α_s in Eq. (64) is a well-behaved series through order α_s^4 .

There are subtleties in the definition of the MRS mass in presence of massive fermions in the sea. These subtleties are discussed in detail in Ref. [112].

Let us now discuss the MRS mass in connection to the HQET description of heavy-light meson masses in Eq. (63). HQET as an effective theory of QCD can be reformulated in presence of a residual mass term [125]. With this reformulation, one is allowed to shift the mass of the heavy quark by an amount of order of QCD Lambda and redefine the HQET matrix elements such as \bar{A} . In deriving Eq. (64), the ambiguous part of the Borel sum of $\sum R_n \alpha_s^{n+1}$, which itself is of order of QCD Lambda, is swept from m_h to \bar{A} rendering it unambiguous too. We write $m_{h,\text{MRS}}$ and \bar{A}_{MRS} to denote the unambiguous definitions of m_h and \bar{A} in the MRS scheme. Equation (63) then reads

$$M_H = m_{h,\text{MRS}} + \bar{A}_{\text{MRS}} + \frac{\mu_\pi^2 - \mu_G^2(m_h)}{2m_{h,\text{MRS}}} + \mathcal{O}(m_{h,\text{MRS}}^{-2}) \quad (68)$$

in the MRS scheme. We emphasize that the only difference between Eqs. (63) and (68) is that in the later one the definitions of the heavy quark mass and the matrix element corresponding to the energy of the light quarks and gluons are fixed to the MRS scheme. We do not attribute the MRS scheme to the kinetic term μ_π^2 nor the chromomagnetic term μ_G^2 in Eq. (68). The chromomagnetic term is indeed related to the hyperfine splitting in the masses of the vector and pseudoscalar mesons; therefore, it can be simply estimated from experimental data up to an uncertainty suppressed by an inverse power of the heavy quark mass. The kinetic term is expected to have very small intrinsic ambiguity (if not zero) simply because its corresponding ambiguity in the pole mass is very small. This can be seen from the fact that in Eq. (67) the coefficients are all small without any sign of divergence through order α_s^4 .

As an alternative scheme to organize the HQET expansion, one can consider the so-called principal value (PV) mass (e.g., [126, 128, 129]). A practical and transparent definition for the PV mass is presented in Ref. [112] via the MRS mass as

$$m_{\text{PV}} = m_{\text{MRS}} + cA_{\overline{\text{MS}}}, \quad (69)$$

where the constant c is given in Eq. (2.30) of Ref. [112]. The scheme conversion is simply a shift by an amount independent of the quark mass. The shift is indeed small for QCD with three light quarks; $cA_{\overline{\text{MS}}} \approx 0.1$ GeV. Similarly, we have

$$\bar{A}_{\text{PV}} = \bar{A}_{\text{MRS}} - cA_{\overline{\text{MS}}} \quad (70)$$

so that Eq. (68) remains unchanged with this scheme conversion. Both the MRS and PV masses can be used in the analysis. In practice, for QCD with three light quarks, there is no need to perform a simple shift to the MRS mass to obtain the PV mass. Moreover, it turns out that the PV mass becomes slightly less precise than the MRS mass due to uncertainties in the ingredients of $cA_{\overline{\text{MS}}}$ including $A_{\overline{\text{MS}}}$. As a result this analysis prefers the MRS scheme.

This concludes the derivation and implementation of the MRS scheme in the continuum. In the context of lattice QCD, one still needs to discuss how to calculate the MRS mass of a heavy quark from its simulation mass on a lattice.

7.1.2. Simulation and renormalized masses

The Fermilab lattice, MILC, and TUMQCD collaborations use a nonperturbative approach to relate the simulation mass of a heavy quark on a lattice to its MRS mass. With staggered fermions, they introduce a “reference quark” and rewrite $m_{h,\text{MRS}}$ as

$$m_{h,\text{MRS}} = m_{r,\overline{\text{MS}}}(\mu) \frac{\overline{m}_h}{m_{h,\overline{\text{MS}}}(\mu)} \frac{m_{h,\text{MRS}}}{\overline{m}_h} \frac{am_h}{am_r} \quad (71)$$

with the four factors as follows. The first factor is the mass of the reference quark in the $\overline{\text{MS}}$ scheme, which can be treated as a fit parameter. The second is a factor to run the heavy quark mass in the $\overline{\text{MS}}$ scheme from scale μ to the self-consistent scale $\overline{m}_h = m_{h,\overline{\text{MS}}}(\overline{m}_h)$

$$\frac{\overline{m}_h}{m_{h,\overline{\text{MS}}}(\mu)} = \frac{C(\alpha_{\overline{\text{MS}}}(\overline{m}_h))}{C(\alpha_{\overline{\text{MS}}}(\mu))}, \quad (72)$$

where with four active flavors [130]

$$C(\pi u) = u^{12/25} [1 + 1.01413u + 1.38921u^2 + 1.09054u^3 + 5.8304u^4 + \mathcal{O}(u^5)]. \quad (73)$$

The coefficient of u^4 is obtained from the five-loop results for the beta function [131] and the quark-mass anomalous dimension [130]. The third factor is basically the big parentheses in Eq. (64). Finally, the fourth factor is the ratio of the simulation masses (in lattice units) of the heavy quark and the reference quark.

It is worth mentioning that the remnant chiral symmetry of staggered fermions plays a key role in Eq. (71). To be more specific, Eq. (71) is constructed based on the identity

$$\frac{m_{h,\overline{\text{MS}}}(\mu)}{m_{r,\overline{\text{MS}}}(\mu)} = \frac{am_h}{am_r} + \mathcal{O}(a^2), \quad (74)$$

which holds for staggered fermions.

In Ref. [113], the reference mass am_r is set to 0.4 times the bare mass of the strange quark obtained from an analysis of light mesons with the so-called $p4s$ method. Therefore, when the analysis is completed, this method yields m_s in addition to the heavy-quark masses m_c and m_b .

7.1.3. Heavy-light mesons in EFTs and construction of a fit function

The technique of constructing EFTs is very powerful in tackling problems with several scales such as problems involving very heavy and/or very light quarks. HQET, χ PT, and a merger of them HM χ PT are among the well-known EFTs developed to study the low-energy dynamics of QCD. Our main aim is to use EFTs along with lattice-QCD data to extract quark masses from heavy-light meson masses. To this end

we could simply use the EFTs that are developed in the continuum to analyze lattice data. An alternative approach, which we use here, is to develop new EFTs based on symmetries of the lattice action. This helps us have more control on artifacts of discretization of the lattice action and be able to extrapolate the lattice results to the continuum in a more systematic way.

With staggered fermions, the appropriate theory for this analysis is known as heavy-meson, rooted, all-staggered chiral perturbation theory (HMrAS χ PT) [132]. This is a cascade of EFTs describing, for example, how the mass of a heavy-light meson composed of staggered quarks depends on the simulation quark masses, the lattice spacing, and the volume of the lattice. Within the framework of this theory, one-loop corrections to heavy-light meson masses are calculated in Ref. [112]. We summarize the results in Appendix B.

The one-loop corrections contain effects of flavor, hyperfine, and (staggered) taste splittings as well as effects of finite lattice size. They are needed to describe the next-to-leading order behavior of the lattice data. They, however, are not enough to fully describe the quark-mass and lattice-spacing dependence. Therefore, the authors of Ref. [113] extend the function containing one-loop corrections by adding higher-order analytic corrections in powers of light-quark masses, the lattice spacing, and the heavy quark mass in lattice units, and also in inverse powers of the heavy-quark mass. The extended function, which is given in Eq. (3.26) of Ref. [113], contains 67 fit parameters. Because of lengthy expressions, we do not reproduce them here. We simply use

$$M_{H_x}(\{m_h, m_x\}, \{m'_l, m'_l, m'_s, m'_c\}, \{a, V\}; \{p_1, \dots, p_{67}\}) \quad (75)$$

to denote this function, which takes as inputs the simulation masses of the valence heavy and light quarks (in the first braces), the simulation masses of four flavors of sea quarks (in the second braces), and the lattice spacing and volume (in the third braces). Note that in this analysis the up and down sea-quark masses are taken equal and denoted by m'_l in Eq. (75). The fourth braces in Eq. (75) lists the 67 parameters of M_{H_x} . The main physical parameters correspond to $m_{r,\overline{\text{MS}}}(\mu)$ in Eq. (71), which is set to 0.4 times the strange quark mass $m_{s,\overline{\text{MS}}}(2\text{ GeV})$, and the HQET matrix elements in Eq. (68):

$$p_1 = m_{p_{4s},\overline{\text{MS}}}(2\text{ GeV}), \quad p_2 = \bar{A}_{\text{MRS}}, \quad p_3 = \mu_\pi^2, \quad p_4 = \mu_G^2(m_b), \dots, \quad (76)$$

where $m_{p_{4s},\overline{\text{MS}}} \equiv 0.4 m_{s,\overline{\text{MS}}}$.

The effective function M_{H_x} can be readily used to perform a combined EFT fit to lattice data of heavy-light meson masses computed at multiple lattice spacings and various valence- and sea-quark masses. This determines the fit parameters in Eq. (76), including the strange quark mass $m_{s,\overline{\text{MS}}}$, and enables us to calculate heavy quark masses m_c and m_b . This is discussed further in Sec. 7.3.

7.2. Lattice setup and simulations parameters

This analysis uses a data set from 24 ensembles generated by the MILC collaboration [100, 133] with four flavors of sea quarks using the HISQ action [35]. The data set includes ensembles with six values of lattice spacings ranging from approximately 0.15 fm to 0.03 fm; ensembles with the light (up-down), strange, and charm sea masses close to their physical values; and ensembles with the light and strange sea masses heavier or lighter than in nature, respectively. These ensembles with a wide range of simulation parameters provide a good control over the continuum extrapolation and the dependence on sea quark masses.

In order to control the dependence of heavy-light meson masses on their valence-quark masses, this analysis uses a wide range of masses for valence heavy and light quarks. On the coarsest ensembles, there are only two different values for the valence heavy quark: $m_h = m'_c$ and $m_h = 0.9m'_c$. Here m'_c denotes the simulation value of the sea charm-quark mass in each ensemble, which is slightly different from the physical charm mass m_c because of tuning errors. On the finest ensembles, there are several data with $0.9m'_c \leq m_h \leq 5m'_c$. The analysis uses the data with $am_h < 0.9$ to avoid large lattice artifacts. For every valence heavy quark, several light valence quarks are used with masses $m_l \lesssim m_x \lesssim m_s$. Altogether 384 data points are used in the main analysis of heavy-light meson masses.

The full description of the lattice setup and simulation parameters is given in Table I of Ref. [134]. The procedures for calculating pseudoscalar meson correlators and for finding masses from these correlators are also described in Refs. [134, 135]. Moreover, the scale setting and tuning the masses of light quarks are performed in Ref. [134] with a two-step procedure that uses the pion decay constant f_π to set the overall scale combined with the so-called $p4s$ method, which yields a simultaneous determination of the lattice spacing a and $m_{p4s} \equiv 0.4 m_s$.

In the tuning procedure of the light quark masses, the values of the bare masses corresponding to the light and strange quarks are obtained from combinations of the physical pion and kaon masses. Because the gauge-field ensembles omit electromagnetism, electromagnetic effects should be subtracted (in a specific scheme) from the experimentally measured masses. In this analysis, the subtraction is performed using the results of Ref. [136], which presents a lattice computation of the electromagnetic contributions to kaon and pion masses. As we discuss below, a similar treatment is used for heavy quarks.

We conclude this part by a comment on the topological charge in lattice simulations. In production of the gauge configurations at very small lattice spacings a very slow evolution of topological charge has been seen. This in principle leads to incorrect sampling and causes small finite-volume effects. In Ref. [137], the topological-charge evolution in the ensembles used in this analysis is investigated, and it is discussed how to correct lattice data for the leading effects of unequilibrated topological charge. Although the corrections are negligible for masses of heavy-light mesons, lattice data at the finest ensembles are corrected accordingly, and uncertainties in the corrections are included in the systematic errors.

7.3. Quark mass results from EFT fit to lattice data

In Sec. 7.1, we discussed how using a cascade of EFTs we construct an effective function M_{H_x} with 67 free parameters. Here, we discuss how we determine the free parameters by fitting M_{H_x} to the lattice data summarized in Sec. 7.2.

As discussed in Sec. 7.2, the data set used in this analysis contains several lattice spacings and various masses for valence and sea quarks. In particular, a wide range of heavy-quark masses are used from near charm-quark mass to bottom-quark mass. To avoid large lattice artifacts, the heavy quark masses are restricted to $am_h < 0.9$ in the fitting procedure. The MRS mass of each heavy quark is calculated using Eq. (71).

The calculation of the MRS mass relies on having a precise value for the strong coupling. This analysis uses

$$\alpha_{\overline{\text{MS}}}(5 \text{ GeV}; n_f = 4) = 0.2128(25), \quad (77)$$

which is obtained by HPQCD collaboration [99]; this value corresponds to $\alpha_{\overline{\text{MS}}}(m_Z; n_f = 5) = 0.11822(74)$. The mean value is used in the base fit, and an uncertainty associated with $\alpha_{\overline{\text{MS}}}$ is introduced by varying its value by 1σ . To run the coupling constant to the scale μ , the QCD beta function at five-loop order accuracy [131] is employed and the differential equation is integrated numerically.

The data for the heavy-light meson masses are more precise than the data for scale-setting quantities. To account for the uncertainties in scale setting quantities, the so-called penalty trick [138] is employed. With this trick the optimized values for the scale setting quantities are obtained simultaneously in the EFT fit. Because the base fit uses data at 5 different lattice spacings, 10 additional parameters are required.

Altogether there are 384 lattice data points and 77 parameters in the base fit: 67 parameters in the effective fit function and 10 parameters for optimized values of scale-setting quantities. The analysis is performed using a constrained fitting procedure [139] with prior distributions of parameters set mainly according to expectations from EFTs and in several cases from external considerations. (See Ref. [113] for details.) The fit returns a correlated $\chi^2_{\text{data}}/\text{dof} = 320/307$, giving a p value of $p = 0.3$.

Figure 12 illustrates a snapshot of the fit for the physical mass ensembles at four lattice spacings as well as the continuum extrapolation of the fit function. The valence light mass m_x is tuned to m_s ; the graphs illustrate heavy-strange meson masses. The meson mass or the difference of the meson mass and the h -quark MRS mass are plotted versus the continuum limit of the h -quark MRS mass in Fig. 12. Data points with open symbols to the right of the dashed vertical line of the corresponding color in Fig. 12 are not included in the fit because they have $am_h > 0.9$. At nonzero lattice spacing the masses of the sea quarks are set to their simulation values, while in the continuum extrapolation the masses of sea quarks are tuned to the physical quark masses m_l , m_s and m_c .

The widths of the fit lines in Fig. 12 correspond to a part of the statistical error coming from the fit. They

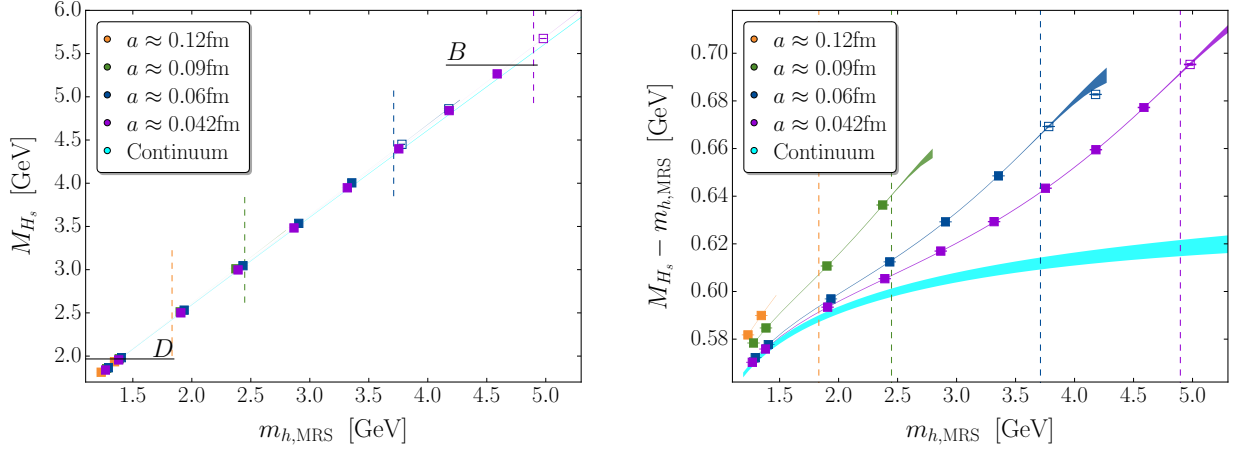


Figure 12: A snapshot of the base fit and the lattice data for heavy-strange meson masses. Only ensembles with physical light sea mass are shown. Left: heavy-strange meson mass vs. heavy-quark MRS mass. Right: difference of the heavy-strange meson mass and the heavy-quark MRS mass vs. heavy-quark MRS mass. The dashed vertical lines indicate the cut $am_h = 0.9$ for each lattice spacing, and data points with open symbols to the right of them are not included in the fit. Here $m_{h,\text{MRS}}$ is the continuum limit of the MRS mass of the heavy quark h , and its error bar is suppressed for clarity. From Ref. [113].

do not include the statistical errors coming from scale setting and tuning light quark masses. Moreover, they are sensitive to numerical errors in computing the fit parameters' covariance matrix. A jackknife procedure, with 20 jackknife resamples, is used for a robust determination of the total statistical error of each output quantity.

The fit determines the 67 free parameters of M_{H_x} including $p_1 = m_{p4s,\overline{\text{MS}}}(2\text{ GeV})$ and $p_2 = \bar{\Lambda}_{\text{MRS}}$. Moreover, the fit function evaluated at zero lattice spacing, infinite volume and physical sea-quark masses, i.e.

$$M_{H_x}(\{m_h, m_x\}, \{m_l, m_l, m_s, m_c\}, \{0, \infty\}; \{p_1, \dots, p_{67}\}), \quad (78)$$

yields the meson masses as a function of the valence heavy and light quark masses. We now define the physical charm and bottom quarks such that the D_s - and B_s -meson masses take their physical values, albeit after subtracting the electromagnetic effects from the meson masses. We use the phenomenological formula

$$M_{H_x}^{\text{expt}} = M_{H_x}^{\text{QCD}} + A e_x e_h + B e_x^2, \quad (79)$$

to relate the experimental masses to the “pure-QCD” masses. In Eq. (79), e_h and e_x are charges of the valence heavy and light components, respectively, and the coefficients are $A = 4.44\text{ MeV}$ and $B = 2.4\text{ MeV}$ [134]. For details of calculation one should consult Refs. [113, 134]. Using the experimental meson masses $M_{D_s}^{\text{expt}} = 1968.27(10)\text{ MeV}$ and $M_{B_s}^{\text{expt}} = 5366.82(22)\text{ MeV}$ [140], Eq. (79) yields the pure-QCD masses: $M_{D_s}^{\text{QCD}} = 1967.01\text{ MeV}$ and $M_{B_s}^{\text{QCD}} = 5367.04\text{ MeV}$.

Before reporting the final results for quark masses, we discuss the effects from truncating perturbative

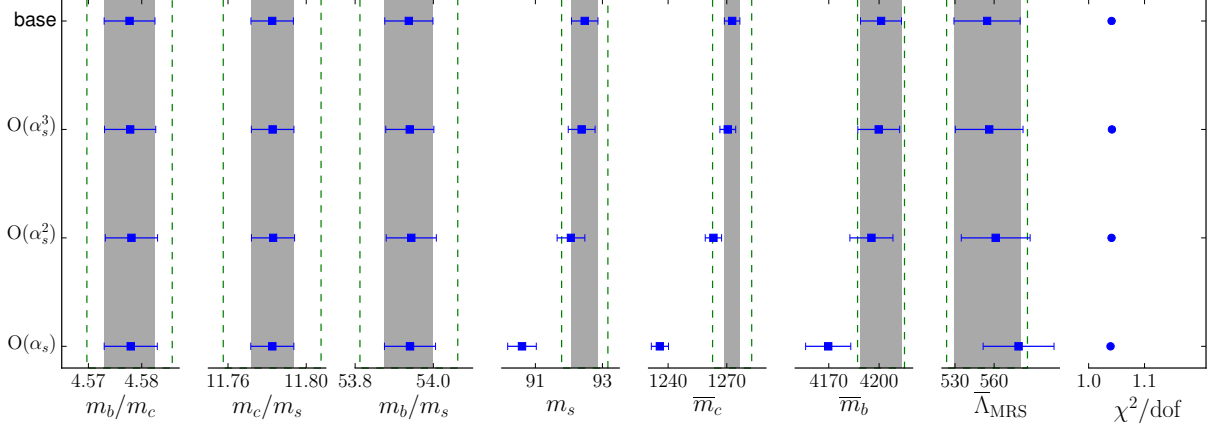


Figure 13: Stability plot showing the sensitivity to truncation error in perturbative-QCD relations. The perturbative series in the base fit are accurate through order α_s^4 . Here the strange-quark mass is given at 2 GeV, and the charm- and bottom-quark masses given in their self-consistent scales. The error bars show only the statistical errors, the gray error bands correspond to the statistical error of the base fit, and the dashed green lines correspond to total errors. From Ref. [113].

QCD in the relation between quark-mass definitions and the beta function. The analysis uses the fit parameter $m_{p4s,\overline{\text{MS}}}(2 \text{ GeV})$ and am_h/am_{p4s} to calculate $m_{h,\overline{\text{MS}}}(2 \text{ GeV})$ for each heavy quark. Then Eqs. (72) and (73) are used to calculate \overline{m}_h and Eq. (64) to calculate $m_{h,\text{MRS}}$. For these calculations we rely on known perturbative QCD results: the beta function and quark-mass anomalous dimension at five loops [130, 131] and the pole mass at four loops [127, 141]. By rerunning the analysis with fewer orders in Eqs. (73) and (64) and in the beta function one can monitor the truncation errors in perturbative QCD. Figure 13 shows the stability of the results as the order of perturbation theory is increased; $O(\alpha_s^n)$ denotes a fit that includes n orders beyond the leading terms in Eqs. (73), (64), and the beta function. The quark mass ratios are not sensitive to the truncations in the perturbative-QCD relations. This is expected because these ratios are essentially the continuum limit of the corresponding bare masses; they do not need to get renormalized. The masses of the strange, charm, and bottom quarks as well as the HQET matrix element $\overline{\Lambda}_{\text{MRS}}$ show good convergence as the order of α_s in the perturbative expressions is increased. As a result there is no need to introduce any additional systematic error associated with truncation in perturbative-QCD results. The fact that the truncation effects are negligible is a consequence of using the MRS mass in the analysis because the renormalon-subtracted perturbative coefficients in the MRS mass are all very small; see Eq. (67).

We now present the final results of this analysis. As discussed above, the first factor in Eq. (71) is the mass of the reference quark, which is set to 0.4 times the mass of the strange quark (denoted by m_{p4s}) and treated as a fit parameter. The analysis yields

$$m_{s,\overline{\text{MS}}}(2 \text{ GeV}) = 92.47(39)_{\text{stat}}(18)_{\text{syst}}(52)_{\alpha_s}(11)_{f_{\pi,\text{PDG}}} \text{ MeV}. \quad (80)$$

There are four uncertainties: statistical, which includes uncertainties from statistics and EFT fit, systematic,

discussed below, the uncertainty from the parametric input α_s , given in Eq. (77), and the uncertainty in the value of f_π used for scale setting. Note that the α_s uncertainty is the largest uncertainty in Eq. (80) where the strange quark mass is reported at 2 GeV. When running the strange quark mass, using Eqs. (72) and (73), from 2 GeV to higher scales, it turns out that the α_s uncertainty shrinks much faster than the other sources of uncertainties because of the obvious correlation with the value of α_s used in the running procedure. This is discussed further below.

We now solve M_{H_x} in Eq. (78) to obtain the points that give the pure-QCD masses $M_{D_s}^{\text{QCD}} = 1967.01$ MeV and $M_{B_s}^{\text{QCD}} = 5367.04$ MeV. This yields the mass ratios

$$m_c/m_s = 11.783(11)_{\text{stat}}(21)_{\text{syst}}(00)_{\alpha_s}(08)_{f_{\pi, \text{PDG}}}, \quad (81)$$

$$m_b/m_s = 53.94(6)_{\text{stat}}(10)_{\text{syst}}(1)_{\alpha_s}(5)_{f_{\pi, \text{PDG}}}. \quad (82)$$

Multiplying the strange quark mass in Eq. (80) and the quark mass ratios in Eqs. (81) and (82) then gives the charm- and bottom-quark masses in the $\overline{\text{MS}}$ at scale 2 GeV. For the heavy quarks, it is customary to present the quark masses at the self-consistent scale $\overline{m}_h = m_{h, \overline{\text{MS}}}(m_{h, \overline{\text{MS}}})$, which can be iteratively calculated using Eqs. (72) and (73). For the charm quark, we then obtain

$$\overline{m}_c = 1273(4)_{\text{stat}}(1)_{\text{syst}}(10)_{\alpha_s}(0)_{f_{\pi, \text{PDG}}} \text{ MeV}. \quad (83)$$

For the bottom quark, because the lattice simulations used in this analysis contain only the effects of four flavors in the sea, we should adjust the mass to include effects of the bottom quark in the sea. The adjustment can be calculated perturbatively by matching a theory with four active quarks in the sea to a theory with five active quarks. Specifically, we use [142]

$$\begin{aligned} m_b^{(n_l)}(\mu) = \overline{m}_b^{(n_f)} \left[1 + 0.2060 \left(\frac{\alpha_s^{(n_f)}(\mu)}{\pi} \right)^2 + (1.8476 + 0.0247n_l) \left(\frac{\alpha_s^{(n_f)}(\mu)}{\pi} \right)^3 \right. \\ \left. + (6.850 - 1.466n_l + 0.05616n_l^2) \left(\frac{\alpha_s^{(n_f)}(\mu)}{\pi} \right)^4 + \dots \right], \end{aligned}$$

where $n_l = n_f - 1$ and $\mu = \overline{m}_b^{(n_f)}$, and we obtain

$$\overline{m}_b^{(n_f=5)} = 4195(12)_{\text{stat}}(1)_{\text{syst}}(8)_{\alpha_s}(1)_{f_{\pi, \text{PDG}}} \text{ MeV} \quad (84)$$

in a theory with five active quarks in the sea.

In addition to the strange-, charm- and bottom-quark masses, Ref. [113] presents the up and down quark masses by combining their analysis with a separate, but correlated, analysis of light mesons from Ref. [134].

The light quark masses read

$$m_{l,\overline{\text{MS}}}(2 \text{ GeV}) = 3.402(15)_{\text{stat}}(05)_{\text{syst}}(19)_{\alpha_s}(04)_{f_{\pi,\text{PDG}}} \text{ MeV}, \quad (85)$$

$$m_{u,\overline{\text{MS}}}(2 \text{ GeV}) = 2.130(18)_{\text{stat}}(35)_{\text{syst}}(12)_{\alpha_s}(03)_{f_{\pi,\text{PDG}}} \text{ MeV}, \quad (86)$$

$$m_{d,\overline{\text{MS}}}(2 \text{ GeV}) = 4.675(30)_{\text{stat}}(39)_{\text{syst}}(26)_{\alpha_s}(06)_{f_{\pi,\text{PDG}}} \text{ MeV}, \quad (87)$$

where m_l is the average of the up- and down-quark masses.

This analysis directly yields results for the HQET matrix elements. It is worthwhile to present the HQET matrix element $\bar{\Lambda}$ in the MRS scheme:

$$\bar{\Lambda}_{\text{MRS}} = 555(25)_{\text{stat}}(8)_{\text{syst}}(16)_{\alpha_s}(1)_{f_{\pi,\text{PDG}}} \text{ MeV}. \quad (88)$$

In addition to computing the quark masses, mass ratios, and HQET matrix elements, the fit function can be used to investigate flavor splittings in the D - and B -meson systems as well as their SU(2) and SU(3) chiral limits. We refer the readers to Ref. [113] for the results and end this section with a few remarks.

A brief discussion on different sources of uncertainties in quark masses may be in order. The systematic error of each quantity includes systematic effects that are not captured in the EFT fit to lattice data. These are systematic uncertainties in scale setting quantities, light quark mass tuning, finite volume effects, topological charge distribution, the excited-state contamination in two-point correlator fits, and finally electromagnetic effects. For the full descriptions of the systematic error the reader should see Ref. [113]. In particular, Table I in Ref. [113] tabulates the contribution of each source of uncertainty. One can see that these systematic effects are relatively small for quark masses especially for the heavy quark masses. They, however, get enhanced in ratios of quark masses; see Eqs. (81) and (82). This is due to the fact that the statistical, α_s , and $f_{\pi,\text{PDG}}$ uncertainties in the quark masses are highly correlated and thus they cancel in the quark mass ratios while this is not the case for the systematic errors.

The α_s uncertainty in the results for quark masses in Eqs. (80) and (83)–(87) is one of the largest uncertainties. As mentioned above, when we run the quark masses to higher scales, using (72) and (73), the error bars corresponding to the α_s uncertainty shrinks faster than the other sources of uncertainties. This happens because there is 100% correlation between the α_s uncertainty in the quark masses and the uncertainty in the value of α_s given in Eq. (77), which is used for running the quark masses. For convenience, we also present the up-, down-, strange-, and charm-quark masses at 3 GeV and the bottom-quark mass at

10 GeV:

$$m_{l,\overline{\text{MS}}}(3 \text{ GeV}) = 3.072(13)_{\text{stat}}(04)_{\text{syst}}(10)_{\alpha_s}(04)_{f_{\pi,\text{PDG}}} \text{ MeV}, \quad (89)$$

$$m_{u,\overline{\text{MS}}}(3 \text{ GeV}) = 1.923(16)_{\text{stat}}(32)_{\text{syst}}(06)_{\alpha_s}(02)_{f_{\pi,\text{PDG}}} \text{ MeV}, \quad (90)$$

$$m_{d,\overline{\text{MS}}}(3 \text{ GeV}) = 4.221(27)_{\text{stat}}(35)_{\text{syst}}(14)_{\alpha_s}(05)_{f_{\pi,\text{PDG}}} \text{ MeV}, \quad (91)$$

$$m_{s,\overline{\text{MS}}}(3 \text{ GeV}) = 83.49(36)_{\text{stat}}(16)_{\text{syst}}(28)_{\alpha_s}(10)_{f_{\pi,\text{PDG}}} \text{ MeV}, \quad (92)$$

$$m_{c,\overline{\text{MS}}}(3 \text{ GeV}) = 983.7(4.3)_{\text{stat}}(1.4)_{\text{syst}}(3.3)_{\alpha_s}(0.5)_{f_{\pi,\text{PDG}}} \text{ MeV}, \quad (93)$$

$$m_{b,\overline{\text{MS}}}(10 \text{ GeV}; n_f = 5) = 3665(11)_{\text{stat}}(1)_{\text{syst}}(1)_{\alpha_s}(1)_{f_{\pi,\text{PDG}}} \text{ MeV}. \quad (94)$$

Remarkably, the α_s uncertainty becomes negligible at 10 GeV and higher scales relevant to the physics beyond the Standard Model.

The results presented here show that the combined EFT and lattice QCD program developed in Refs. [112, 113] and highlighted here is both qualitatively and quantitatively successful. The qualitative success relies on the clean separation of scales provided by HQET with the MRS definition of the heavy-quark mass. The quantitative success relies on the high statistics of the MILC collaboration's HISQ ensembles [100, 133], as well as the availability of high order coefficients in perturbation theory: the order- α_s^5 coefficient for the running of the quark mass [130] and strong coupling [131], and the order- α_s^4 coefficient for relating the $\overline{\text{MS}}$ mass to the pole mass and, consequently, the MRS mass [127, 141].

As the concluding remark, note that this program can be considered, on the one hand, as an application of EFTs in extracting real-world results (quark masses) from lattice simulations and, on the other hand, as an application of lattice simulations in computing parameters of EFTs (such as \bar{A}_{MRS}). For a review on different aspects of connection between EFTs and lattice QCD see, for example, Ref. [143].

8. Other determination of α_s

In the previous sections we discussed α_s determinations using the static quark-antiquark energy and moments of quarkonium correlators. In this section we will briefly review other lattice determinations of the strong coupling constant. We will only consider α_s determinations that are based on $2 + 1$ flavor and $2 + 1 + 1$ flavor calculations since these are the only phenomenologically relevant ones. We note, however, that determinations of the strong coupling constant for smaller number of dynamical quark flavors, including no dynamical quarks, are interesting for understanding of systematic effects in the underlying calculations. These are discussed in detail in the FLAG review [46].

In the following subsection we will discuss α_s determinations from step scaling analysis, small Wilson loops, hadronic vacuum polarization, QCD vertices and eigenvalues of the Dirac operators. We will present average values of $\alpha_s(M_Z)$ obtained from each of these methods.

8.1. α_s determination from step scaling

The step scaling method allows to calculate α_s at large energy scales while avoiding the window problem. In this method one defines a coupling $g_S^2(1/L)$, where L is the size of the lattice with the specified boundary conditions. The boundary conditions here define the scheme for the coupling constant. Then one decreases the box size, while keeping $L \gg a$ and follows the running of the coupling constant. For sufficiently small L the coupling constant $g_S^2(1/L)$ can be related to the coupling constant in $\overline{\text{MS}}$ scheme, $g_{\overline{\text{MS}}}^2(1/L) = g_S^2(1/L)(1 + c^1 g_S^2(1/L) + c^2 g_S^4(1/L) + \dots)$. One first starts at some $g_S^2(1/L_{\text{max}})$ with $L_{\text{max}} \sim 1$ fm. Using lattice calculations in large volumes and the same lattice action one determines L_{max} in the continuum limit for example by performing calculations of L_{max}/r_0 at several lattice spacings and then extrapolating to the continuum, $a \rightarrow 0$ limit. Then one studies the change of the coupling constant as ν changes from $1/L_{\text{max}}$ to s^n/L_{max} for $n = 2, 3, 4, \dots$ until ν reaches a large enough energy scale, where the resulting coupling can be converted to $\overline{\text{MS}}$ scheme.

In practice Schrödinger functional (SF) boundary conditions are used because the relation of the coupling constant in this scheme to the $\overline{\text{MS}}$ coupling is known to two-loop order. In the SF scheme Dirichlet boundary conditions are imposed in the time direction [144]

$$A_k(x)|_{x_0=0} = C_k, \quad A_k(x)|_{x_0=L} = C'_k, \quad k = 1, 2, 3. \quad (95)$$

Periodic boundary conditions are imposed on gluon and quark fields. Here C_k and C'_k are diagonal 3×3 matrices that depend on a real dimensionless parameter η [144]. The coupling constant in this scheme is defined in terms of the derivative of the effective action

$$\partial_\eta \langle S \rangle|_{\eta=0} = \frac{12\pi}{g_{SF}^2}. \quad (96)$$

One could also use the gradient flow coupling for the step scaling method [145–147]. The first step scaling analysis in 2+1+1 flavor QCD was done by the PACS collaboration using the SF scheme [148]. They obtained $\alpha_s = 0.1183$ [148]. More recently the ALPHA collaboration determined α_s using a step scaling analysis of the gradient flow coupling and the SF coupling [149]. For $2 \text{ GeV} < \nu < 4 \text{ GeV}$ the gradient flow coupling was used. They switched to SF coupling at 4 GeV and determined the running of the SF coupling until $\nu = 70 \text{ GeV}$, where the two-loop relation to the $\overline{\text{MS}}$ coupling is sufficiently accurate. The use of the gradient flow coupling allowed the ALPHA collaboration to significantly reduce the statistical errors at small values of ν and obtain a precise determination [149]

$$\alpha_s(M_Z) = 0.11852(84). \quad (97)$$

This result agrees well with the PACS determination but has much smaller error. Therefore we will use it as the α_s value from the step scaling method. The experimental input of this result is the scale $f_{\pi K} = (2f_K + f_\pi)/3 = 147.6(5) \text{ MeV}$, which is sub-leading in the error budget.

8.2. α_s from small Wilson loops

One could try to determine the strong coupling constant from short distance quantities calculated on the lattice. In this case the relevant scale is $\mu \sim 1/a$. Examples of such short distance quantities are the small Wilson loops or quantities derived from them, e.g. Creutz ratios. If the lattice spacing is sufficiently small the quantities can be calculated in lattice perturbation theory. However, it is well known that the convergence of lattice perturbation theory is poor. This problem can be cured if the perturbative series are expressed in terms of some renormalized coupling like α_V [86]. For quantities X obtained from small Wilson loops the perturbative series can be written as

$$X = \sum_n c_n^X \alpha_V(q^*). \quad (98)$$

The coefficients c_n^X are known through $n = 3$ and the scale $q^* = d^X/a$ [150], where d^X slightly depends on the chosen quantity [151], but typically $d^X \sim \pi$. Comparing results from lattice QCD calculations with the above perturbative expression one obtains $\alpha_V(q^*)$, which then can be converted to α_s in $\overline{\text{MS}}$ scheme. In this approach there is no problem with the continuum extrapolations since the comparison to perturbation theory is performed at finite lattice spacing. The reliability of this method is limited by the accuracy of the perturbative result and the smallness of the lattice spacing. Typically relatively large scales can be achieved since q^* is larger than the inverse lattice spacing.

The strong coupling constant has been determined by the HPQCD collaboration [95, 150, 152] as well as by Maltman et al [153] using this approach. The lattice data sets entering the above analyses largely overlap. The analysis of Ref. [95] results in $\alpha_s(M_Z) = 0.1184(6)$ and supersedes the previous HPQCD determinations since it uses finer lattices. Maltman et al use a different analysis strategy of the perturbative expansion and the condensates. They also use a subset of the data from Ref. [152] and obtain $\alpha_s(M_Z) = 0.1192(11)$ [153]. Performing the weighted average of the above values we estimate the central value and error of $\alpha_s(M_Z)$ to be $0.1185^{+0.0006}_{-0.0005}$. The uncertainty of the experimental input, f_π , which contributes to the uncertainty of the lattice scale r_1 , is sub-leading in the error budget in both studies.

8.3. The strong coupling constant from hadronic vacuum polarization

The idea behind this approach is similar to the one based on the moments of quarkonium correlation functions but uses the vector or axial-vector current of light quarks. Let us consider the correlator

$$\Pi_{\mu\nu}(q) = \int d^4x e^{iqx} \langle j_\mu(x) j_\nu^\dagger(0) \rangle, \quad (99)$$

where j_μ is the non-singlet vector or axial vector current. The correlator can be decomposed into transverse and longitudinal components

$$\Pi_{\mu\nu}(q) = (q^2 g_{\mu\nu} - q_\mu q_\nu) \Pi^1(q^2) - q_\mu q_\nu \Pi^0(q^2). \quad (100)$$

In the isospin symmetric limit $\Pi_{\mu\nu}(q)$ is purely transverse, i.e. $\Pi^0 = 0$. For Euclidean momenta $Q^2 = -q^2 > 0$, Π^1 can be calculated in terms of OPE. Here the large scale is given by the momentum transfer not by the quark masses. The OPE is conveniently formulated in terms of Adler function, defined as

$$D(Q^2) = -q^2 \frac{d\Pi^1}{dq^2}, \quad (101)$$

which is regularization and scheme independent. The OPE in terms of Adler function is written as

$$D(Q^2) = D^{(0)}(Q^2, \nu^2) + \frac{m_l^2}{Q^2} D^{(2)}(Q^2, \nu^2) + \sum_{n=2} \frac{c_{2n}}{Q^{2n}}. \quad (102)$$

$D^{(0)}$ is known to five-loop [27, 154–156], i.e. to order α_s^4 , $D^{(2)}$ is known only to two-loop, but the corresponding contribution being proportional to m_l^2 is numerically small. The last term in the above expression parametrizes the nonperturbative contribution to the Adler function in terms of the local condensates. For sufficiently large Q^2 the nonperturbative contribution to $D(Q^2)$ is small, and comparing the Adler function obtained on the lattice to Eq. (102), we can extract $\alpha_s(\nu)$ at some scale ν that is not too different from Q . A first analysis of this kind was performed by JLQCD/TWQCD for two flavors of light dynamical quarks [157] and then by the JLQCD collaboration in 2+1 flavor case [158]. While the perturbative calculation of the Adler function is available at high orders this method is very challenging because of the window problem. For small values of a the contribution of the condensates is significant, while at large Q^2 we have to deal with large discretization effects. The determination in Ref. [158] resulted in a very low value of α_s , $\alpha_s(M_Z) = 0.1118(3)(+16)(-17)$. The systematic errors in this method have been carefully studied in Ref. [159] involving the lead authors of the previous work. In particular, the values of Q were limited to the one closest to the diagonal in order to minimize the discretization effects. This analysis resulted in $\alpha_s(M_Z) = 0.1184(27)(+8)(-22) = 0.1184(34)$. We added the errors in quadrature and symmetrized the final error in the last equation. The experimental input for this study is the Omega baryon mass, which is sub-leading in the error budget.

8.4. The strong coupling constant from QCD vertices

A straightforward way to obtain the strong coupling constant is to calculate three- and four-gluon vertices or quark-gluon and ghost-gluon vertices in a fixed gauge on the lattice. The QCD coupling constant can be related to the renormalization constants of these vertices. In practice one uses the Landau gauge and the renormalized coupling constant is defined in some intermediate MOM like scheme. For pioneering studies within this approach we refer the reader to Refs. [160, 161]. The ghost-gluon vertex offers an attractive possibility to extract α_s because it involves only the calculation of the ghost and gluon two-point functions [162]. Furthermore, it is practical to use the MOM Taylor scheme in which the renormalized running coupling constant is defined as [163]

$$\alpha_T(\nu) = \frac{g_T^2(\nu)}{4\pi} = Z_3(\nu^2, a^2) \tilde{Z}_3(\nu^2, a^2) \frac{g_0^2(a)}{4\pi}, \quad (103)$$

where $Z_3(\nu^2, a^2)$ and $\tilde{Z}_3(\nu^2, a^2)$ are the gluon and ghost propagator renormalization constants and g_0^2 is the bare lattice gauge coupling. For a large value of ν , the strong coupling constant in this scheme, $\alpha_T(\nu)$ can be written as sum of the perturbative result and a nonperturbative contribution due to the dimension-two gluon condensate $\langle A^2 \rangle$ in Landau gauge [163]. The running of α_T is known to four-loop [164], and the relation between the Λ parameter of the MOM Taylor scheme and the $\overline{\text{MS}}$ scheme is also known [164]. As many other methods this approach, too, suffers from the window problem: for small ν the nonperturbative contributions like the ones from the dimension-two gluon condensate are large, while for large ν discretization errors are important. Determinations of the strong coupling constant along these lines have been carried out by ETM collaboration for 2+1+1 flavors using twisted mass fermions [165–167]. Discretization effects have been carefully studied in the above publications. The latest ETM analysis gave $\alpha_s(M_Z) = 0.1196(4)(8)(6)$ [167] or 0.1196(11) if all errors are combined in quadrature. The experimental input for this study is the pion decay constant, which is sub-leading in the error budget. This result supersedes the previous ETM determinations. Very recently the determination of α_s using this approach but the DWF formulation and 2+1 flavors has been reported [168]. This study finds $\alpha_s(M_Z) = 0.1172(11)$ [168]. The experimental input for this study is the Omega baryon mass, which is sub-leading in the error budget. This clearly deviates from the previous result by more than one sigma, possibly indicating that not all systematic errors in this method are under control. Taking the weighted average of the above result gives $\alpha_s(M_Z) = 0.1184$. We assign an error of 0.0012 to this result to cover the spread in individual determinations.

8.5. The strong coupling constant from eigenvalues of the Dirac operator

One can also determine the strong coupling constant from the eigenvalues λ of the Dirac operator. For sufficiently large λ values the density of eigenvalues can be calculated in perturbation theory

$$\rho(\lambda) = \frac{3}{4\pi^3} \lambda^3 (1 + \alpha_s \rho_1 + \alpha_s^2 \rho_2 + \alpha_s^3 \rho_3 + \dots), \quad (104)$$

with known coefficients ρ_1, ρ_2 and ρ_3 in the $\overline{\text{MS}}$ scheme [169, 170]. The eigenvalues of the Dirac operator using overlap fermions have been analyzed in Ref. [171]. The analysis gives [171]

$$\alpha_s(M_Z) = 0.1226(36). \quad (105)$$

The experimental input for this study is the Omega baryon mass used in setting the gradient flow scale $\sqrt{t_0}$, which is sub-leading in the error budget.

9. Other heavy quark mass determinations

In the sections 4 and 5 we discussed the quark mass determination using reduced moments of quarkonium correlators and the EFT approach. In the EFT approach the quark mass determination relies on HQET

and chiral perturbation theory to interpolate the hadron mass dependence on the quark masses. In other approaches one calculates the bare quark masses that correspond to physical values of a set of hadron masses and then performs the renormalization to obtain the quark masses in the $\overline{\text{MS}}$ scheme. The calculations of the reduced moments can be viewed as a special method to calculate these renormalization constants. A more conventional approach to calculate the quark mass renormalization is to use some intermediate scheme like MOM or SF non-perturbatively on the lattice and then use the relation of these intermediate schemes to the $\overline{\text{MS}}$ scheme to finally obtain the $\overline{\text{MS}}$ scheme quark masses. In the following subsection we will briefly review the determination of the charm quark and bottom quark masses using this approach. As has already been pointed out, the determination of the bottom quark mass on the lattice is challenging because the bare bottom quark mass in lattice units is not small. In this case using some form of EFT approach and perturbation theory is necessary. It is customary to quote the charm quark mass in the $\overline{\text{MS}}$ scheme at a scale equal to the charm quark mass, i.e. $m_c = m_c(m_c)$ for four active flavors, see e.g. [49]. Similarly, the bottom quark mass, m_b is quoted at the scale of the bottom quark mass, $m_b = m_b(m_b)$ and five active flavors. In what follows we will show the results for the charm and bottom quark masses using this convention unless stated otherwise.

9.1. Charm quark mass determination

In 2+1 flavor QCD there is a determination of the charm quark mass from the χ QCD collaboration using overlap fermions in the valence sector and domain wall fermions for the sea quarks. They use two lattice spacings $a = 0.087$ fm and $a = 0.11$ fm and several light quark masses corresponding to a pion mass in the range of 290 MeV to 420 MeV. They obtain $1.304(5)(20)$ GeV [172]. We note, however, that using only two lattice spacings may be problematic for obtaining reliable continuum results for the charm quark mass. There are two charm quark mass determinations by the ETM collaboration using $N_f = 2 + 1 + 1$ and twisted mass fermion action [173, 174]. In Ref. [173] the bare charm quark mass was determined using D and D_s meson masses resulting in $m_c = 1.348(46)$ GeV, while in Ref. [174] the Ω_c^+ was used to fix the bare charm quark mass leading to $m_c = 1.3478(27)(195)$ GeV. The HPQCD collaboration used the same lattice setup as for the calculation of moments of quarkonium correlators to determine the renormalization factors for the quark masses in RI-sMOM scheme [175]. Using these for the charm quark mass they obtain $m_c = 1.2757(84)$ GeV. This value agrees well with the HPQCD determination using the moments of quarkonium correlators.

9.2. Bottom quark mass determination

To deal with the problem of the large bottom quark mass one can use NRQCD. The HPQCD collaboration calculated the Υ masses using NRQCD and $N_f = 2 + 1$ [176]. The NRQCD mass parameter, m_{b0} , can be related to the $\overline{\text{MS}}$ bottom quark mass using three-loop perturbation theory [176]. With this approach the HPQCD collaboration obtained $m_b = 4.166(43)$ GeV using a single volume and pion mass of around

300 MeV [176]. Using only one lattice volume and a single value of the pion mass that is larger than the physical value may be of some concern. However, we note that the \mathcal{V} mass is largely insensitive to the pion mass and is not much affected by the volume. One can also calculate the moments of bottomonium correlators also in NRQCD [177]. Such calculations have been performed by the HPQCD collaboration using the HISQ action for the sea quarks and $N_f = 2 + 1 + 1$. The ratio of the moments of bottomonium correlators together with the ratio of the lattice kinetic mass of bottomonium and the lattice NRQCD mass parameter, m_{b0} , can be related to the ratio of the experimental bottomonium mass and the $\overline{\text{MS}}$ b-quark mass. Using this relation the HPQCD obtained $m_b = 4.196(23)$ GeV.

The ETM collaboration calculated the heavy-light and heavy-strange meson masses using the twisted mass action in (2+1+1)-flavor QCD [178]. Using HQET analysis these masses can be related to the pole mass in the static limit [178], which then can be converted to the $\overline{\text{MS}}$ b-quark mass. With this approach the ETM collaboration obtains $m_b(\mu = m_b, N_f = 4) = 4.26(10)$ GeV. Finally Gambino et al used the same gauge configurations as the above ETM study and a very similar method to obtain m_b [179]. The main difference in their analysis is that they relate the bottom quark mass to the kinetic mass, and obtain $m_b(\mu = m_b, N_f = 4) = 4.26(18)$ [179].

10. Executive summary of the strong coupling constant and heavy quark mass determinations

In this section we present an executive summary of the lattice determinations of the strong coupling constant and heavy quark masses.

We reviewed lattice determinations of α_s using different methods. For all the methods, with the exception of the Dirac operator eigenvalue approach, there are calculations performed by different groups. This allows to cross-check the error estimates within a given method. We performed pre-averages for each of the methods of α_s determination and assigned errors to these pre-averages to cover the spread in the individual determination within one method. The summary of different lattice determinations is shown in Fig. 14. The pre-averages are indicated by the green bands in the figure. As one can see from the figure there is no large tension between different lattice determinations of α_s . We note that different methods have quite different sources of systematic errors, so the lack of significant tension is non-trivial check of the lattice methods. As has been pointed out the major uncertainties are due to the perturbative errors and the continuum extrapolation for most of the methods. The step scaling method has control over these effects as large scales can be reached with controllable discretization errors. Because of the high energy scale the perturbative errors in this method are negligible. Since different lattice methods have different systematic errors it makes sense to perform a weighted average of α_s performed by different methods using the pre-averages. This procedure is similar to the one used by PDG and FLAG.

Performing the weighted averages of the pre-averages as well as the α_s determination from hadronic

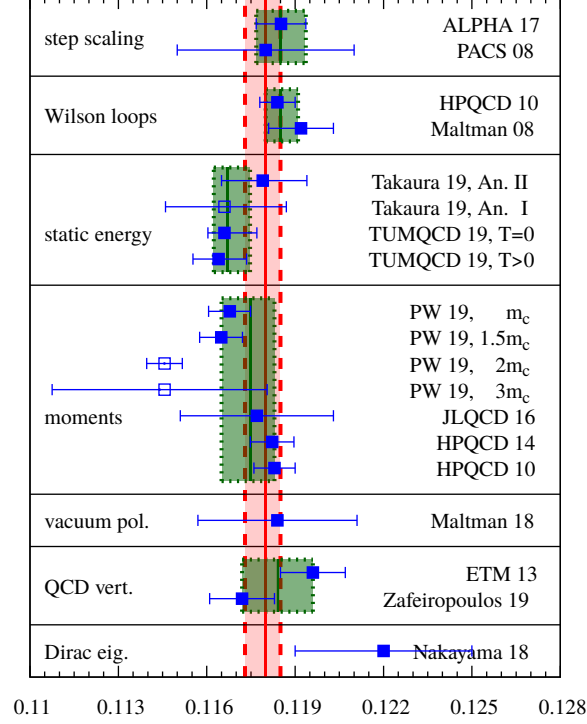


Figure 14: Summary of lattice determinations of $\alpha_s(M_Z)$ using different methods. Green boxes show the pre-averages for the different observables. Open symbols do not enter the averaging procedure, see text.

vacuum polarization and eigenvalues of the Dirac operators we obtain

$$\alpha_s(M_Z) = 0.11803^{+0.00047}_{-0.00068}, \quad \chi^2/\text{d.o.f.} = 6.54/6. \quad (106)$$

The combined lattice result has a smaller error than the step scaling method, $\alpha_s(M_Z) = 0.11852(84)$, which can be considered as the most reliable. On the one hand, if we perform the average without the static energy result, we obtain $\alpha_s(M_Z) = 0.11838^{+0.00044}_{-0.00048}$, $\chi^2/\text{d.o.f.} = 2.75/5$. Furthermore, if we perform the average without the eigenvalues of the Dirac operator, we obtain $\alpha_s(M_Z) = 0.11802^{+0.00046}_{-0.00069}$, $\chi^2/\text{d.o.f.} = 4.79/5$. Finally, if we perform the average without the step scaling result, we obtain $\alpha_s(M_Z) = 0.11791^{+0.00054}_{-0.00074}$, $\chi^2/\text{d.o.f.} = 6.39/5$, which agrees well with the other numbers. Thus, the combination of all lattice determinations other than the step scaling analysis leads to consistent and similarly accurate results. The consistency of different lattice averages confirms that the errors of the lattice determinations are indeed realistic.

There are several determinations of the charm quark mass. The determination of the charm quark mass first involves the determination of the bare charm quark mass in the lattice scheme by matching the

masses of hadrons with charm quarks to the corresponding experimental values, and then performing the renormalization to obtain the charm quark mass in $\overline{\text{MS}}$ scheme. Typically the renormalization involves the use of some intermediate scheme like RI-MOM. The method of reduced moments can be considered as a special method of calculating the renormalization constant. The perturbative errors as well as the errors of the continuum extrapolation in the charm quark mass determination are mostly under control. Perhaps the largest uncertainty is due to the determination of the lattice spacing. In Fig. 15 we show the summary of the charm quark mass determinations on the lattice. Different lattice determination of m_c are consistent with each other, except for the ETM result. There is a clear tension between the results from ETM collaboration and other lattice calculations. There are several determinations of the charm quark mass using the reduced moments of quarkonium correlators. These determinations are grouped together in Fig. 15 and agree well with each other. We performed a weighted average of the corresponding results, which gave $m_c^{\text{mom}} = 1.2729(42)$ GeV and $\chi^2/\text{d.o.f.} = 0.66$. Taking this value together with m_c determinations from other methods we calculated the weighted average of m_c . When results from ETM collaborations are included in the averaging we obtain $m_c = 1.2768(64)$ and $\chi^2/\text{d.o.f.} = 3.53$. The large value of $\chi^2/\text{d.o.f.}$ indicates the incompatibility of ETM results with other lattice determinations. If we perform the averaging excluding the ETM results we obtain

$$m_c(\mu = m_c, N_f = 4) = 1.2743(35), \quad \chi^2/\text{d.o.f.} = 0.72. \quad (107)$$

The central value of m_c did not change within errors but the resulting error is reduced almost by factor two. We will use the above value as our final estimate for the charm quark mass. The above value of the charm quark mass is considerably more precise than the PDG value. This is partly due to the averaging procedure but also to some quite precise individual lattice determinations. We note that the two most precise determination of m_c , the TUMQCD/MILC/FNAL determination and the combined determination from the moment method agree very well with each other. This suggests that the error in Eq. (107) is realistic, since the two methods have different systematic errors.

The lattice determination of the bottom quark mass is challenging because of the large discretization effects that are proportional to powers of am_b . In the moment method one has to use very fine lattices to ensure that the continuum extrapolation is under control. The problem of the large bottom-quark mass causing large discretization effects can be avoided by combining EFT and lattice approaches as discussed in sections 7 and 9. The determination of the bottom quark mass using such methods can be very precise. The lattice determinations of the bottom quark mass is summarized in Fig. 16. The different lattice determinations agree well with each other. The bottom quark mass determination by TUMQCD/MILC/FNAL collaboration [113] is the most precise one. The bottom quark mass in Refs. [178, 179] was given for four active flavors. We converted the results for the five flavor theory using perturbative decoupling at the value of $m_b(\mu = m_b)$ [101]. As for the charm quarks we took a pre-average of the bottom quark mass determinations

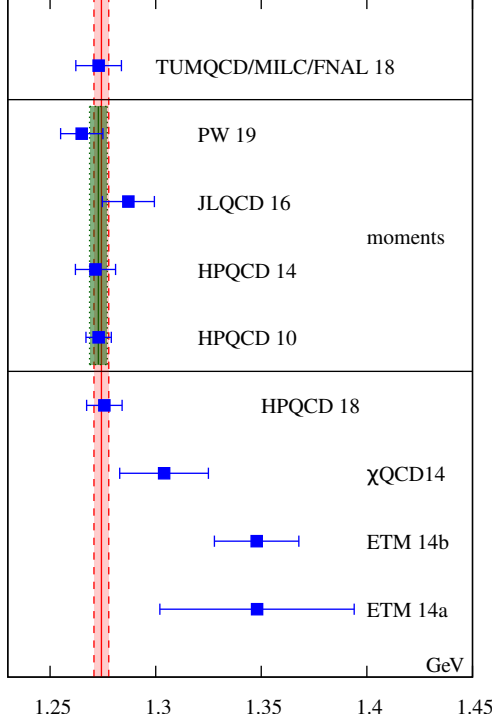


Figure 15: The summary of charm quark mass determinations by different lattice groups. The labels TUMQCD/MILC/FNAL 18, PW 19, JLQCD 16, HPQCD 14, HPQCD 10, HPQCD 18, χ QCD14, ETM 14b, ETM 14a correspond to the results from Refs. [113], [97], [98], [99], [95], [175], [172], [173] and [174], respectively. The vertical line and band correspond to the value of the charm quark mass given in Eq. (107) and its uncertainty. The green box shows the pre-average for the moments.

from the moments of quarkonium correlators which resulted in $m_b^{\text{mom}} = 4.169(19)$ GeV and $\chi^2/\text{d.o.f.} = 0.17$. Using this value together with other lattice determinations and performing the weighted average results in

$$m_b(\mu = m_b, N_f = 5) = 4.188(10), \quad \chi^2/\text{d.o.f.} = 0.46. \quad (108)$$

This average value is shown in Fig. 16 as the vertical line with the corresponding error band. This value is more precise than the PDG value and the consistency of different approaches suggest that the error is indeed realistic.

11. Conclusions

In this review paper we discussed the lattice determinations of the strong coupling constant and the heavy quark masses. We emphasized the role of the EFT approach in the determinations of these parameters. We explained how the use of combined lattice and EFT approaches helps the determination of the quark masses

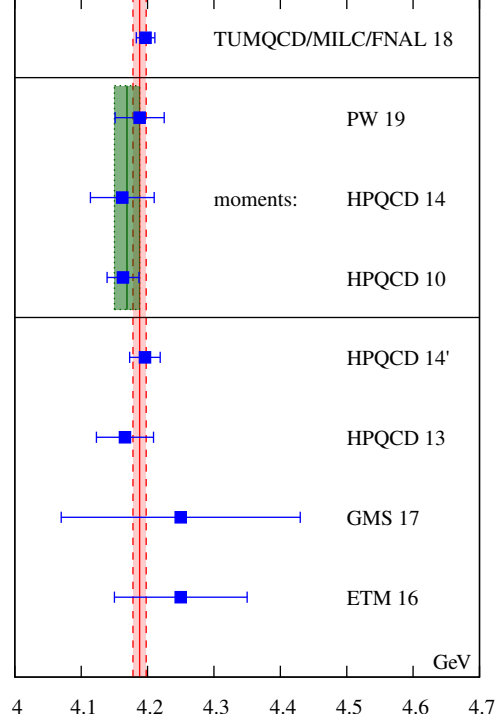


Figure 16: The summary of bottom quark mass determinations by different lattice groups. The labels TUMQCD/MILC/FNAL 18, PW 19, HPQCD 14, HPQCD 10, HPQCD 14', HPQCD 13, GMS 17, ETM 16 refer to results from Refs. [113], [97], [99], [95], [177], [176], [179] and [178], respectively. The vertical line and band correspond to the value of the bottom quark mass given in Eq. (108)) and its uncertainty. The green box shows the pre-average for the moments.

and the strong coupling constant. The use of NRQCD and HQET is very important for the determination of the bottom quark masses. Combining lattice calculations with HMrAS χ PT leads to the most accurate determination of strange, charm and bottom quark masses. We have found that with very few exceptions the lattice determinations are consistent with each other and therefore the lattice determination of the heavy quark masses and α_s can be considered as quite reliable. Our main results are given by Eqs. (106), (107) and (108). These lattice results on the strong coupling constant, charm-quark mass and bottom-quark mass are considerably more precise than the ones obtained by PDG.

Acknowledgments

JK would like to thank the Fermilab Lattice, MILC, and TUMQCD collaborations for such a fruitful collaboration. JHW would like to thank the TUMQCD collaboration for the productive work, and, in particular, Y. Kiyo for the useful discussions and the correspondence of the static energy results with

domain-wall fermions. JHW was supported by the U.S. Department of Energy, Office of Science, Office of Nuclear Physics and Office of Advanced Scientific Computing Research within the framework of Scientific Discovery through Advance Computing (SciDAC) award Computing the Properties of Matter with Leadership Computing Resources. PP was supported by the U.S. Department of Energy under Contract No. DE-SC0012704.

Appendix A. Coefficients of the force at N³LL

In this appendix, we summarize the set of coefficients that appear in the various weak-coupling results that are used in this review.

For N_c being the number of colors, the $SU(N_c)$ color factors read

$$C_F = \frac{N_c^2 - 1}{2N_c}, \quad C_A = N_c, \quad T_F = \frac{1}{2}. \quad (\text{A.1})$$

The QCD beta function is

$$\frac{d\alpha_s(\nu)}{d\ln\nu} = \alpha_s\beta(\alpha_s) = -\frac{\alpha_s^2}{2\pi} \sum_{n=0}^{\infty} \left(\frac{\alpha_s}{4\pi}\right)^n \beta_n = -2\alpha_s \left[\beta_0 \frac{\alpha_s}{4\pi} + \beta_1 \left(\frac{\alpha_s}{4\pi}\right)^2 + \dots \right], \quad (\text{A.2})$$

where the first three coefficients read [180, 181]

$$\beta_0 = \frac{11}{3}C_A - \frac{4}{3}T_F N_f, \quad (\text{A.3})$$

$$\beta_1 = \frac{34}{3}C_A^2 - \frac{20}{3}C_A N_f T_F - 4C_F N_f T_F, \quad (\text{A.4})$$

$$\beta_2 = \frac{2857}{54}C_A^3 + \left(-\frac{1415}{27}C_A^2 - \frac{205}{9}C_A C_F + 2C_F^2\right) N_f T_F + \left(\frac{158}{27}C_A + \frac{44}{9}C_F\right) N_f^2 T_F^2. \quad (\text{A.5})$$

N_f is the number of active massless quarks. The higher-order coefficients β_3 , and β_4 are also known [180, 181], but are not reproduced for brevity's sake.

The singlet potential V_s in Eq. (13) is given in terms of the coupling $\alpha_V(q^2)$, or in terms of the integral of the N³LO force with or without the resummation of leading ultrasoft logarithms, i.e. Eqs. (19) or (20), respectively. In the following we collect the coefficients in these weak-coupling expressions. We reproduce the coefficients \tilde{a}_i as given in Ref. [71]

$$\tilde{a}_1 = a_1 + 2\gamma_E \beta_0, \quad (\text{A.6})$$

$$\tilde{a}_2 = a_2 + \left(\frac{\pi^2}{3} + 4\gamma_E^2\right) \beta_0^2 + \gamma_E (4a_1 \beta_0 + 2\beta_1), \quad (\text{A.7})$$

$$\begin{aligned} \tilde{a}_3 = & a_3 + \left(8\gamma_E^3 + 2\gamma_E \pi^2 + 16\zeta(3)\right) \beta_0^3 + 2\gamma_E \beta_2 \\ & + \left[(12\gamma_E^2 + \pi^2) \beta_0^2 + 4\gamma_E \beta_1\right] a_1 + \left[6a_2 \gamma_E + \frac{5}{2} \left(4\gamma_E^2 + \frac{\pi^2}{3}\right) \beta_1\right] \beta_0, \end{aligned} \quad (\text{A.8})$$

where the coefficients a_1 and a_2 read [57–59]

$$a_1 = \frac{31}{9}C_A - \frac{20}{9}T_F N_f, \quad (\text{A.9})$$

$$a_2 = \left(\frac{4343}{162} + 4\pi^2 - \frac{\pi^4}{4} + \frac{22}{3}\zeta(3) \right) C_A^2 - \left(\frac{1798}{81} + \frac{56}{3}\zeta(3) \right) C_A T_F N_f - \left(\frac{55}{3} - 16\zeta(3) \right) C_F T_F N_f + \left(\frac{20}{9} T_F N_f \right)^2. \quad (\text{A.10})$$

The coefficient a_3 reads [62, 63]

$$a_3 = a_3^{(3)} N_f^3 + a_3^{(2)} N_f^2 + a_3^{(1)} N_f + a_3^{(0)}, \quad (\text{A.11})$$

$$a_3^{(3)} = - \left(\frac{20}{9} \right)^3 T_F^3$$

$$a_3^{(2)} = \left(\frac{12541}{243} + \frac{368}{3}\zeta(3) + \frac{64\pi^4}{135} \right) C_A T_F^2 + \left(\frac{14002}{81} - \frac{416}{3}\zeta(3) \right) C_F T_F^2 \quad (\text{A.12})$$

$$a_3^{(1)} = (-709.717) C_A^2 T_F + \left(-\frac{71281}{162} + 264\zeta(3) + 80\zeta(5) \right) C_A C_F T_F$$

$$+ \left(\frac{286}{9} + \frac{296}{3}\zeta(3) - 160\zeta(5) \right) C_F^2 T_F + (-56.83(1)) \frac{18 - 6N_c^2 + N_c^4}{96N_c^2} \quad (\text{A.13})$$

$$a_3^{(0)} = 502.24(1) C_A^3 - 136.39(12) \frac{N_c^3 + 6N_c}{48} + \frac{8}{3} \pi^2 C_A^3 \left(-\frac{5}{3} + 2\gamma_E + 2\log 2 \right). \quad (\text{A.14})$$

The three numerical values given above are nowadays known analytically [64, 65]. Lastly, we reproduce the coefficient a_3^L as given in Ref. [60], which multiplies the leading finite term of the perturbative piece of the ultrasoft contribution in Eq. (13),

$$a_3^L = \frac{16\pi^2}{3} C_A^3. \quad (\text{A.15})$$

Appendix B. One-loop chiral corrections to heavy-light mesons masses

In HMrAS χ PT, the mass of H_x meson is described by Eq. (4.2) of Ref. [112]

$$M_{H_x}(\{m_h, m_x\}, \{m'_l, m'_l, m'_s\}, \{a\}) = m_{h,\text{MRS}} + \bar{L}_{\text{MRS}} + \frac{\mu_\pi^2 - \mu_G^2(m_h)}{2m_{h,\text{MRS}}} + 2\lambda_1 B_0 m_x$$

$$+ 2\lambda'_1 B_0 (2m'_l + m'_s) + \delta M_{H_x}(\{m_h, m_x\}, \{m'_l, m'_l, m'_s\}, \{a, V\}) - \mathcal{C}, \quad (\text{B.1})$$

where B_0 is the low energy constant (LEC) in the relation $m_\pi^2 = B_0(m_u + m_d)$ between the pion mass and light quark masses, λ_1 and λ'_1 are LECs independent of the heavy quark mass, δM_{H_x} is the one-loop corrections to the mass of the H_x meson, and \mathcal{C} is a constant elaborated below. The arguments of M_{H_x} and δM_{H_x} correspond to the heavy and light valence-quark mass, the set of three light sea-quark masses, and the lattice spacing a . δM_{H_x} contains effects of flavor, hyperfine, and order- a^2 (staggered) taste splittings as

well as finite lattice size. For a theory with $(2+1)$ light flavors in the sea, we have

$$\begin{aligned} \delta M_{H_x} = & -\frac{3g_\pi^2}{16\pi^2 f^2} \left\{ \frac{1}{16} \sum_{\mathcal{S}, \Xi} K_1(m_{\mathcal{S}x\Xi}, \Delta^* + \delta_{\mathcal{S}x}) \right. \\ & + \frac{1}{3} \sum_{j \in \mathcal{M}_I^{(2,x)}} \frac{\partial}{\partial m_{X_I}^2} \left[R_j^{[2,2]}(\mathcal{M}_I^{(2,x)}; \mu_I^{(2)}) K_1(m_j, \Delta^*) \right] \\ & + \left(a^2 \delta'_V \sum_{j \in \mathcal{M}_V^{(3,x)}} \frac{\partial}{\partial m_{X_V}^2} \left[R_j^{[3,2]}(\mathcal{M}_V^{(3,x)}; \mu_V^{(2)}) K_1(m_j, \Delta^*) \right] + [V \rightarrow A] \right) \Big\} \\ & + a^2 \frac{3g_\pi^2}{16\pi^2 f^2} \left[\lambda'_{a^2} \bar{\Delta} \sum_{\mathcal{S}} \delta_{\mathcal{S}x} + \lambda_{a^2} \Delta^* \left(3\bar{\Delta} - \frac{1}{3} \Delta_I + \delta'_V + \delta'_A \right) \right]. \end{aligned} \quad (\text{B.2})$$

For the full description of each term one should see Refs. [112, 113]. Here we give a brief description of the main indices and terms. g_π is the H - H^* - π coupling, and Δ^* is the lowest-order hyperfine splitting between pseudoscalar and vector mesons. The indices \mathcal{S} and Ξ denote the light sea-quark flavors and meson tastes, respectively. There are 16 mesonic tastes labeled with $\{I, V, T, A, P\}$ corresponding to multiplets of $(1, 4, 6, 4, 1)$, respectively [182]. $m_{\mathcal{S}x, \Xi}$ is the mass of the pseudoscalar meson with taste Ξ and flavors \mathcal{S} and x ; at the tree level we have [[183], Eq. (18)]

$$m_{\mathcal{S}x, \Xi}^2 = B_0(m_{\mathcal{S}} + m_x) + a^2 \Delta_{\Xi}, \quad (\text{B.3})$$

where $\Delta_P = 0$. $\delta_{\mathcal{S}x}$ is the flavor splitting between a heavy-light meson with light quark of flavor \mathcal{S} and one of flavor x . δ'_A and δ'_V are the taste-breaking hairpin parameters. λ_{a^2} and λ'_{a^2} are parameters in S χ PT related to taste breaking in meson masses, and

$$a^2 \bar{\Delta} = \frac{1}{16} \sum_{\Xi} (m_{\mathcal{S}x, \Xi}^2 - m_{\mathcal{S}x, P}^2), \quad (\text{B.4})$$

$$a^2 \Delta_I = m_{\mathcal{S}x, I}^2 - m_{\mathcal{S}x, P}^2. \quad (\text{B.5})$$

Definitions of the chiral-log function K_1 at infinite and finite volumes, the residue functions $R_j^{[n,k]}$, and the sets of masses in the residues are given in Ref. [112] and references therein.

In Eq. (B.1), \mathcal{C} is a constant that can be set to

$$\mathcal{C} = 2\lambda_1 B_0 m_l + 2\lambda'_1 B_0 (2m_l + m_s) + \delta M_{H_x}(\{m_h, m_l\}, \{m_l, m_l, m_s\}, \{0\}) \quad (\text{B.6})$$

so that in the continuum limit, for physical values of sea-quark masses, and $m_x = m_l$ one obtains

$$M_{H_x}(\{m_h, m_l\}, \{m_l, m_l, m_s\}, \{0\}) = m_{h, \text{MRS}} + \bar{A}_{\text{MRS}} + \frac{\mu_\pi^2 - \mu_G^2(m_h)}{2m_{h, \text{MRS}}}. \quad (\text{B.7})$$

References

- [1] G. Peter Lepage, Paul B. Mackenzie, and Michael E. Peskin. Expected Precision of Higgs Boson Partial Widths within the Standard Model. 2014.

- [2] Jens Erler and Rodolfo Ferro-Hernandez. Weak Mixing Angle in the Thomson Limit. *JHEP*, 03:196, 2018.
- [3] Jens Erler and Ming-xing Luo. Hadronic loop corrections to the muon anomalous magnetic moment. *Phys. Rev. Lett.*, 87:071804, 2001.
- [4] Jens Erler and Genaro Toledo Sanchez. An Upper Bound on the Hadronic Light-by-Light Contribution to the Muon $g-2$. *Phys. Rev. Lett.*, 97:161801, 2006.
- [5] Sally Dawson et al. Working Group Report: Higgs Boson. In *Proceedings, 2013 Community Summer Study on the Future of U.S. Particle Physics: Snowmass on the Mississippi (CSS2013): Minneapolis, MN, USA, July 29-August 6, 2013*, 2013.
- [6] Dario Buttazzo, Giuseppe Degrandi, Pier Paolo Giardino, Gian F. Giudice, Filippo Sala, Alberto Salvio, and Alessandro Strumia. Investigating the near-criticality of the Higgs boson. *JHEP*, 12:089, 2013.
- [7] Jos Ramn Espinosa. Vacuum Stability and the Higgs Boson. *PoS, LATTICE2013:010*, 2014.
- [8] V. M. Abazov et al. Determination of the strong coupling constant from the inclusive jet cross section in $p\bar{p}$ collisions at $\sqrt{s}=1.96$ TeV. *Phys. Rev.*, D80:111107, 2009.
- [9] Bogdan Malaescu and Pavel Starovoitov. Evaluation of the Strong Coupling Constant α_s Using the ATLAS Inclusive Jet Cross-Section Data. *Eur. Phys. J.*, C72:2041, 2012.
- [10] Serguei Chatrchyan et al. Measurement of the ratio of the inclusive 3-jet cross section to the inclusive 2-jet cross section in pp collisions at $\sqrt{s} = 7$ TeV and first determination of the strong coupling constant in the TeV range. *Eur. Phys. J.*, C73(10):2604, 2013.
- [11] Vardan Khachatryan et al. Measurement of the inclusive 3-jet production differential cross section in proton-proton collisions at 7 TeV and determination of the strong coupling constant in the TeV range. *Eur. Phys. J.*, C75(5):186, 2015.
- [12] Vardan Khachatryan et al. Constraints on parton distribution functions and extraction of the strong coupling constant from the inclusive jet cross section in pp collisions at $\sqrt{s} = 7$ TeV. *Eur. Phys. J.*, C75(6):288, 2015.
- [13] G. Dissertori, A. Gehrmann-De Ridder, T. Gehrmann, E. W. N. Glover, G. Heinrich, G. Luisoni, and H. Stenzel. Determination of the strong coupling constant using matched NNLO+NLLA predictions for hadronic event shapes in e^+e^- annihilations. *JHEP*, 08:036, 2009.
- [14] G. Dissertori, A. Gehrmann-De Ridder, T. Gehrmann, E. W. N. Glover, G. Heinrich, and H. Stenzel. Precise determination of the strong coupling constant at NNLO in QCD from the three-jet rate in electron-positron annihilation at LEP. *Phys. Rev. Lett.*, 104:072002, 2010.
- [15] G. Abbiendi et al. Determination of α_s using OPAL hadronic event shapes at $\sqrt{s} = 91 - 209$ GeV and resummed NNLO calculations. *Eur. Phys. J.*, C71:1733, 2011.
- [16] S. Bethke, S. Kluth, C. Pahl, and J. Schieck. Determination of the Strong Coupling $\alpha(s)$ from hadronic Event Shapes with $\mathcal{O}(\alpha^3(s))$ and resummed QCD predictions using JADE Data. *Eur. Phys. J.*, C64:351–360, 2009.
- [17] R. A. Davison and B. R. Webber. Non-Perturbative Contribution to the Thrust Distribution in e^+e^- Annihilation. *Eur. Phys. J.*, C59:13–25, 2009.
- [18] Riccardo Abbate, Michael Fickinger, Andre H. Hoang, Vicent Mateu, and Iain W. Stewart. Thrust at N3LL with Power Corrections and a Precision Global Fit for $\alpha_s(m_Z)$. *Phys. Rev.*, D83:074021, 2011.
- [19] Thomas Gehrmann, Gionata Luisoni, and Pier Francesco Monni. Power corrections in the dispersive model for a determination of the strong coupling constant from the thrust distribution. *Eur. Phys. J.*, C73(1):2265, 2013.
- [20] Andr. Hoang, Daniel W. Kolodrubetz, Vicent Mateu, and Iain W. Stewart. Precise determination of α_s from the C -parameter distribution. *Phys. Rev.*, D91(9):094018, 2015.
- [21] Johannes Blumlein, Helmut Bottcher, and Alberto Guffanti. Non-singlet QCD analysis of deep inelastic world data at $\mathcal{O}(\alpha^3(s))$. *Nucl. Phys.*, B774:182–207, 2007.
- [22] S. Alekhin, J. Blumlein, and S. Moch. Parton Distribution Functions and Benchmark Cross Sections at NNLO. *Phys.*

Rev., D86:054009, 2012.

- [23] P. Jimenez-Delgado and E. Reya. Dynamical NNLO parton distributions. *Phys. Rev.*, D79:074023, 2009.
- [24] A. D. Martin, W. J. Stirling, R. S. Thorne, and G. Watt. Uncertainties on $\alpha(S)$ in global PDF analyses and implications for predicted hadronic cross sections. *Eur. Phys. J.*, C64:653–680, 2009.
- [25] L. A. Harland-Lang, A. D. Martin, P. Motylinski, and R. S. Thorne. Uncertainties on α_S in the MMHT2014 global PDF analysis and implications for SM predictions. *Eur. Phys. J.*, C75(9):435, 2015.
- [26] Richard D. Ball, Valerio Bertone, Luigi Del Debbio, Stefano Forte, Alberto Guffanti, Jose I. Latorre, Simone Lionetti, Juan Rojo, and Maria Ubiali. Precision NNLO determination of $\alpha_s(M_Z)$ using an unbiased global parton set. *Phys. Lett.*, B707:66–71, 2012.
- [27] P. A. Baikov, K. G. Chetyrkin, and Johann H. Kuhn. Order $\alpha_s^4(s)$ QCD Corrections to Z and tau Decays. *Phys. Rev. Lett.*, 101:012002, 2008.
- [28] Antonio Pich. Precision Tau Physics. *Prog. Part. Nucl. Phys.*, 75:41–85, 2014.
- [29] Michel Davier, Andreas Hr, Bogdan Malaescu, Chang-Zheng Yuan, and Zhiqing Zhang. Update of the ALEPH non-strange spectral functions from hadronic τ decays. *Eur. Phys. J.*, C74(3):2803, 2014.
- [30] Diogo Boito, Maarten Golterman, Kim Maltman, James Osborne, and Santiago Peris. Strong coupling from the revised ALEPH data for hadronic τ decays. *Phys. Rev.*, D91(3):034003, 2015.
- [31] Johann H. Kuhn and M. Steinhauser. Determination of α_s and heavy quark masses from recent measurements of $R(s)$. *Nucl. Phys.*, B619:588–602, 2001. [Erratum: Nucl. Phys.B640,415(2002)].
- [32] Bahman Dehnadi, Andre H. Hoang, and Vicent Mateu. Bottom and Charm Mass Determinations with a Convergence Test. *JHEP*, 08:155, 2015.
- [33] S. Alekhin, Bluemlein J., K. Daum, K. Lipka, and S. Moch. Precise charm-quark mass from deep-inelastic scattering. *Phys. Lett.*, B720:172–176, 2013.
- [34] Kostas Orginos, Doug Toussaint, and R. L. Sugar. Variants of fattening and flavor symmetry restoration. *Phys. Rev.*, D60:054503, 1999.
- [35] E. Follana et al. Highly improved staggered quarks on the lattice, with applications to charm physics. *Phys. Rev.*, D75:054502, 2007.
- [36] Roberto Frezzotti, Pietro Antonio Grassi, Stefan Sint, and Peter Weisz. Lattice QCD with a chirally twisted mass term. *JHEP*, 08:058, 2001.
- [37] David B. Kaplan. A Method for simulating chiral fermions on the lattice. *Phys. Lett.*, B288:342–347, 1992.
- [38] A. Bazavov et al. Nonperturbative QCD Simulations with 2+1 Flavors of Improved Staggered Quarks. *Rev. Mod. Phys.*, 82:1349–1417, 2010.
- [39] Alexei Bazavov, Nora Brambilla, Peter Petreczky, Antonio Vairo, and Johannes Heinrich Weber. Color screening in (2+1)-flavor QCD. *Phys. Rev.*, D98(5):054511, 2018.
- [40] A. Bazavov, P. Petreczky, and J. H. Weber. Equation of State in 2+1 Flavor QCD at High Temperatures. *Phys. Rev.*, D97(1):014510, 2018.
- [41] A. Bazavov, N. Brambilla, H. T. Ding, P. Petreczky, H. P. Schadler, A. Vairo, and J. H. Weber. Polyakov loop in 2+1 flavor QCD from low to high temperatures. *Phys. Rev.*, D93(11):114502, 2016.
- [42] Matthias Berwein, Nora Brambilla, Peter Petreczky, and Antonio Vairo. Polyakov loop at next-to-next-to-leading order. *Phys. Rev.*, D93(3):034010, 2016.
- [43] H. T. Ding, Swagato Mukherjee, H. Ohno, P. Petreczky, and H. P. Schadler. Diagonal and off-diagonal quark number susceptibilities at high temperatures. *Phys. Rev.*, D92(7):074043, 2015.
- [44] Najmul Haque, Aritra Bandyopadhyay, Jens O. Andersen, Munshi G. Mustafa, Michael Strickland, and Nan Su. Three-loop HTLpt thermodynamics at finite temperature and chemical potential. *JHEP*, 05:027, 2014.

- [45] A. Bazavov, H. T. Ding, P. Hegde, F. Karsch, C. Miao, Swagato Mukherjee, P. Petreczky, C. Schmidt, and A. Velytsky. Quark number susceptibilities at high temperatures. *Phys. Rev.*, D88(9):094021, 2013.
- [46] S. Aoki et al. FLAG Review 2019. *Eur. Phys. J.*, C80(2):113, 2020.
- [47] Andreas Athenodorou, Jacob Finkenrath, Francesco Knechtli, Tomasz Korzec, Björn Leder, Marina Krsti Marinković, and Rainer Sommer. How perturbative are heavy sea quarks? *Nucl. Phys.*, B943:114612, 2019.
- [48] C. Aubin, C. Bernard, C. DeTar, J. Osborn, Steven Gottlieb, E. B. Gregory, D. Toussaint, U. M. Heller, J. E. Hetrick, and R. Sugar. Light hadrons with improved staggered quarks: Approaching the continuum limit. *Phys. Rev.*, D70:094505, 2004.
- [49] M. Tanabashi et al. *Phys. Rev. D*, 98:030001, Aug 2018.
- [50] R. Sommer. A New way to set the energy scale in lattice gauge theories and its applications to the static force and α_s in $SU(2)$ Yang-Mills theory. *Nucl. Phys.*, B411:839–854, 1994.
- [51] Martin Lüscher. Properties and uses of the Wilson flow in lattice QCD. *JHEP*, 08:071, 2010. [Erratum: *JHEP*03,092(2014)].
- [52] Szabolcs Borsanyi et al. High-precision scale setting in lattice QCD. *JHEP*, 09:010, 2012.
- [53] A. Bazavov et al. Results for light pseudoscalar mesons. *PoS, LATTICE2010*:074, 2010.
- [54] Rainer Sommer. Scale setting in lattice QCD. *PoS, LATTICE2013*:015, 2014.
- [55] Y. Maezawa and P. Petreczky. Quark masses and strong coupling constant in 2+1 flavor QCD. *Phys. Rev.*, D94(3):034507, 2016.
- [56] Thomas Appelquist, Michael Dine, and I. J. Muzinich. The Static Potential in Quantum Chromodynamics. *Phys. Lett.*, 69B:231–236, 1977.
- [57] W. Fischler. Quark - anti-Quark Potential in QCD. *Nucl. Phys.*, B129:157–174, 1977.
- [58] A. Billoire. How Heavy Must Be Quarks in Order to Build Coulombic q anti- q Bound States. *Phys. Lett.*, 92B:343–347, 1980.
- [59] York Schröder. The Static potential in QCD to two loops. *Phys. Lett.*, B447:321–326, 1999.
- [60] Nora Brambilla, Antonio Pineda, Joan Soto, and Antonio Vairo. The Infrared behavior of the static potential in perturbative QCD. *Phys. Rev.*, D60:091502, 1999.
- [61] Nora Brambilla, Antonio Vairo, Xavier Garcia i Tormo, and Joan Soto. The QCD static energy at N³LL. *Phys. Rev.*, D80:034016, 2009.
- [62] C. Anzai, Y. Kiyo, and Y. Sumino. Static QCD potential at three-loop order. *Phys. Rev. Lett.*, 104:112003, 2010.
- [63] Alexander V. Smirnov, Vladimir A. Smirnov, and Matthias Steinhauser. Three-loop static potential. *Phys. Rev. Lett.*, 104:112002, 2010.
- [64] Roman N. Lee, Alexander V. Smirnov, Vladimir A. Smirnov, and Matthias Steinhauser. Analytic three-loop static potential. *Phys. Rev.*, D94(5):054029, 2016.
- [65] Roman N. Lee and Vladimir A. Smirnov. Evaluating the last missing ingredient for the three-loop quark static potential by differential equations. *JHEP*, 10:089, 2016.
- [66] Dolores Eiras and Joan Soto. Light fermion finite mass effects in non-relativistic bound states. *Phys. Lett.*, B491:101–110, 2000.
- [67] Nora Brambilla, Antonio Pineda, Joan Soto, and Antonio Vairo. Potential NRQCD: An Effective theory for heavy quarkonium. *Nucl. Phys.*, B566:275, 2000.
- [68] M. Beneke. Renormalons. *Phys. Rept.*, 317:1–142, 1999.
- [69] U. Aglietti and Zoltan Ligeti. Renormalons and confinement. *Phys. Lett.*, B364:75, 1995.
- [70] Silvia Necco and Rainer Sommer. The $N(f) = 0$ heavy quark potential from short to intermediate distances. *Nucl. Phys.*, B622:328–346, 2002.

- [71] Xavier Garcia i Tormo. Review on the determination of α_s from the QCD static energy. *Mod. Phys. Lett.*, A28:1330028, 2013.
- [72] Alexei Bazavov, Nora Brambilla, Xavier Garcia i Tormo, Peter Petreczky, Joan Soto, and Antonio Vairo. Determination of α_s from the QCD static energy. *Phys. Rev.*, D86:114031, 2012.
- [73] Alexei Bazavov, Nora Brambilla, Xavier Garcia i Tormo, Peter Petreczky, Joan Soto, and Antonio Vairo. Determination of α_s from the QCD static energy: An update. *Phys. Rev.*, D90(7):074038, 2014.
- [74] Hiromasa Takaura, Takashi Kaneko, Yuichiro Kiyo, and Yukinari Sumino. Determination of α_s from static QCD potential: OPE with renormalon subtraction and lattice QCD. *JHEP*, 04:155, 2019.
- [75] H. Takaura, T. Kaneko, Y. Kiyo, and Y. Sumino. Determination of α_s from static QCD potential with renormalon subtraction. *Phys. Lett.*, B789:598–602, 2019.
- [76] Antonio Pineda and Joan Soto. The Renormalization group improvement of the QCD static potentials. *Phys. Lett.*, B495:323–328, 2000.
- [77] Nora Brambilla, Antonio Pineda, Joan Soto, and Antonio Vairo. Effective field theories for heavy quarkonium. *Rev. Mod. Phys.*, 77:1423, 2005.
- [78] Alexei Bazavov, Nora Brambilla, Xavier Garcia i Tormo, Peter Petreczky, Joan Soto, Antonio Vairo, and Johannes Heinrich Weber. Determination of the QCD coupling from the static energy and the free energy. *Phys. Rev.*, D100(11):114511, 2019.
- [79] Y. Sumino. Static QCD potential at $r < \Lambda(\text{QCD})^{-1}$: Perturbative expansion and operator-product expansion. *Phys. Rev.*, D76:114009, 2007.
- [80] Go Mishima, Yukinari Sumino, and Hiromasa Takaura. Subtracting infrared renormalons from Wilson coefficients: Uniqueness and power dependences on ΛQCD . *Phys. Rev.*, D95(11):114016, 2017.
- [81] M. Albanese et al. Glueball Masses and String Tension in Lattice QCD. *Phys. Lett.*, B192:163–169, 1987.
- [82] Anna Hasenfratz and Francesco Knechtli. Flavor symmetry and the static potential with hypercubic blocking. *Phys. Rev.*, D64:034504, 2001.
- [83] Colin Morningstar and Mike J. Peardon. Analytic smearing of SU(3) link variables in lattice QCD. *Phys. Rev.*, D69:054501, 2004.
- [84] Martin Lüscher and Peter Weisz. Perturbative analysis of the gradient flow in non-abelian gauge theories. *JHEP*, 02:051, 2011.
- [85] M. Lüscher and P. Weisz. Computation of the Action for On-Shell Improved Lattice Gauge Theories at Weak Coupling. *Phys. Lett.*, 158B:250–254, 1985.
- [86] G. Peter Lepage and Paul B. Mackenzie. On the viability of lattice perturbation theory. *Phys. Rev.*, D48:2250–2264, 1993.
- [87] Johannes Heinrich Weber, Alexei Bazavov, and Peter Petreczky. Equation of state in (2+1) flavor QCD at high temperatures. In *13th Conference on Quark Confinement and the Hadron Spectrum (Confinement XIII) Maynooth, Ireland, July 31-August 6, 2018*, 2018.
- [88] Matthias Berwein, Nora Brambilla, Peter Petreczky, and Antonio Vairo. Polyakov loop correlator in perturbation theory. *Phys. Rev.*, D96(1):014025, 2017.
- [89] Christian Sturm. Moments of Heavy Quark Current Correlators at Four-Loop Order in Perturbative QCD. *JHEP*, 09:075, 2008.
- [90] Y. Kiyo, A. Maier, P. Maierhofer, and P. Marquard. Reconstruction of heavy quark current correlators at $\mathcal{O}(\alpha_s^3)$. *Nucl. Phys.*, B823:269–287, 2009.
- [91] A. Maier, P. Maierhofer, P. Marquard, and A. V. Smirnov. Low energy moments of heavy quark current correlators at four loops. *Nucl. Phys.*, B824:1–18, 2010.

- [92] I. Allison et al. High-Precision Charm-Quark Mass from Current-Current Correlators in Lattice and Continuum QCD. *Phys. Rev.*, D78:054513, 2008.
- [93] David J. Broadhurst, P. A. Baikov, V. A. Ilyin, J. Fleischer, O. V. Tarasov, and Vladimir A. Smirnov. Two loop gluon condensate contributions to heavy quark current correlators: Exact results and approximations. *Phys. Lett.*, B329:103–110, 1994.
- [94] B. V. Geshkenbein, B. L. Ioffe, and K. N. Zybalyuk. The Check of QCD based on the tau - decay data analysis in the complex q^2 - plane. *Phys. Rev.*, D64:093009, 2001.
- [95] C. McNeile, C. T. H. Davies, E. Follana, K. Hornbostel, and G. P. Lepage. High-Precision c and b Masses, and QCD Coupling from Current-Current Correlators in Lattice and Continuum QCD. *Phys. Rev.*, D82:034512, 2010.
- [96] A. Bazavov et al. Equation of state in (2+1)-flavor QCD. *Phys. Rev.*, D90:094503, 2014.
- [97] P. Petreczky and J. H. Weber. Strong coupling constant and heavy quark masses in (2+1)-flavor QCD. *Phys. Rev.*, D100(3):034519, 2019.
- [98] Katsumasa Nakayama, Brendan Fahy, and Shoji Hashimoto. Short-distance charmonium correlator on the lattice with Möbius domain-wall fermion and a determination of charm quark mass. *Phys. Rev.*, D94(5):054507, 2016.
- [99] Bipasha Chakraborty, C. T. H. Davies, B. Galloway, P. Knecht, J. Koponen, G. C. Donald, R. J. Dowdall, G. P. Lepage, and C. McNeile. High-precision quark masses and QCD coupling from $n_f = 4$ lattice QCD. *Phys. Rev.*, D91(5):054508, 2015.
- [100] A. Bazavov et al. Lattice QCD Ensembles with Four Flavors of Highly Improved Staggered Quarks. *Phys. Rev.*, D87(5):054505, 2013.
- [101] Chetyrkin, K. G. and Kühn, Johann H. and Steinhauser, M. RunDec: A Mathematica package for running and decoupling the strong coupling and quark masses. *Comput. Phys. Commun.*, 133:43–65, 2000.
- [102] Diogo Boito and Vicent Mateu. Precise determination of α_s from relativistic quarkonium sum rules. *JHEP*, 03:094, 2020.
- [103] Diogo Boito and Vicent Mateu. Precise α_s determination from charmonium sum rules. 2019.
- [104] Adam F. Falk and Matthias Neubert. Second order power corrections in the heavy quark effective theory. 1. Formalism and meson form-factors. *Phys. Rev.*, D47:2965–2981, 1993.
- [105] Andreas S. Kronfeld and James N. Simone. Computation of $\Lambda_{\overline{\text{MS}}}$ and $\Lambda(1)$ with lattice QCD. *Phys. Lett.*, B490:228–235, 2000. [Erratum: *Phys. Lett.* B495,441(2000)].
- [106] Gustavo Burdman and John F. Donoghue. Union of chiral and heavy quark symmetries. *Phys. Lett.*, B280:287–291, 1992.
- [107] Tung-Mow Yan, Hai-Yang Cheng, Chi-Yee Cheung, Guey-Lin Lin, Y. C. Lin, and Hoi-Lai Yu. Heavy quark symmetry and chiral dynamics. *Phys. Rev.*, D46:1148–1164, 1992. [Erratum: *Phys. Rev.* D55,5851(1997)].
- [108] Mark B. Wise. Chiral perturbation theory for hadrons containing a heavy quark. *Phys. Rev.*, D45(7):R2188, 1992.
- [109] K. Symanzik. Continuum limit and improved action in lattice theories 1: Principles and ϕ^4 theory. *Nucl. Phys.*, B226:187–204, 1983.
- [110] J. Komijani et al. Decay constants f_B and f_{B_s} and quark masses m_b and m_c from HISQ simulations. *PoS, LATTICE2016*:294, 2016.
- [111] Javad Komijani. A discussion on leading renormalon in the pole mass. *JHEP*, 08:062, 2017.
- [112] Nora Brambilla, Javad Komijani, Andreas S. Kronfeld, and Antonio Vairo. Relations between heavy-light meson and quark masses. *Phys. Rev.*, D97(3):034503, 2018.
- [113] A. Bazavov et al. Up-, down-, strange-, charm-, and bottom-quark masses from four-flavor lattice QCD. *Phys. Rev.*, D98(5):054517, 2018.
- [114] A. Bazavov et al. B- and D-meson leptonic decay constants and quark masses from four-flavor lattice QCD. In *13th Conference on the Intersections of Particle and Nuclear Physics (CIPANP 2018) Palm Springs, California, USA, May*

29-June 3, 2018, 2018.

- [115] Andreas S. Kronfeld. The Perturbative pole mass in QCD. *Phys. Rev.*, D58:051501, 1998.
- [116] J. C. Breckenridge, M. J. Lavelle, and Thomas G. Steele. The Nielsen identities for the two point functions of QED and QCD. *Z. Phys.*, C65:155–164, 1995.
- [117] Ikaros I. Bigi, Mikhail A. Shifman, N. G. Uraltsev, and A. I. Vainshtein. The Pole mass of the heavy quark: Perturbation theory and beyond. *Phys. Rev.*, D50:2234–2246, 1994.
- [118] M. Beneke and Vladimir M. Braun. Heavy quark effective theory beyond perturbation theory: Renormalons, the pole mass and the residual mass term. *Nucl. Phys.*, B426:301–343, 1994.
- [119] Nikolai Uraltsev. BLM resummation and OPE in heavy flavor transitions. *Nucl. Phys.*, B491:303–322, 1997.
- [120] Nikolai Uraltsev. On the chromomagnetic expectation value $\mu^{**2}(G)$ and higher power corrections in heavy flavor mesons. *Phys. Lett.*, B545:337–344, 2002.
- [121] Antonio Pineda. Determination of the bottom quark mass from the Upsilon(1S) system. *JHEP*, 06:022, 2001.
- [122] Andre H. Hoang, Ambar Jain, Ignazio Scimemi, and Iain W. Stewart. Infrared Renormalization Group Flow for Heavy Quark Masses. *Phys. Rev. Lett.*, 101:151602, 2008.
- [123] A. H. Hoang. 1S and $\overline{\text{MS}}$ bottom quark masses from Upsilon sum rules. *Phys. Rev.*, D61:034005, 2000.
- [124] M. Beneke. A Quark mass definition adequate for threshold problems. *Phys. Lett.*, B434:115–125, 1998.
- [125] Adam F. Falk, Matthias Neubert, and Michael E. Luke. The Residual mass term in the heavy quark effective theory. *Nucl. Phys.*, B388:363–375, 1992.
- [126] M. Beneke. More on ambiguities in the pole mass. *Phys. Lett.*, B344:341–347, 1995.
- [127] Peter Marquard, Alexander V. Smirnov, Vladimir A. Smirnov, Matthias Steinhauser, and David Wellmann. $\overline{\text{MS}}$ -on-shell quark mass relation up to four loops in QCD and a general $\text{SU}(N)$ gauge group. *Phys. Rev.*, D94(7):074025, 2016.
- [128] Taekoon Lee. Heavy quark mass determination from the quarkonium ground state energy: A Pole mass approach. *JHEP*, 10:044, 2003.
- [129] Gunnar S. Bali and Antonio Pineda. QCD phenomenology of static sources and gluonic excitations at short distances. *Phys. Rev.*, D69:094001, 2004.
- [130] P. A. Baikov, K. G. Chetyrkin, and J. H. Kühn. Quark Mass and Field Anomalous Dimensions to $O(\alpha_s^5)$. *JHEP*, 10:076, 2014.
- [131] P. A. Baikov, K. G. Chetyrkin, and J. H. Kühn. Five-Loop Running of the QCD coupling constant. *Phys. Rev. Lett.*, 118(8):082002, 2017.
- [132] Claude Bernard and Javad Komijani. Chiral Perturbation Theory for All-Staggered Heavy-Light Mesons. *Phys. Rev.*, D88(9):094017, 2013.
- [133] A. Bazavov et al. Scaling studies of QCD with the dynamical HISQ action. *Phys. Rev.*, D82:074501, 2010.
- [134] A. Bazavov et al. B - and D -meson leptonic decay constants from four-flavor lattice QCD. *Phys. Rev.*, D98(7):074512, 2018.
- [135] A. Bazavov et al. Charmed and light pseudoscalar meson decay constants from four-flavor lattice QCD with physical light quarks. *Phys. Rev.*, D90(7):074509, 2014.
- [136] S. Basak et al. Lattice computation of the electromagnetic contributions to kaon and pion masses. *Phys. Rev.*, D99(3):034503, 2019.
- [137] C. Bernard and D. Toussaint. Effects of nonequilibrated topological charge distributions on pseudoscalar meson masses and decay constants. *Phys. Rev.*, D97(7):074502, 2018.
- [138] Richard D. Ball, Luigi Del Debbio, Stefano Forte, Alberto Guffanti, Jose I. Latorre, Juan Rojo, and Maria Ubiali. Fitting Parton Distribution Data with Multiplicative Normalization Uncertainties. *JHEP*, 05:075, 2010.
- [139] G. P. Lepage, B. Clark, C. T. H. Davies, K. Hornbostel, P. B. Mackenzie, C. Morningstar, and H. Trottier. Constrained

- curve fitting. *Nucl. Phys. Proc. Suppl.*, 106:12–20, 2002.
- [140] C. Patrignani et al. Review of Particle Physics. *Chin. Phys.*, C40(10):100001, 2016.
 - [141] Peter Marquard, Alexander V. Smirnov, Vladimir A. Smirnov, and Matthias Steinhauser. Quark Mass Relations to Four-Loop Order in Perturbative QCD. *Phys. Rev. Lett.*, 114(14):142002, 2015.
 - [142] Tao Liu and Matthias Steinhauser. Decoupling of heavy quarks at four loops and effective Higgs-fermion coupling. *Phys. Lett.*, B746:330–334, 2015.
 - [143] C. Bernard. Effective Field Theories and Lattice QCD. *PoS*, CD15:004, 2015.
 - [144] Martin Lüscher, Rajamani Narayanan, Peter Weisz, and Ulli Wolff. The Schrödinger functional: A Renormalizable probe for nonAbelian gauge theories. *Nucl. Phys.*, B384:168–228, 1992.
 - [145] R. Narayanan and H. Neuberger. Infinite N phase transitions in continuum Wilson loop operators. *JHEP*, 03:064, 2006.
 - [146] Zoltan Fodor, Kieran Holland, Julius Kuti, Daniel Nogradi, and Chik Him Wong. The Yang-Mills gradient flow in finite volume. *JHEP*, 11:007, 2012.
 - [147] Patrick Fritzsch and Alberto Ramos. The gradient flow coupling in the Schrger Functional. *JHEP*, 10:008, 2013.
 - [148] S. Aoki et al. Precise determination of the strong coupling constant in $N_f = 2+1$ lattice QCD with the Schrödinger functional scheme. *JHEP*, 10:053, 2009.
 - [149] Mattia Bruno, Mattia Dalla Brida, Patrick Fritzsch, Tomasz Korzec, Alberto Ramos, Stefan Schaefer, Hubert Simma, Stefan Sint, and Rainer Sommer. QCD Coupling from a Nonperturbative Determination of the Three-Flavor Λ Parameter. *Phys. Rev. Lett.*, 119(10):102001, 2017.
 - [150] Q. Mason, H. D. Trottier, C. T. H. Davies, K. Foley, A. Gray, G. P. Lepage, M. Nobes, and J. Shigemitsu. Accurate determinations of $\alpha(s)$ from realistic lattice QCD. *Phys. Rev. Lett.*, 95:052002, 2005.
 - [151] K. Hornbostel, G. P. Lepage, and C. Morningstar. Scale setting for $\alpha(s)$ beyond leading order. *Phys. Rev.*, D67:034023, 2003.
 - [152] C. T. H. Davies, K. Hornbostel, I. D. Kendall, G. P. Lepage, C. McNeile, J. Shigemitsu, and H. Trottier. Update: Accurate Determinations of $\alpha(s)$ from Realistic Lattice QCD. *Phys. Rev.*, D78:114507, 2008.
 - [153] K. Maltman, D. Leinweber, P. Moran, and A. Sternbeck. The Realistic Lattice Determination of $\alpha(s)(M(Z))$ Revisited. *Phys. Rev.*, D78:114504, 2008.
 - [154] K. G. Chetyrkin, A. L. Kataev, and F. V. Tkachov. Higher Order Corrections to Σ -t ($e^+ e^- \rightarrow \text{Hadrons}$) in Quantum Chromodynamics. *Phys. Lett.*, 85B:277–279, 1979.
 - [155] Levan R. Surguladze and Mark A. Samuel. Total hadronic cross-section in $e^+ e^-$ annihilation at the four loop level of perturbative QCD. *Phys. Rev. Lett.*, 66:560–563, 1991. [Erratum: *Phys. Rev. Lett.* 66,2416(1991)].
 - [156] S. G. Gorishnii, A. L. Kataev, and S. A. Larin. The $O(\alpha_s^3)$ -corrections to $\sigma_{tot}(e^+e^- \rightarrow \text{hadrons})$ and $\Gamma(\tau^- \rightarrow \nu_\tau + \text{hadrons})$ in QCD. *Phys. Lett.*, B259:144–150, 1991.
 - [157] E. Shintani, S. Aoki, T. W. Chiu, S. Hashimoto, T. H. Hsieh, T. Kaneko, H. Matsufuru, J. Noaki, T. Onogi, and N. Yamada. Lattice study of the vacuum polarization function and determination of the strong coupling constant. *Phys. Rev.*, D79:074510, 2009.
 - [158] E. Shintani, S. Aoki, H. Fukaya, S. Hashimoto, T. Kaneko, T. Onogi, and N. Yamada. Strong coupling constant from vacuum polarization functions in three-flavor lattice QCD with dynamical overlap fermions. *Phys. Rev.*, D82(7):074505, 2010. [Erratum: *Phys. Rev.* D89, no.9, 099903(2014)].
 - [159] Renwick J. Hudspith, Randy Lewis, Kim Maltman, and Eigo Shintani. α_s from the Lattice Hadronic Vacuum Polarisation. 2018.
 - [160] B. Alles, D. Henty, H. Panagopoulos, C. Parrinello, C. Pittori, and D. G. Richards. α_s from the nonperturbatively renormalised lattice three gluon vertex. *Nucl. Phys.*, B502:325–342, 1997.
 - [161] Philippe Boucaud, J. P. Leroy, H. Moutarde, J. Micheli, O. Pene, J. Rodriguez-Quintero, and C. Roiesnel. Preliminary

- calculation of $\alpha(s)$ from Green functions with dynamical quarks. *JHEP*, 01:046, 2002.
- [162] Philippe Boucaud, F. De Soto, J. P. Leroy, A. Le Yaouanc, J. Micheli, O. Pene, and J. Rodriguez-Quintero. Ghost-gluon running coupling, power corrections and the determination of $\Lambda(\overline{\text{MS}})$. *Phys. Rev.*, D79:014508, 2009.
 - [163] B. Blossier, Ph. Boucaud, F. De soto, V. Morenas, M. Gravina, O. Pene, and J. Rodriguez-Quintero. Ghost-gluon coupling, power corrections and $\Lambda_{\overline{\text{MS}}}$ from twisted-mass lattice QCD at $N_f=2$. *Phys. Rev.*, D82:034510, 2010.
 - [164] K. G. Chetyrkin and A. Retey. Three loop three linear vertices and four loop similar to MOM beta functions in massless QCD. 2000.
 - [165] B. Blossier, Ph. Boucaud, M. Brinet, F. De Soto, X. Du, M. Gravina, V. Morenas, O. Pene, K. Petrov, and J. Rodriguez-Quintero. Ghost-gluon coupling, power corrections and $\Lambda_{\overline{\text{MS}}}$ from lattice QCD with a dynamical charm. *Phys. Rev.*, D85:034503, 2012.
 - [166] B. Blossier, Ph. Boucaud, M. Brinet, F. De Soto, X. Du, V. Morenas, O. Pene, K. Petrov, and J. Rodriguez-Quintero. The Strong running coupling at τ and Z_0 mass scales from lattice QCD. *Phys. Rev. Lett.*, 108:262002, 2012.
 - [167] B. Blossier, Ph. Boucaud, M. Brinet, F. De Soto, V. Morenas, O. Pene, K. Petrov, and J. Rodriguez-Quintero. High statistics determination of the strong coupling constant in Taylor scheme and its OPE Wilson coefficient from lattice QCD with a dynamical charm. *Phys. Rev.*, D89(1):014507, 2014.
 - [168] S. Zafeiropoulos, P. Boucaud, F. De Soto, J. Rodrez-Quintero, and J. Segovia. Strong Running Coupling from the Gauge Sector of Domain Wall Lattice QCD with Physical Quark Masses. *Phys. Rev. Lett.*, 122(16):162002, 2019.
 - [169] K. G. Chetyrkin and Johann H. Kuhn. Quartic mass corrections to $R(\text{had})$. *Nucl. Phys.*, B432:337–350, 1994.
 - [170] Andre Kneur, Jean-Loiand Neveu. Chiral condensate from renormalization group optimized perturbation. *Phys. Rev.*, D92(7):074027, 2015.
 - [171] Katsumasa Nakayama, Hidenori Fukaya, and Shoji Hashimoto. Lattice computation of the Dirac eigenvalue density in the perturbative regime of QCD. *Phys. Rev.*, D98(1):014501, 2018.
 - [172] Yi-Bo Yang et al. Charm and strange quark masses and f_{D_s} from overlap fermions. *Phys. Rev.*, D92(3):034517, 2015.
 - [173] N. Carrasco et al. Up, down, strange and charm quark masses with $N_f = 2+1+1$ twisted mass lattice QCD. *Nucl. Phys.*, B887:19–68, 2014.
 - [174] C. Alexandrou, V. Drach, K. Jansen, C. Kallidonis, and G. Koutsou. Baryon spectrum with $N_f = 2 + 1 + 1$ twisted mass fermions. *Phys. Rev.*, D90(7):074501, 2014.
 - [175] A. T. Lytle, C. T. H. Davies, D. Hatton, G. P. Lepage, and C. Sturm. Determination of quark masses from $\mathbf{n_f} = \mathbf{4}$ lattice QCD and the RI-SMOM intermediate scheme. *Phys. Rev.*, D98(1):014513, 2018.
 - [176] A. J. Lee, C. J. Monahan, R. R. Horgan, C. T. H. Davies, R. J. Dowdall, and J. Koponen. Mass of the b quark from lattice NRQCD and lattice perturbation theory. *Phys. Rev.*, D87(7):074018, 2013.
 - [177] B. Colquhoun, R. J. Dowdall, C. T. H. Davies, K. Hornbostel, and G. P. Lepage. Υ and Υ' Leptonic Widths, a_μ^b and m_b from full lattice QCD. *Phys. Rev.*, D91(7):074514, 2015.
 - [178] A. Bussone et al. Mass of the b quark and B -meson decay constants from $N_f = 2 + 1 + 1$ twisted-mass lattice QCD. *Phys. Rev.*, D93(11):114505, 2016.
 - [179] P. Gambino, A. Melis, and S. Simula. Extraction of heavy-quark-expansion parameters from unquenched lattice data on pseudoscalar and vector heavy-light meson masses. *Phys. Rev.*, D96(1):014511, 2017.
 - [180] F. Herzog, B. Ruijl, T. Ueda, J. A. M. Vermaseren, and A. Vogt. The five-loop beta function of Yang-Mills theory with fermions. *JHEP*, 02:090, 2017.
 - [181] Thomas Luthe, Andreas Maier, Peter Marquard, and York Schröder. The five-loop Beta function for a general gauge group and anomalous dimensions beyond Feynman gauge. *JHEP*, 10:166, 2017.
 - [182] Andreas S. Kronfeld. Lattice gauge theory with staggered fermions: How, where, and why (not). *PoS, LAT2007*:016, 2007.

- [183] C. Aubin and C. Bernard. Pion and kaon masses in staggered chiral perturbation theory. *Phys. Rev.*, D68:034014, 2003.